MASTER THESIS

Earthing System Design, Modelling and Evaluation of a Typical PV Plant of 1kV or Larger

Author:
Tristan LAKER

Supervisors:
Prof. Dr. Veit Dominik KUNZ
Mr. Martin URBAN

A thesis submitted in fulfillment of the requirements
for the degree of Master of Renewable Energy Systems - Environmental and
Process Engineering

on

September 14, 2017

Declaration of Authorship

I, Tristan LAKER, declare that this thesis titled, "Earthing System Design, Modelling and Evaluation of a Typical PV Plant of 1kV or Larger" and the work presented in it is my own. I confirm that:

- This work was done wholly or mainly while in candidature for a research degree at this University.

- Where any part of this thesis has previously been submitted for a degree or any other qualification at this University or any other institution, this has been clearly stated.

- Where I have consulted the published work of others, this is always clearly attributed.

- Where I have quoted from the work of others, the source is always given. With the exception of such quotations, this thesis is entirely my own work.

- I have acknowledged all main sources of help.

- Where the thesis is based on work done by myself jointly with others, I have made clear exactly what was done by others and what I have contributed myself.

Signed:

_____

Date:

_____

Abstract

The work in this thesis presents a detailed study into the behaviour of an earthing system associated with a grid connected solar photovoltaic plant. A computer simulation model is developed and used for conducting experiments to investigate how a solar plant earthing system reacts to variations in plant configuration and other conditions associated with the plant. Also infield measurements were conducted on an existing soar plant earthing system to verify the accuracy of the developed model.

The key findings of the study have shown that solar plants with an isolated or resonant earthed neutral point are in all practical cases safe under the worst possible fault scenarios. Also larger plants are inherently more safe than smaller plants.

Furthermore the effect on the earthing system of the length of the MV cables connecting the plant to the grid, the short circuit power of the grid and the phase angle of the grid have been investigated with the results showing minimal impact on the behaviour of the earthing system.

Keywords: Earthing System, Grounding System, Photovoltaic Plant, LTspice

Acknowledgements

During the completion of this project I have received the help and support of many people and without their generous assistance this thesis would never have succeeded.

First my wonderful girlfriend Marei has always been there for me and put up with me throughout the project and my heartfelt thanks is extended to her for always cheering me up and putting me in a good frame of mind to tackle any challenges I have faced.

My supervisors, Martin Urban and Veit Dominik Kunz have provided a wealth of knowledge and direction in guiding me through this thesis and I believe without their help this thesis would lack technical integrity and professionalism.

To all of the great people at Enerparc AG, I thank you, I have learnt a great deal in my time there and having the backing of everyone there made this project a reality.

My family have also provided me with a lot of support and guidance during the completion of not only this project but the entire degree. Being the youngest of the family their experience and knowledge has always guided me along a path to success and for this I am eternally grateful.

And finally to the boys at the Dockers Australian Football Club, although you may not realise you all have a significant contribution to this piece of work for which I thank you.

Contents

x

List of Figures

List of Tables

List of Abbreviations

EPR	**E**arth **P**otential **R**ise
ESPR	**E**arth **S**urface **P**otential **R**ise
NPT	**N**eutral **P**oint **T**reatment
PV	**P**hoto**V**oltaic
RMS	**R**oot **M**ean **S**quare
FOP	**F**all **O**f **P**otential
DC	**D**irect **C**urrent
AC	**A**lternating **C**urrent
GES	**G**lobal **E**arthing **S**ystem
SPICE	**S**imulation **P**rogram with **I**integrated **C**ircuit **E**mphasis
PEN	**P**rotective **E**arth **N**eutral
MV	**M**edium **V**oltage
LES	**L**ocal **E**arthing **S**ystem
HEC	**H**orizontal **E**arthing **Conductor**
NP	**N**eutral **P**oint

List of Symbols

B	Radius of Hemispherical Earthing Electrode	m
C_E	Line to Earth Capacitance	F
C_S	Surface Layer Derating Factor	
D_F	Fault Current Decrement Factor	
E	Electrical Field Strength	N/C
i	Current Density	A/m^2
$I_{C,U}, I_{C,V}, I_{C,W}$	Phase U, V, W Capacitive Current	A
I_E	Earth Current	A
I_F	Fault Current	A
$I_{L,N}$	Neutral Point Inductive Current	A
I_N	Neutral Point Current	A
I_{OC}	Open Circuit Current	A
I_{SC}	Short Circuit Current	A
I_0	Zero Sequence Current	A
L_{grid}	Grid Inductance	H
L_N	Neutral Point Inductance	H
R_E	Resistance to Earth	Ω
$R_{E,App}$	Apparent Resistance to Earth	Ω
R_{grid}	Grid Resistance	Ω
R_N	Neutral Point Resistance	Ω
R_U, R_V, R_W	Phase Loads	Ω
ρ	Soil Resistivity	Ωm
ρ_r	Apparent Soil Resistivity	Ωm
ρ_s	Soil Surface Resistivity	Ωm
S_F	Fault Current Division Factor	
T_a	DC Offset Time Constant	
t_f	Duration of Electrical Fault	s
t_s	Duration of Electrical Shock	s
U, V, W	Phases in a Three Phase System	
V_E	Electrical Potential of an Earthing Electrode	V
V_f	Fault Voltage	V
V_S	Step Voltage	V
V_T	Touch Voltage	V
$V_{step,allow}$	Allowable Step Voltage	V
$V_{touch,allow}$	Allowable Touch Voltage	V
V_{OC}	Open Circuit Voltage	V
V_{SC}	Short Circuit Voltage	V
Z_{grid}	Grid Impedance	Ω
Z_N	Neutral Point Impedance	Ω
Z_0, Z_1, Z_2	Zero, Positive and Negative Sequence Impedance	Ω

1 Introduction

1.1 Motivation

Medium and high voltage electrical facilities pose a danger to humans within their vicinity. Under fault conditions unintended current pathways may form potentially exposing humans to high electrical voltages which can have negative health effects and in some cases can lead to death. An earthing system is used to ensure the safety of humans and also to ensure any fault current does not exceed the maximum allowable current limit of electrical equipment within the facility.

In recent years the threat of human induced global warming has driven a transformation in electrical energy production away from traditional fossil fuel fired power plants to renewable energy power plants such as wind, solar thermal and solar photovoltaic. Solar photovoltaic power plants range in size from private household rooftop systems typically ranging from 1-5 kWp to commercial scale grid connected systems typically larger that 1 MWp of power output. Such commercial scale solar plants represent a medium to high voltage electrical facility and as such require a correctly functioning earthing system to ensure safe operation of the system.

The design and operation of earthing systems for traditional fossil fuel power plants has been thoroughly studied and there exist various papers and design standards pertaining to this [1] [2] [3]. Grid connected solar power plants share very few similarities with fossil fuel power plants and as such the earthing system design and operation is very different. Studies into solar plant earthing systems are currently quite limited [4] and there exists demand for further investigation into this topic.

1.2 Project Partner Enerparc AG

Enerparc AG, head quartered in Hamburg, Germany are a company offering services in all aspects of grid connected solar plants such as project development and finance, engineering, construction and operation and maintenance. Enerparc AG have successfully installed 1,700 MW of solar plant capacity in Europe, the USA and Asia and as such have strong experience in the industry [5].

Enerparc AG are acting as the industry partner supporting this study, plants owned and operated by Enerparc AG will be used for conducting in field experiments and providing real world data to verify the operation of the computer simulations conducted in this study.

1.3 Problems with Solar Plant Earthing System Design

The current approach to solar plant earthing system design at lacks a formal design process bringing rise to several risks. Under the current design process a standard earthing system design is used for each plant and after construction of the system the resistance to earth of the system is measured. If the resistance to earth of the system is equal to or below a predetermined acceptable limit the system is certified

safe, if however the resistance to earth is greater than the predetermined acceptable limit design modifications to the earthing system are made and the measurement and certification process is repeated.

A problem arising from this process is that there exists uncertainty with the performance of the system upon construction and in the case the system is not certified safe project budget and schedule over runs are possible.

Also rather than the system being designed to protect equipment from high currents and protect humans from high voltages only the resistance to earth of the system is used as a performance indicator. This could lead to unsafe systems being certified safe or safe systems being certified unsafe.

Finally the current design process lacks an in depth understanding of the behaviour of the system. Such an understanding would prove valuable as the behaviour of the system for various plant conditions and configurations could be predicted prior to construction and any necessary design modifications could be implemented.

1.4   Aim and Purpose

The aim of this thesis is to develop a cost effective solar plant earthing system design philosophy which delivers earthing systems that meet all operational and safety requirements. Such requirements include the protection of equipment from high currents and the protection of humans from high voltages.

In addition this thesis aims to develop a quantitative understanding of the behaviour of the earthing system under various plant conditions and configurations. This is to be achieved by developing a computer model of an earthing system and conducting simulations with the model to understand the behaviour of the system. Investigations are to be conducted under single and double phase faults and with various different grid characteristics such as neutral point treatment, short circuit power and phase angle. Also various plant sizes will be investigated and the behaviour of the earthing system will be studied under different soil conditions.

A further aim of this thesis is to investigate the concept of a Global Earthing System (GES), a type of earthing system introduced in HD 637 S1, Power installations exceeding 1kV ac [6] which is safe under all conditions, and to find a method to certify a particular earthing system as a GES.

Finally this study aims to make a quantitative comparison of the available international earthing standards.

1.5   Scope

The scope of this thesis shall be limited to grid connected solar plants with a grid connection voltage of 20 kV and a minimum power output of 1 MW. The electrical current generated by the solar modules in the studied plants is converted to 3 phase 400 V power by solar inverters before being stepped up to the 20 kV level by the medium voltage transformers. Only solar pants mounted on land will be considered, roof top mounted systems are not considered.

When investigating faults in the solar plants only power faults will be considered, analysing lightening strike conditions will not form any part of this thesis. Also dynamic control behaviour of the solar plant or the grid will be ignored, only the worst case fault situations will be investigated.

2 Background Theory

2.1 Earthing Problem

Earthing, or grounding, is an electrical concept to ensure the safe and continuous operation of an electrical installation [1]. An effective earthing system will return any fault current to the neutral point(s) of the system without exceeding the operational limits of the equipment and ensuring personnel are not exposed to voltages exceeding a pre-determined safe limit [1]. To achieve this all metallic or conductive enclosures, structures and other exposed non-current carrying materials are electrically bonded and provided with a current path to the earth [7]. The earthed equipment is electrically connected to the earth via an earthing electrode arrangement whereby conductive materials are physically inserted into the earth, this is usually a set of rods driven into the earth, a metallic grid buried in the earth or other electrodes such as the metallic footings of a building [3] [8]. In the case of an electrical fault an unintentional current path may form, electrifying normally non-current carrying equipment and the physical body of the earth is used to return fault currents to the neutral point of the system. For the earthing system to be effective there must be low enough impedance of the return path to ensure the occurring fault current does not induce dangerous voltages in the earthed equipment [3].

2.2 Earth Potential Rise

As discussed in section 2.1 the earth is used to form a return path for fault currents, the earth also is used as a reference value for electrical potential in the earthing system, which is referred to as remote earth i.e. the potential of the earth at a sufficient distance that the effect of the earthing system is not observed. During an earth fault the potential of the earthing system will rise in relation to remote earth due to the impedance of the earthing system, the maximum value of this is known as the Earth Potential Rise (EPR) in V. Also as fault current flows through the earth via the earthing system the resistivity of the soil will cause an increase in electrical potential of the soil. The rise in potential of the earth at the surface due to an earth current above the electrical potential of remote earth is called Earth Surface Potential Rise (ESPR) in V [1].

To understand this further consider a hemispherical earthing electrode of radius B in m buried in soil with homogenous electrical resistivity of ρ in Ωm carrying an earth current I_E in A to the earth as in Figure 2.1 (a). The resulting current density i in A/m^2 at a distance x in m from the centre of the electrode in the earth surrounding the electrode is given by Equation 2.1 [3].

$$i = \frac{I_E}{2\pi x^2} \tag{2.1}$$

And according to Ohm's law the electrical field strength E in N/C produced is:

$$E = \rho i = \frac{\rho I_E}{2\pi x^2} \tag{2.2}$$

And integrating Equation 2.2 yields the electric potential of the electrode $V_{electrode}$ in V in relation to the potential of the earth at a distance x in m from the centre of the electrode [3].

$$V_E = \int_B^x E dx = \int_B^x \frac{\rho I_E}{2\pi x^2} dx = \frac{\rho I_E}{2\pi}\left(\frac{1}{B} - \frac{1}{x}\right) \qquad x \geq B \tag{2.3}$$

Now to find the electric potential of the soil in relation to remote earth, i.e. ESPR, the interval of the definite integral in Equation 2.3 must be changed as in Equation 2.4 [3].

$$ESPR = \int_x^\infty E dx = \int_x^\infty \frac{\rho I_E}{2\pi x^2} dx = \frac{\rho I_E}{2\pi}\left(\frac{1}{x} - \frac{1}{\infty}\right) = \frac{\rho I_E}{2\pi}\left(\frac{1}{x}\right) \qquad x \geq B \tag{2.4}$$

And the EPR corresponds to the maximum value of Equation 2.4 as in Equation 2.5.

$$EPR = max\left(\frac{\rho I_E}{2\pi}\left(\frac{1}{x}\right)\right) = \frac{\rho I_E}{2\pi B} \tag{2.5}$$

Figure 2.1 (b) provides a visualization of the EPR and ESPR corresponding to the hemispherical earthing electrode carrying an earth current I_E to earth shown in Figure 2.1 (a).
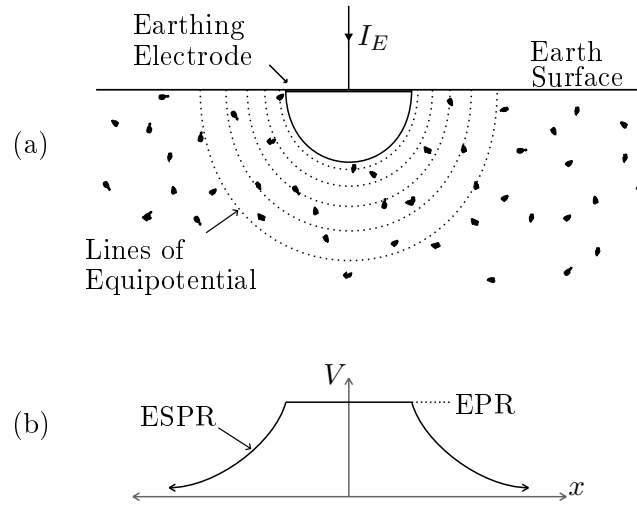
FIGURE 2.1: The EPR and ESPR caused by a hemispherical earthing electrode carrying a fault current I_E to earth. Figure (a) shows the electrode buried in the earth with lines of equipotential emanating out from the electrode, figure (b) graphs the EPR and ESPR caused by the arrangement as described by Equations 2.5 and 2.4 [3].

It must be noted that this analysis has been conducted for the ideal case of homogeneous earth and an electrode of simple geometry, in reality however the earth displays significant inhomogeneity and earthing electrodes exhibit complex geometries making such an analysis far more complex.

2.3 Neutral Point Treatment

In three phase power generation and distribution the neutral point is defined as the common point in a star or Y topology. The method that is selected to earth the neutral point in such a system significantly effects the values of fault currents and voltages that may occur [9] [10]. In general there are four methods to treat the neutral point.

Isolated Neutral Point: In this arrangement no intentional contact to the earth from the neutral point is made and the system is earthed via the line to earth capacitance C_E [11]. During a fault the earth return current I_E must flow through the line to earth capacitances of the unfaulty phases [12]. For these systems an earth fault can cause high EPR as the return path for the fault current encounters high impedance and consequently the fault currents are relatively low see Figure 2.2 (a).

Directly Earthed Neutral Point: In this system the neutral point is directly connected to the earth via an earthing system without any intentional impedance between the neutral point and the earth [12]. This arrangement provides a low impedance pathway for fault current and as such the observed EPR is relatively low and the fault currents are relatively high see Figure 2.2 (b).

Impedance Earthed Neutral Point: Impedance earthed neutral points involves the intentional installation of impedance, Z_N, between the neutral point and the earthing system [13]. This arrangement is usually designed so the installed impedance limits the fault current to below the safe operating limit of the equipment in the system and consequently the observed EPR is relatively high see Figure 2.2 (c).

Resonant Earthing or Petersen Coil Neutral Point: In this system an adjustable high impedance reactor (Petersen Coil), L_N, is installed between the neutral point and the earthing system. The Petersen coil reactance is tuned to match the system phase to earth capacitive reactance [13]. With a correctly tuned coil the inductive current across the neutral point is opposed and equal to the capacitive current caused by the line to earth capacitances of the unfaulty phases, $I_{L,N} = -(I_{C,U} + I_{C,V})$, and the resulting fault current is theoretically reduced to zero see Figure 2.2 (d). In reality however an ohmic residual fault current will flow caused by the resistance of the Petersen coil, insulator leakage, resistance of the lines and other components of the system and corona losses [14].
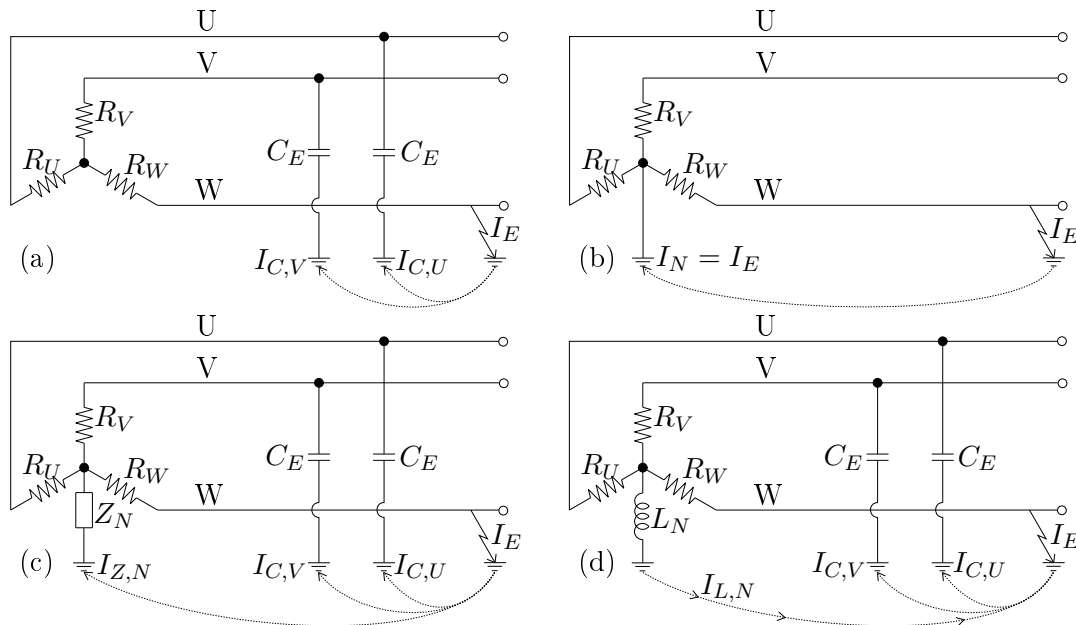
FIGURE 2.2: The four methods of earthing the neutral point with
earth currents indicated under a single phase to earth fault. Figure
(a) an isolated neutral point with earth current returning via the line
to earth capacitances. Figure (b) a directly earthed neutral point with
earth current returning via the neutral point. Figure (c) an impedance
earthed neutral point with the earth current returning via the line
to earth capacitances and the neutral point. Figure (d) a resonant
earthed neutral point with the inductive current from the neutral point
opposing the capacitive current from the healthy phases [2].

2.4   Design Approach and Design Codes

The design of an earthing system for an electrical substation follows the same basic
procedure regardless of the nature of the installation and is as follows [15].

Step 1) Soil resistivity study undertaken to model the soil characteristics;

Step 2) Maximum permissible step and touch voltages calculated;

Step 3) Fault analysis undertaken to determine the maximum possible fault current;

Step 4) The earthing system is designed, modelled and simulated under fault condi-
tions;

Step 5) Simulation is evaluated to ensure maximum step and touch voltages remain
below or equal to the safe limit.

There exist several national and international design codes providing guidelines
on the design of earthing systems, the most commonly used are:

1. IEEE 80-2000: Guide for Safety in AC Substation Grounding. From the Insti-
tute of Electrical and Electronics Engineers, USA.

2. ENA TS 41-24: Guidelines for the Design, Installation, Testing and Mainte-
nance of Main Earthing Systems in Substations. From the Energy Networks
Association of the United Kingdom.

3. BS 7354: Code of Practice for Design of High-Voltage Open-Terminal Stations. From the British Standards Institute.

4. DIN EN 50522 VDE 0101-2:2011-11: Earthing of power installations exceeding 1 kV a.c. From the Verband der Elektrotechnik, Elektronik und Informationstechnik, Germany.

Sections 2.5 through 2.9 shall cover the details of the design process.

2.5 Soil Characteristics

The resistivity of the soil at the location of the earthing system significantly effects the design of the system and the safe design of the system relies on an accurate analysis of the soil characteristics [16]. The first step in conducting a soil characteristics study is to take field measurements of the resistivity of the soil. Today the Wenner method is the most commonly practiced technique for obtaining soil resistivity measurements [4].

The Wenner method was presented by F. Wenner in 1915 and involves four electrodes inserted into the soil at an equal spacing of a meters in a straight line. The two outermost electrodes have a current source applied and the inner two electrodes measure the resulting voltage [17], as seen in Figure 2.3.
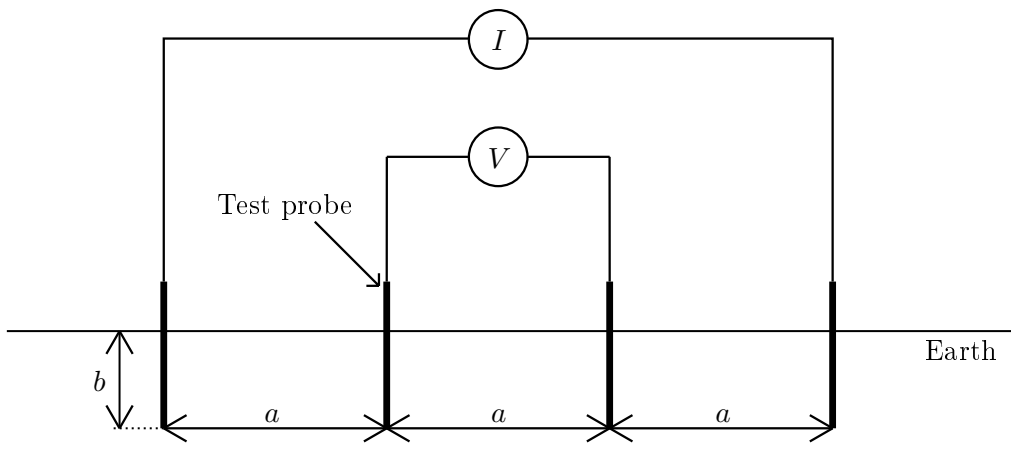
FIGURE 2.3: The Wenner method showing four equally spaced electrodes inserted into the earth. A current is circulated between the two outer electrodes and the two inner electrodes measure voltage. The ratio of voltage to current gives the apparant resistance and from this the apparant soil resistivity is calculated with Equation 2.6 [17].

The measured voltage is then divided by the applied current to obtain the value of resistance, R in Ω. If the distance of spacing a is equal to or larger than ten times the depth of the electrodes b in m an approximation for the apparent soil resistivity ρ_r in Ωm can be calculated using Equation 2.6 [18].

$$\rho_r = 2\pi a R \qquad (2.6)$$

Now Wenner assumes that the earth under measurement exhibits constant resistivity and so the the current travels in a circular profile hence it is a reasonable approximation to assume the apparent soil resistivity at a depth of a is equal to the measured soil resistivity with an electrode spacing of a [17] allowing the investigation

of soil resistivity to significant depths.

Once the soil resistivity measurements have been taken the acquired data must be interpreted and a model developed to allow the analytical evaluation of the earthing system. Typically observed soil structures exhibit non-homogenous properties both vertically and horizontally which is observed in the resistivity measurements of the soil [19]. Selecting a model to accurately represent the soil resistivity structure can be done either manually or by computer analysis and consists of fitting the parameters of each proposed model with the measured data then selecting the model that displays the lowest Root Mean Square (RMS) error [1]. In practice three different types of models are used, the single-layer model, the two-layer model and the multi-layer model.

Single-Layer Model: The single-layer model is used when resistivity measurements display very little deviation with respect to measurement depth. This model assumes the soil is homogenous in its resistivity and the average value of the resistivity measurements is taken as the overall value [19].

Two-Layer Model: The two layer model is used when apparent soil resistivity measurements display large variations with increasing measurement depth. This model assigns a constant resistivity value to the top layer of soil of a finite depth and a different resistivity value to the bottom layer of soil of infinite depth [19]. In practice this is the most commonly employed model [1].

Multi-Layer Model: In cases where the soil structure displays a highly varying resistivity with respect to measurement depth a multi-layer model can be utilized. This model is effectively the same as the two layer model only with more layers of different resistivities with finite depth modelled on top of the final layer of infinite depth [20].

It must be noted that the models used for representing soil resistivity are, at best, an approximation and will not exactly predict the soil behavior [21]. Furthermore it is noted extensively in the literature that soil resistivity varies with moisture content and temperature which vary seasonally [22] [23]. Due to this the IEEE std. 80 guideline recommends that moisture content is recorded at the time resistivity measurements are recorded to indicate if the acquired data is taken at a time of abnormal soil resistivities. It should be noted that seasonal temperature changes do not have a geat impact because soil acts as a strong resistor to heat transfer and so seasonal temperature changes are only manifested in the upper layers of the earth not greatly effecting the buried earthing system [24].

2.6   Safe Voltage Limits

During an earth fault a person within the vicinity of the electrical installation may be exposed to an electrical shock due to the gradient of the ESPR. Step voltage, V_S, is defined as the potential difference a person is exposed to when taking a step of one meter in the ESPR zone. Touch voltage, V_T is defined as the potential difference between an earthed structure which a person is toching and the location of feet contact to earth of that person [1], as shown in Figure 2.4.

Each of the design codes discussed in Section 2.4 details a permissible step and touch voltage calculation methodology [25]. ENA TS 41-24, BS 7354 and DIN EN 50522 use the methodology outlined in the technical report released by the International Electrotechnical Commission in 1994 IEC 479-1 Effects of Current on Human
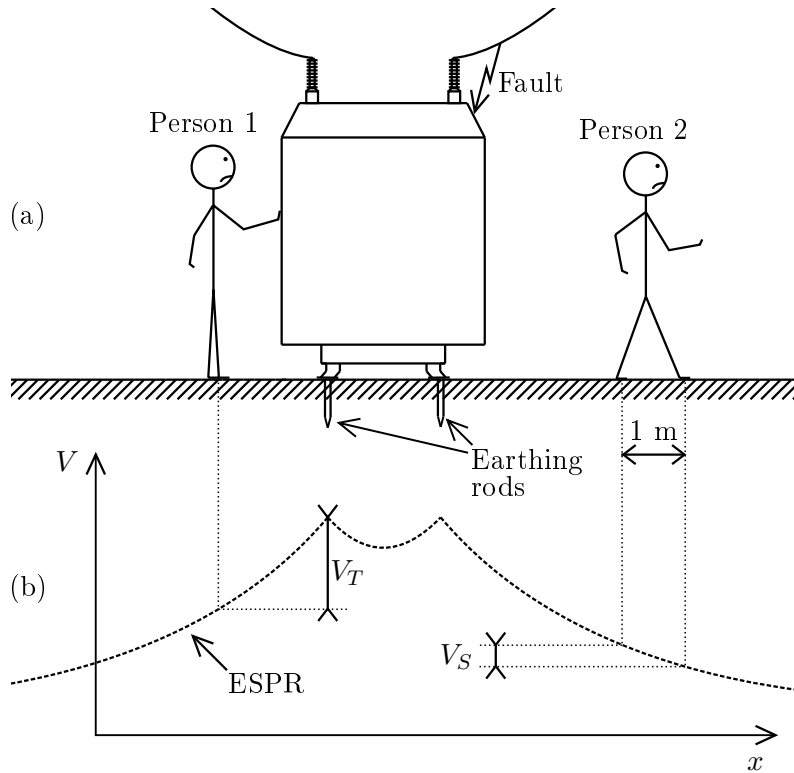
FIGURE 2.4: Step and touch voltages encountered under an electrical fault on an earthed piece of equipment. Person 1 (touch voltage) is shown touching the electrified equipment in figure (a) and the voltage difference between the point of contact with the equipment and the ground is displayed on the ESPR graph in figure (b). Person 2 (step voltage) is shown walking in the vicinity in figure (a) and the voltage difference between the point of contact with the ground of each foot is displayed on the ESPR graph in figure (b) [2].

Beings and Livestock whereas IEEE std. 80 uses the methodology developed by Dalziel [26] [27] [28].

The IEC 479-1 method uses data for the body resistance as a function of body voltage and current path as well as data of tolerable body current as a function of current duration. Tabulated and graphical data is presented for total body resistance along the hand-to-hand path for various contact area sizes and dry, water wet and saltwater wet contact conditions [29], see Appendix A for full details. DIN EN 50522 summarises the IEC 479-1 method for touch voltage and provides a graph of allowable touch voltage as a function of current exposure, shown in Figure 2.5, note that step voltage is ignored as touch voltage is inherently more dangerous.

The IEEE std. 80 method assumes a constant body resistance of 1000 Ω and analytically calculates the contact resistance in the two cases of step and touch voltage based on the contact resistance of one foot being $3C_s\rho_s$ Ω where ρ_s is the soil surface resistivity and C_s is the surface layer derating factor used in situations where a layer of high resistivity material (eg gravel) has been spread on the surface. So for step voltage where the feet act in series the total contact resistance is $6C_s\rho_s$ Ω and for touch voltage, where the feet act in parallel, the contact resistance is $1.5C_s\rho_s$ Ω. Also the allowable body currents for a 50 kg and 70 kg person have been empirically determined using mammals of similar body weight to humans as being $\frac{0.116}{\sqrt{t_s}}$ and
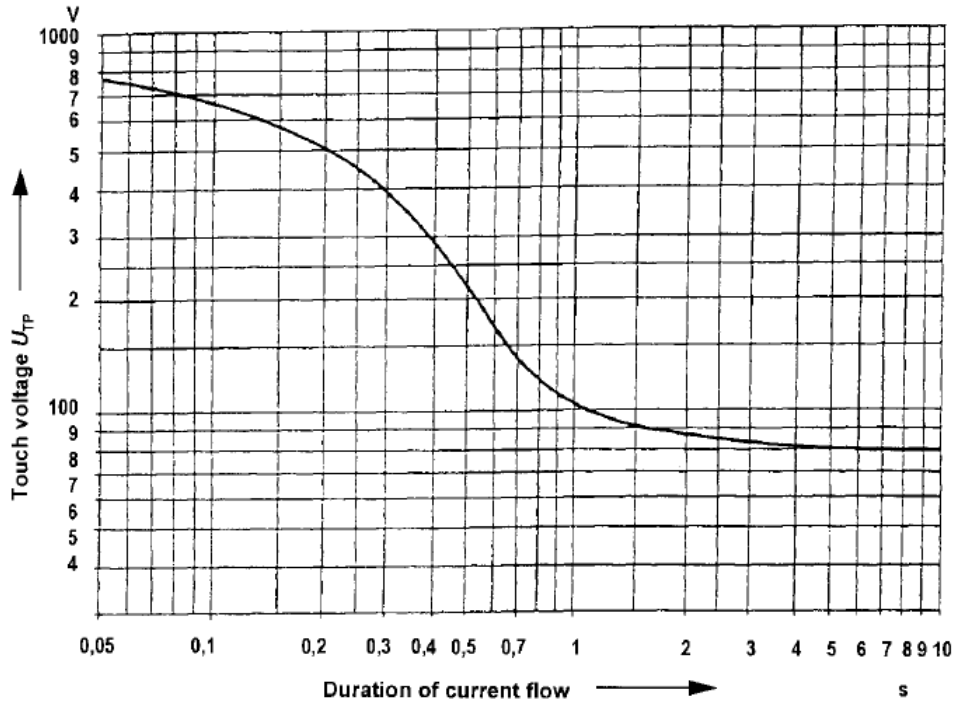
FIGURE 2.5:   Allowable touch voltage as a function of current flow
duration according to DIN EN 50522.

$\frac{0.157}{\sqrt{t_s}}$ respectively where t_s is the duration of current exposure. Equations 2.7 and
2.8 present the step voltage limits for a person of 50 kg and 70 kg respectively and
Equations 2.9 and 2.10 present the touch voltage limits for a person of 50 kg and 70
kg respectively. It should be noted that due to the large area of a typical solar PV
plant spreading an additional layer of high resistivity material on the soil surface is
rarely practical and so the surface layer derating factor C_s is always assumed equal
to 1.

$$V_{step50,allow} = (1000 + 6C_s\rho_s)\frac{0.116}{\sqrt{t_s}} \tag{2.7}$$

$$V_{step70,allow} = (1000 + 6C_s\rho_s)\frac{0.157}{\sqrt{t_s}} \tag{2.8}$$

$$V_{touch50,allow} = (1000 + 1.5C_s\rho_s)\frac{0.116}{\sqrt{t_s}} \tag{2.9}$$

$$V_{touch70,allow} = (1000 + 1.5C_s\rho_s)\frac{0.157}{\sqrt{t_s}} \tag{2.10}$$

Table 2.1 shows values of step and touch voltage limits for various current durations
of a 50 kg and 70 kg person with surface soil resistivity of 300 Ωm.

The work done comparing the two methods by A. Meliopoulos and C. Lee demon-
strates that in some cases the IEC method delivers more conservative results and vice
versa in other cases. As the IEEE method is simpler than the IEC method and both
methods exhibit ample safety margins the recommended method is that presented by
IEEE std. 80 [30].

$\mathbf{t_s}$ (s)	0.1	0.25	0.5	1.0
$\mathbf{V_{step50,allow}}$ (V)	1027.11	649.60	459.34	324.80
$\mathbf{V_{step70,allow}}$ (V)	1390.14	879.20	621.69	439.60
$\mathbf{V_{touch50,allow}}$ (V)	531.90	336.40	237.87	168.20
$\mathbf{V_{touch70,allow}}$ (V)	719.89	455.30	321.95	227.65

TABLE 2.1: Step and touch voltage limits according to IEEE std. 80 with surface soil resistivity of 300 Ωm and a surface layer derating factor of 1.

2.7 Fault Analysis

An electrical fault is an abnormal condition in an electrical system involving failure of one or more components and can be classified as either a short circuit fault or an open circuit fault. A short circuit fault can result from an insulation failure or an overvoltage in the system and causes a current flow through an unintended path, an open circuit fault results from mechanical failure of a component and causes the cessation of current flow. For earthing systems only short circuit faults are considered. In a three phase system short circuits can form between phases, between phases and earth or both resulting in five types of fault, single phase to earth, double phase to earth, triple phase to earth, phase to phase and triple phase [31]. In the case of single or double phase to earth faults the voltage in the faulted phase(s) will collapse and the voltage in the sound phase(s) will rise [32], triple phase to earth and triple phase faults are the only balanced faults resulting in no zero sequence current.

For the design purpose of an earthing system the maximum earth current must be determined, that is the maximum current flowing between the earthing system and the surrounding earth. IEEE std. 80 provides a four step process to determine this value:

Step 1) Assess type and location of fault likely to cause the greatest fault current. The worst type of earth fault is the one that causes the highest value of zero sequence current and can be either a single phase to earth or double phase to earth fault depending on the system impedances. For the case that the product of the positive sequence impedance and the zero sequence impedance is greater than the square of the negative sequence impedance then a single phase to earth fault will result in the greatest zero sequence current. For the case that the product of the positive sequence impedance and the zero sequence impedance is less than the square of the negative sequence impedance then a double phase to earth fault will result in the greatest zero sequence current.

For assessing the worst fault location there are no universal rules, it is a matter of assessing each system upon its individual merits and calculating the zero sequence current at each identified location. For a photovoltaic power plant the worst fault location is typically at the high voltage side of the step-up transformers [15]. For the calculation of the zero sequence current IEEE std. 80 provides equations based upon Ohm's law for a single phase to earth fault Equation 2.11 and for a double phase to earth fault Equation 2.12.

$$I_0 = \frac{V_f}{Z_1 + Z_2 + Z_0} \tag{2.11}$$

$$I_0 = \frac{V_f.Z_2}{Z_1(Z_0 + Z_2) + (Z_0 Z_2)} \tag{2.12}$$

Where:
I_0 is the zero sequence current in A
V_f is the fault voltage in V
Z_1 is the positive sequence impedance in Ω
Z_2 is the negative sequence impedance in Ω
Z_0 is the zero sequence impedance in Ω

It is also interesting to note that for short circuit calculations the International Electrotechnical Commission provides technical report 60909 Short-Circuit Currents in Three-Phase A.C. Systems, which uses equivalent techniques and derives equations that are in essence identical to those presented in IEEE std. 80.

Step 2) Determine the fault current division factor, S_F to calculate the symmetrical earth current. This factor determines the portion of zero sequence current that does not flow via the earthing system back to the neutral point but through other paths such as overhead earth wires, cable sheaths and buried metallic items such as pipes or other cables. To compute this factor the system must be analysed and an equivalent circuit generated with the impedances of each of the alternate current paths calculated. Kirchhoff's law is then applied to the system to determine the current split and the current division factor can be calculated by finding the proportion of total fault current that returns to the neutral point via the earth as in Equation 2.13. This process is unique to each situation and can be a laborious task with many different methods of determining the equivalent circuit available however DIN EN 50522 provides a set of typical reduction factors for several of the most common cases to simplify the process.

$$S_F = \frac{I_E}{3I_0} \tag{2.13}$$

Step 3) Calculate the decrement factor to account for the asymmetrical zero sequence current. Typically an earth fault current will be an asymmetrical current consisting of a sub-transient, transient and steady state AC components and a constant polarity DC offset. The sub-transient, transient AC components and the DC offset display exponential decay but for simplicity of analysis the decay of the AC components is ignored. As the allowable voltage limits calculated in Section 2.6 are based on symmetrical AC currents a decrement factor must be calculated to account for any asymmetry in the fault current. IEEE std. 80 derives Equation 2.14 to calculate this factor and a detailed derivation can be found in Appendix B.

$$D_F = \sqrt{1 + \frac{T_a}{t_f}(1 - e^{(-2t_f/T_a)})} \tag{2.14}$$

Where:
D_F is the decrement factor
T_a is the DC offset time constant $= X/\omega R$
t_f is the fault duration in s

To calculate the decrement factor the fault duration must be estimated, typically this is done by analysing the protection system and determining the fault clearing

time of the installed protection devices such as over current protection devices and calculating the resistance and reactance of the system at the fault location to find the DC offset time constant. Now using Equation 2.15 the maximum earth current, I_E can be calculated:

$$I_E = D_F.S_F(3I_0) \tag{2.15}$$

Where:
I_E is the earth current in A

Step 4) Select the largest value of maximum earth current to give the worst fault conditions. The above analysis must be conducted for each fault location and the maximum earth current calculated must be used for the design of the system. This step is required as there exist many variables effecting the maximum earth current and it is not possible to determine which fault location will give the maximum earth current before the analysis is made [1].

2.7.1 Resistance Earthed and Resonant Earthed Neutral Point Fault Comparison

When a fault occurs in a system with a resonant earthed neutral point the high reactance to resistance ratio of the system will cause a significant transient response upon fault initiation which decays with time until the steady state residual fault current is reached. However in a system with a resistance earthed neutral point the low reactance to resistance ratio of the system will lead to a small to negligible transient response and the steady state fault current is reached almost immediately. Figure 2.6 displays two fault currents from a resistance and resonant earthed neutral point systems initiating at 0.05 seconds and continuing to 0.1 seconds. The transient response of the resonant earthed fault current is clearly visible [31].

Due to the transient response of the resonant earthed system fault the RMS current for shorter fault durations is higher than the RMS current for longer fault durations. For this reason it is recommended that the EPRs are calculated for both the longest possible and shortest possible fault durations and both scenarios are compared to the allowable voltage limits to ensure that neither the initial transient response and the steady state residual fault currents cause dangerous EPRs. As the resistance earthed system does not produce large transient response this is not required for such systems [31].
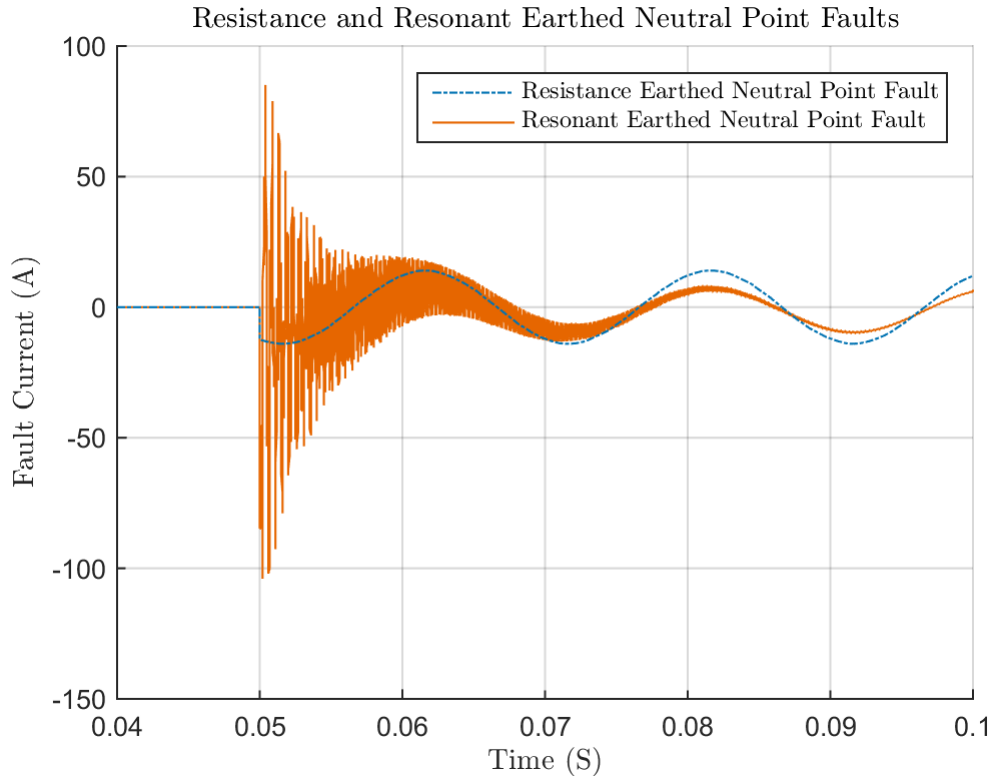
FIGURE 2.6: The fault waveforms arising with a resistance earthed
neutral point and a resonant earthed neutral point.

2.8   Earthing System Design

The design of the earthing system concerns dimensioning the components of the system
so the system impedance is low enough to ensure step and touch voltages remain
below the allowable limits. As well as this the components must be dimensioned and
materials chosen so that their current carrying capacity is not exceeded leading to
excessive heating and the mechanical strength and corrosion resistance is sufficient to
ensure safe operation of the system for the duration of the design life [16]. The critical
design parameters for this are the maximum earth current I_E, fault duration t_f, soil
resistivity ρ, soil surface resistivity ρ_s and the geometry and materials of the system
[1]. Section 2.7 details how maximum grid current is calculated and Section 2.5 details
how soil resistivity is measured which now leaves system material and geometry to be
determined.

Choice of conductor material is based on the electrical properties, corrosion re-
sistance and the cost of the material [1]. A conductor of sufficient conductivity is
required so large voltage differences do not occur in the earthing system, materials
such as copper, aluminium and steel are most often used. Table 2.2 makes a quali-
tative comparison of the properties of the most commonly used materials. It should
also be noted that no mechanical loads are expected to be imparted on the earthing
system and as such a mechanical load analysis is not required [1].

Earthing conductors must also be designed to resist thermal fusing caused by car-
rying high currents. The work done by Sverak [33] in 1981 provides the Equation 2.16
derived from first principle thermodynamic laws to calculate the maximum current
carrying capacity of a conductor based on material constants, ambient conditions and
current duration.

	Conductivity	**Corrosion Resistance**	**Cost**	**Other**
Copper	Highest	Highest	Highest	Forms galvanic cell in soil so is tin plated
Aluminium	Intermediate	Highest	Intermediate	Forms protective corrosion layer of high resistivity
Steel	Lowest	Lowest	Lowest	Requires protective zinc coating

TABLE 2.2: Qualitative comparison of earthing electrode material properties.

$$I_{max} = \frac{A}{10} \sqrt{\left(\frac{TCAP.10^{-4}}{t_f \alpha_r \rho_r}\right) \ln \left(\frac{K_0 + T_m}{K_0 + T_a}\right)} \tag{2.16}$$

Where:
I_{max} = Maximum allowable current in A
A = Conductor Cross-section Area in mm^2
$TCAP$ = Thermal Capacity per Unit Volume in J/(cm^3°C)
t_f = Current Duration in s
α_r = Thermal Coefficient of Resistivity at T_r in 1/°C
ρ_r = Resistivity of the Ground Conductor at T_r in $\mu\Omega$cm
K_0 = Reciprocal of Thermal Coefficient of Resistivity at 0°C in °C
T_m = Maximum Allowable Temperature of Conductor in °C
T_a = Ambient Temperature in °C
T_r = Reference Temperature for Material Constants in °C

The calculated maximum allowable current for given conductor material and dimensions must then be checked against the maximum calculated fault current to ensure thermal fusing is avoided. Alternatively Equation 2.16 can be rearranged to obtain conductor area as a function of current and a minimum conductor cross sectional area can be found. Tabulated data for the material constants used in Equation 2.16 can be found in various engineering handbooks or IEEE std. 80.

Table 2.3 presents that allowable current limits of the materials used to construct the earthing system for Enerparc AG solar plants.

Electrode Material	**Allowable Current Limit (kA)**
10 mm Diameter Galvanised Steel Cable	5.566
70 mm^2 Tinned Copper Cable	20.017
25 mm Diameter Galvanised Steel Rod	34.785

TABLE 2.3: Allowable current limits of the components used to construct a solar plant earthing system.

Once the material and the minimum cross sectional area of the electrodes have been determined the layout of the earthing system must be determined. Earthing electrodes can be split into two categories, auxiliary electrodes, whose primary purpose is

something other than providing an electrical connection to earth and primary earth electrodes whose primary purpose is to provide an electrical connection to earth [1]. Auxiliary earth electrodes can include building/structure foundations, metallic water pipes, etc. and are utilized to reduce earthing system impedance where available. Primary earthing electrodes are either installed vertically (driven rod) or horizontally. Generally a vertical electrode achieves lower impedance to earth as its current carrying capacity is not limited by the surface of the soil as experienced by a horizontal electrode and a vertical electrode can access deeper soil layers with often lower resistivity [34]. Furthermore a vertical rod is less effected by seasonal variations as these effects are mostly manifested in the upper layers of the soil [34] [24]. Horizontal electrodes allow larger areas to be utilized for grounding systems and the interconnection of various electrodes which reduces overall earthing impedance [35]. Typically with photovoltaic power plants the metallic structures used to support the photovoltaic modules are utilsed as auxiliary earth electrodes and they are interconnected with buried earth conductors. Furthermore grid connecting stations and transformer stations are constructed with a local earthing system consisting of a single or double horizontal ring electrode and two or more vertical rod electrodes. This local earthing system is then connected to the buried earth conductors connecting the auxiliary earth electrodes forming an electrically bonded plant earthing system [15] [4] an example of a solar plant earthing system can be seen in Appendix E. From this point an iterative design process is then conducted where the performance of the earthing system is evaluated and the design modified when the performance does not meet requirements until the required performance targets are achieved [1].

2.9   Earthing System Performance Evaluation

Following on from the design stage where the geometric parameters and the construction materials of the earthing system have been determined an analysis confirming the design meets required performance targets must be conducted. Methods for this include computer simulation, measurement of the earthing system impedance and analytical calculation of the earthing system impedance.

2.9.1   Computer Simulation

Today there exists two commercially available computer simulation programs for analyzing earthing systems, CYMGRD provided by EATON Corporation Plc and CDEGS provided by Safe Engineering Services and Technologies Inc. Computer simulation allows the analysis of complex system geometries and analysis in detail of maximum step and touch voltages [1] but with the disadvantage of high costs associated with the purchase of the software and training of personnel. CYMGRD uses the finite element method to calculate the earthing system impedance and the ESPR from which the maximum step and touch voltages can be found. A uniform or two-layer soil model is calculated from input data of soil resistivity taken from the field. The software also has other capabilities such as calculating worst case fault currents and calculating the optimal geometrical properties of electrodes based upon worst case fault currents and material properties. CYMGRD conforms to IEEE std. 80 [36]. CDEGS is a multipackage software tool that has capabilities to analyse soil structure and resistivities and the ESPR under various situations including power faults, lightning strikes and other transients. It utilizes a current distribution algorithm to calculate the potential, electric field and magnetic field at regular points in space and from this can calculate maximum step and touch voltages [37].

2.9.2   Earthing System Impedance Measurement

Field measurement of the earthing system impedance can be conducted after construction of the system to allow the design engineer to calculate expected EPR of the system as an alternative to using computer simulation or to verify calculations made prior to construction. In most cases measuring the earthing impedance is a simple and cost effective technique for obtaining an earthing resistance estimate but there are several sources of error that must be understood to correctly conduct the measurements and interpret the results [18].

The Fall of Potential (FOP) method is widely used for measuring the resistance of an earthing electrode. In the FOP method a known current is circulated between the electrode under test and a return probe inserted into the earth at some large yet finite distance, C, from the electrode. The circulating current causes a voltage rise of the earthing electrode in relation to remote earth and the ratio of this voltage to the circulated current is equal to the apparent resistance of the earthing electrode, R_E, app [38], it is the aim of the FOP method to find this value. To do this a series of measurements are made with a potential probe starting adjacent to the earthing electrode and stepping towards the return probe, the measured values are divided by the value of the circulated current and plotted against distance from the earthing electrode, P, to obtain an FOP curve, see Figure 2.7.

To read the resistance accurately from the FOP curve the location of the potential probe that gives the true value of earthing resistance can be calculated. To understand this lets consider two hemispherical electrodes of radius 0.5 m buried in homogeneous soil of resistivity 50 Ωm separated by 20 m and circulating a 1 A current. The earthing electrode and the return probe both produce an equal ESPR in line with Equation 2.4 as displayed in Figure 2.8.

Due to the nature of the FOP method the measured voltage is the difference in potential of the earthing electrode V_E and the potential electrode V_P. Now the potential of the earthing electrode is constant and is equal to the EPR of the earthing electrode, $V_{E,EPR}$, minus the ESPR at the earthing electrode caused by the return probe, $V_{R,ESPR@E}$. Also the potential of the potential electrode is the ESPR at the potential electrode caused by the earthing electrode $V_{E,ESPR@P}$ minus the ESPR at the potential electrode caused by the return probe $V_{R,ESPR@P}$ [40] as shown in Equation 2.17.

$$V_{FOP} = V_E - V_P = V_{E,EPR} - V_{R,ESPR@E} - V_{E,ESPR@P} + V_{R,ESPR@P} \qquad (2.17)$$

And using Equations 2.4 and 2.5 this becomes:

$$V_{FOP} = \frac{\rho I_E}{2\pi B} - \frac{\rho I_E}{2\pi}\left(\frac{1}{C}\right) - \frac{\rho I_E}{2\pi}\left(\frac{1}{P}\right) + \frac{\rho I_E}{2\pi}\left(\frac{1}{C-P}\right) \qquad (2.18)$$

$$V_{FOP} = \frac{\rho I_E}{2\pi B} + \frac{\rho I_E}{2\pi}\left(\frac{1}{C-P} - \frac{1}{C} - \frac{1}{P}\right) \qquad (2.19)$$

And the apparent earthing resistance is:

$$R_{E,app} = \frac{\rho}{2\pi B} + \frac{\rho}{2\pi}\left(\frac{1}{C-P} - \frac{1}{C} - \frac{1}{P}\right) \qquad (2.20)$$

Now the the true value of R_E is represented by the first term on the right hand side of Equation 2.20 so the location of the potential probe to give the true value of
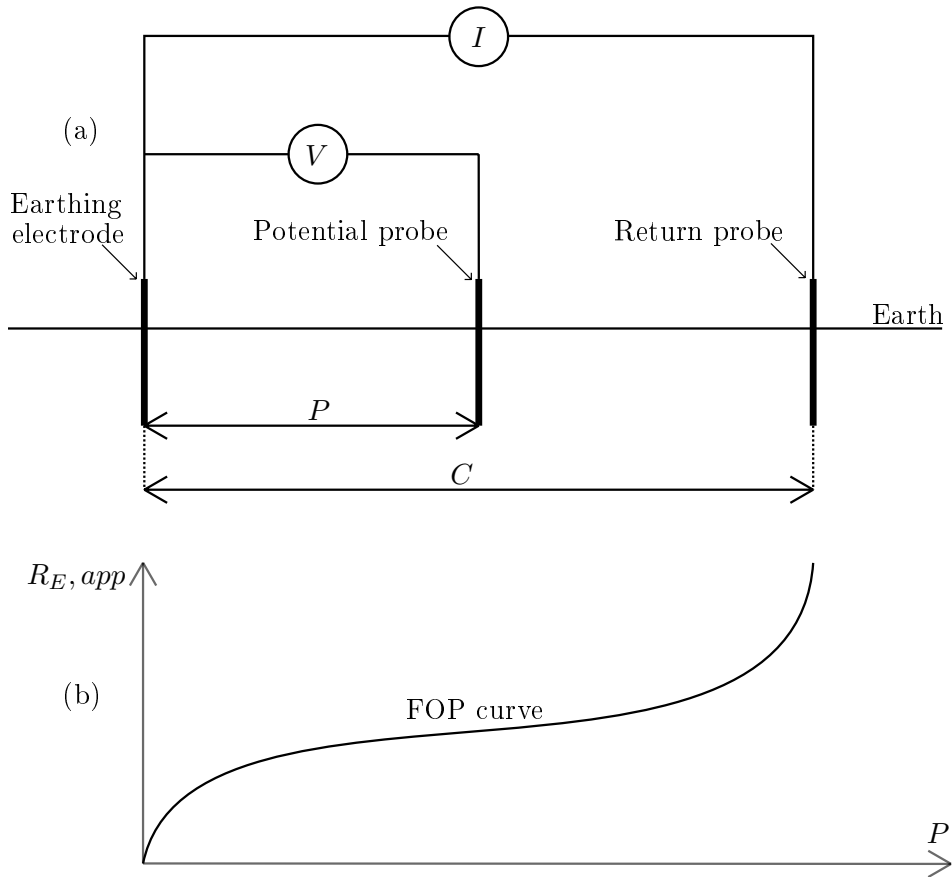
FIGURE 2.7: The fall of potential method showing electrode arrange-
ment and an FOP curve. In figure (a) three electrodes are shown with
a current source circulating a current between the earthing electrode
and the stationary return probe. A voltmeter measures the voltage
difference between the earthing electrode and the variable location
potential probe. Measurements are made increasing the distance P
and the ratio of the measured voltage to circulated current (apparent
earthing resistance) is plotted against P as shown in figure (b) [39].

R_E can be found by finding the roots of $\left(\frac{1}{C-P} - \frac{1}{C} - \frac{1}{P} \right)$ which has only one positive
root of $P = 0.618C$, known as the 0.618 rule [40]. This is displayed graphically in
Figure 2.8 which shows the ESPR caused by the earthing electrode and the return
probe, and the FOP curve with the 0.618 rule marked.

Finding the correct location for the potential probe using the 0.618 rule is a trivial
task for the ideal situation of a hemispherical earthing electrode buried in homoge-
neous soil but for the real situation where complex earthing electrode geometries are
buried in inhomogeneous soil this task requires a more practical approach.

For this the potential probe must be located beyond the limits of significant ESPR
caused by the earthing electrode and the current return probe. Theoretically the limits
of ESPR extend to infinity but practically there is a finite limit as the ESPR varies
inversely with distance from the electrode [18]. Provided that the current return probe
is located at a sufficiently large distance from the earthing electrode this condition
will exist at the midpoint of the line joining the two electrodes and in this vicinity
a plateauing or flattening of the FOP curve shall be observed [18] and the mid-point
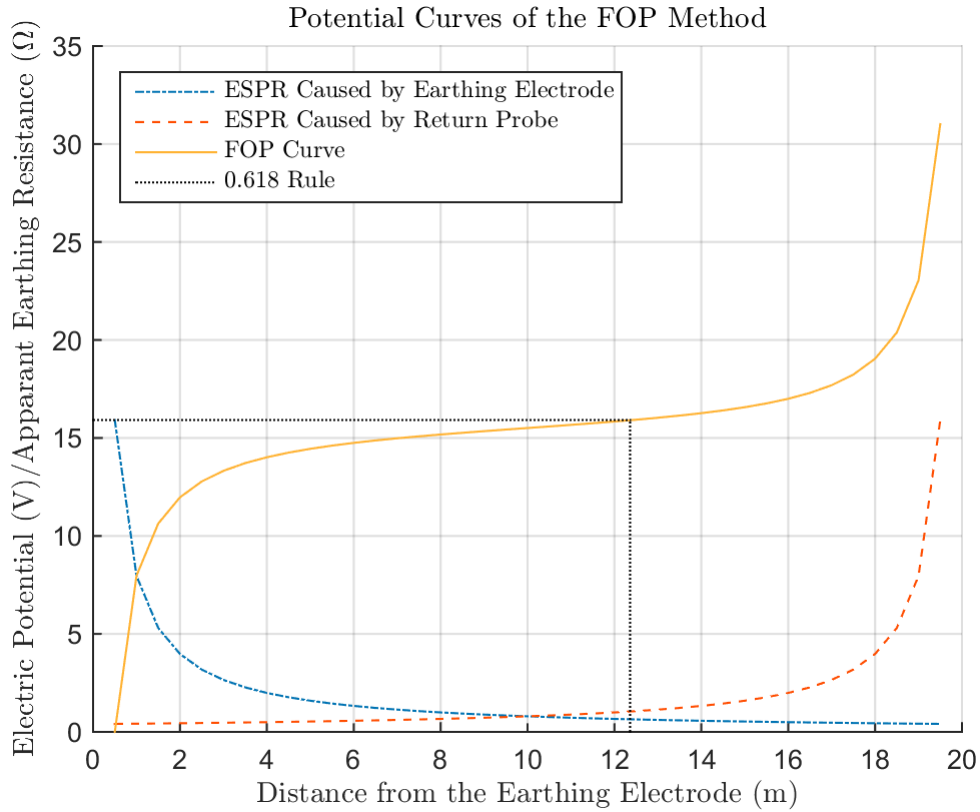
FIGURE 2.8: Analytically calculated FOP curve for the ideal case of a hemispherical earthing electrode of radius 0.5 m buried in homogeneous soil of resistivity 50 Ωm with an identical return probe buried at a 20 m distance from the earthing electrode with a 1 A current circulating between them. The ESPR caused by the earthing and return probes is shown and the resulting FOP curve is shown with the the 0.618 rule marked. Note that the 0.618 rule corresponds with the maximum ESPR of the earthing electrode.

location is read as the location of true R_E.

The work done by Tagg [40] discusses how to quantify any error in using the midpoint method. If Equation 2.20 is examined the error of the FOP method E_{FOP} can be quantified as in Equation 2.21.

$$E_{FOP} = \frac{\rho}{2\pi} \left(\frac{1}{C - P} - \frac{1}{C} - \frac{1}{P} \right) \tag{2.21}$$

And at the midpoint ie $P = C/2$ the error is:

$$E_{FOP,midpoint} = -\frac{\rho}{2\pi C} \tag{2.22}$$

Equation 2.22 shows that when measurements are being carried out using the midpoint method the largest possible electrode spacing should be used which is usually limited by the length of the current circulation cables being used.

Tagg also notes that measuring earthing resistance is far from an accurate science and in practical cases such errors are not analytically quantifiable yet with knowledge of the factors causing them and careful measurement they are tolerable.

Other sources of error associated with the FOP method include the formation of stray currents in the soil and inductive coupling between the voltage measurement and

current circulation cables [18]. Stray currents may form in the soil due to electrolysis and other chemical action or electricity supply leakage in the nearby area, to eliminate these effects an alternating test current of frequency higher than power frequency should be used [40], commercially available system impedance measuring devices such as the Geohm C from Gossen Metrawatt and the MRU 21 from Sonel use 128Hz and 125Hz respectively [41] [42]. To eliminate the effect of inductive coupling between the test cables efforts should be made during measurement to run the cables perpendicular to each other [18].

2.9.3   Analytical calculation of Earthing System Impedance

Another method for evaluating earthing system performance is to analytically calculate the earthing system impedance. IEEE std. 80 and DIN EN 50522 provide equations to calculate the earthing resistance of various earthing electrodes based upon their dimensions and the soil resistivity. The equation from IEEE std. 80 considers the length of the earthing conductor buried in the ground and the area covered by the earthing system as well as the burial depth of the conductor, no distinction is made between a conductor that is installed vertically or horizontally, see Equation 2.23.

$$R_E = \rho \left[\frac{1}{L} + \frac{1}{\sqrt{20A}} \left(1 + \frac{1}{1 + h\sqrt{20A}} \right) \right] \tag{2.23}$$

Where:
R_E = Earthing Resistance in Ω
ρ = Soil resistivity in Ωm
L = Length of conductor in m
A = Area enclosed by earthing system in m^2
h = Burial depth in m

DIN EN 50522 focusses on the contact area of the earthing conductor with the surrounding soil and provides three Equations 2.24, 2.25 and 2.26 for a horizontal strip electrode, a horizontal ring electrode and a vertical rod electrode respectively.

$$R_{E,strip} = \frac{\rho}{\pi L} \ln \left(\frac{2L}{d} \right) \tag{2.24}$$

$$R_{E,ring} = \frac{\rho}{\pi^2 D} \ln \left(\frac{2\pi D}{d} \right) \tag{2.25}$$

$$R_{E,rod} = \frac{\rho}{2\pi L} \ln \left(\frac{4L}{d} \right) \tag{2.26}$$

Where:
$R_E, strip$ = Earthing Resistance of a horizontal strip electrode in Ω
$R_E, ring$ = Earthing Resistance of a horizontal ring electrode in Ω
R_E, rod = Earthing Resistance of a vertical rod electrode in Ω
ρ = Soil resistivity in Ωm
L = Length of conductor in m
d = Diameter of the conductor in m
D = Diameter of the circle enclosed by the electrode in m

From these equations and knowledge of the topology of the earthing system the resistance of each component of the system can be calculated and a thevenin equivalent for total system resistance can be found.

2.9.4 Estimating Step and Touch Voltages

Once an estimate of the resistance to earth of the earthing system has been obtained either through measurement or calculation an estimate of the maximum touch and step voltages must be determined. To do this the EPR and the ESPR must be calculated. The EPR is simply the product of the maximum fault current flowing to earth and the total earthing resistance but finding the ESPR is far more complex. The computer simulation programs discussed utilize computational algorithms to produce a three dimensional plot of the ESPR and from this the maximum touch and step voltages are found [1]. However completing this task analytically becomes practically impossible and alternative methods must be used.

The method proposed by IEEE std. 80 first examines the EPR and compares it to the allowable limits of touch and step voltage. As EPR is inherently greater than touch and step voltage it can be concluded that if EPR falls under the allowable limits then the design is safe and no further analysis needs to be undertaken, however if this is not the case then an estimate for touch and step voltage must be found. Now as step voltage is inherently less dangerous than touch voltage we can simplify the analysis to focus on touch voltage [1] and IEEE std. 80 provides an Equation 2.27 for the calculation of the maximum touch voltage.

$$V_{touch} = \frac{\rho K_S K_i I_E}{L_S} \tag{2.27}$$

Where:
ρ = Soil resistivity in Ωm
K_S = Geometrical factor
K_i = Corrective factor
I_E = Maximum earth current in A
L_S = Effective buried conductor length in m

Expressions to calculate each of the factors and the effective buried conductor length in Equation 2.27 are provided for various system geometries in IEEE std. 80. Results of calculations made with this equation for various earthing systems were compared with the results obtained from computer simulation and an acceptable accuracy of the analytical calculations was demonstrated [1]. Unfortunately the expressions for K_S, K_i and L_S are only presented for simple and regular system geometries, such as those occurring in fossil fuel fired power plants, and as such are not applicable to the complex system geometries existing in solar plants.

DIN EN 50522 does not provide any guidance as to calculating the step or touch voltage but it does however detail a method for measuring touch voltage. The method involves injecting the maximum earth fault current into the system and using two specialised electrodes, one simulating the feet and one the hand which are connected to a voltmeter. The foot electrode must be a minimum of 400 cm^2 and be resting on the ground with a minimum force of 500 N and be placed 1 m from the measured structure, no specifications are provided for the hand electrode. The voltage measured between the two electrodes is taken as being the touch voltage for that location.

Once a touch voltage figure has been obtained it must be compared to the allowable value. If it is below then it can be concluded that the design is safe but if it is higher

than the allowable limit design modifications must be made. Possible solutions for this include extending the amount of eathing conductor in the ground by adding vertical rods to the earthing system or by extending the horizontal conductors which will decrease the total resistance of the earthing system [1]. Also a layer of highly resistive material (eg gravel) can be spread on the surface of the ground to increase the contact resistance of a person's feet to the earth which in turn increases the allowable limits for step and touch voltage [1].

2.10   Global Earthing System

The concept of the Global Garthing Gystem (GES) was introduced by HD 637 S1: Power installations exceeding 1kV ac (the precursor to DIN EN 50522) in 1998 and provides the designer with potential benefits as the identification and classification of an earthing system as a GES removes the requirements of field measurements of soil characteristics and performance levels of the system [43]. A GES is defined as "an equivalent grounding system created by interconnecting local grounding systems and ensuring, by the proximity of the ground electrodes, that there are no dangerous touch and step voltages. Such systems permit the division of the ground fault current in a way that results in a reduction of the ground potential rise at the fault location. Such a system could be said to form a quasi-equipotential surface" [6].

Methods for the verification of a GES are still subject to ongoing research with various proposed methods not yet being approved for usage by any national or international standards organisation [43]. The reason being is that it is simple to identify a specific system as being a GES but defining a set of guidelines to be used for the general case and being valid for all possible situations is difficult [44]. The Campoccia method proposes the use of simplified circuit models to evaluate the behavior of the earthing system under various fault situations [45]. The earthing resistance of each component of the system is estimated from known techniques and using knowledge of the topology of the system a circuit can be developed modelling the system [45]. The modelled circuit can then be analysed with standard techniques to verify the requirements of a GES are met [45]. It is the intention of the author of this thesis to utilize this method to evaluate the performance of earthing systems from large grid connected photovoltaic plants and develop a general model for such cases.

3 Materials and Methods

3.1 Modelling Software

The software chosen to model the photovoltaic (PV) plants and earthing systems is the free circuit simulation package from Linear Technologies LTspice. LTspice utilizes the SPICE (Simulation Program with Integrated Circuit Emphasis) simulation program developed at the University of California Berkeley and incorporates schematic capture and waveform viewer features [46]. SPICE was first launched in 1973 in Canada and was made publicly available, today it is extensively used for circuit analysis and development worldwide. The original development of SPICE focused on the robustness of the programming and as such the user interface was unsophisticated so various commercial enterprises developed it into more user friendly versions, as is the case with LTspice [47]. LTspice takes a set of user defined model parameters in the form of a netlist where the circuit elements and nodes are described in text and develops a set of differential equations to solve for the circuit parameters. LTspice is capable of solving circuits consisting of resistors, inductors, mutual inductors, capacitors, independent current and voltage sources and various semi-conductors [48]. Due to its simplicity of use and its technical capabilities LTspice will be used for the evaluation of the circuit models representing the earthing system and solar plant in this thesis.

3.2 Modelling of the Earthing System

To model the earthing system the sub-circuit capability of LTspice was utilized where a circuit with user defined parameters can be developed and saved in a component library as a discrete component for use in other circuits. Two libraries of components were developed for this study, one conforming to IEEE std. 80 and one to DIN EN 50522.

The earthing system for large scale grid connected solar PV plants typically consists of local earthing systems at each of the transformer/transfer stations consisting of either a single, 70mm^2 copper cable, or double, one 70mm^2 copper cable and one 10mm diameter galvanised steel cable, horizontal earthing loop with two 25mm diameter galvanised steel 1.5 m earthing rods connected to the loops at opposite corners making a total of two/four rods. Also the metallic structures constructed to support the photovoltaic modules act as auxiliary earthing electrodes and are interconnected via a 10mm diameter galvanised steel horizontal earthing conductor buried at 0.5 m which also connects all transformer/transfer stations in the plant. In LTspice three separate components were developed to simulate the earthing system, one each for a transformer/transfer station with a single ring or double ring and one for the horizontal interconnecting earthing conductor. For simplicity in modelling the metallic structures supporting the photovoltaic modules were ignored, note that this is also a conservative assumption. The IEEE component library applies Equation 2.23 and the developed components require input for the soil resistivity and dimensions of the

physical electrode. The DIN library uses Equations 2.24, 2.25 and 2.26 and the developed components require input for the soil resistivity and dimensions of the physical electrode.

To model an earthing system it is a simple task of selecting which library to use then using the earthing layout drawing of the plant to select the types and numbers of the components and wire them together. The layout drawing for each component is then consulted to find the required dimensions and input them into the model. Also the soil resistivity, obtained either through field measurement or estimation from published data must be set and the model is ready for analysis.

3.3   Modelling of the Solar Plant

As well as modelling the earthing system the solar plant was also modelled to allow analysis of the earthing system behaviour under different solar plant configurations. For this a solar plant component library was developed consisting of a solar inverter component, a transformer component, a medium voltage cables component and a grid equivalent component.

3.3.1   Solar Inverters

Solar inverters act as a current source and so modelling them is a simple task of setting three AC current sources at a 120° phase shift from each other. The output current and operating frequency are required inputs.

3.3.2   Transformer

Modelling of the transformers was done using the Steinmetz equivalent circuit diagram shown in Figure 3.1 and the load losses and no-load losses test results published by the manufacturer of the transformer. The transformers used in the solar plants under study operate with a 400 V wye configuration secondary side, with an earthed neutral point, and a 20 kV delta configuration primary side, this is abbreviated as a Dyn transformer.

To determine the values of the components of the equivalent circuit of the transformer two additional equivalent circuits are developed representing the cases of the load losses and no-load losses test.

The no-load losses test is conducted with the primary side of the transformer open-circuited and the secondary side excited at the transformer rated voltage V_{oc} and frequency f. A current will circulate, known as the no-load current I_{oc}, which is due to the no-load losses, primarily the core or ferritic losses caused by ferromagnetic hysteresis and eddy currents [50]. Under this scenario it can be assumed that the stray inductance L_{stray2} and the copper resistance R_{cu2} of the equivalent circuit are small in comparison to the secondary winding inductance L_2 and the ferritic resistance R_{fe} and the equivalent circuit diagram shown in Figure 3.2 can be drawn [49].

Now using the published no-load current I_{oc} and power P_{oc} the unknown values in Figure 3.2 can be determined using Equations 3.1 and 3.2.

$$R_{fe} = \frac{V_{oc}^2}{P_{oc}/3} \tag{3.1}$$
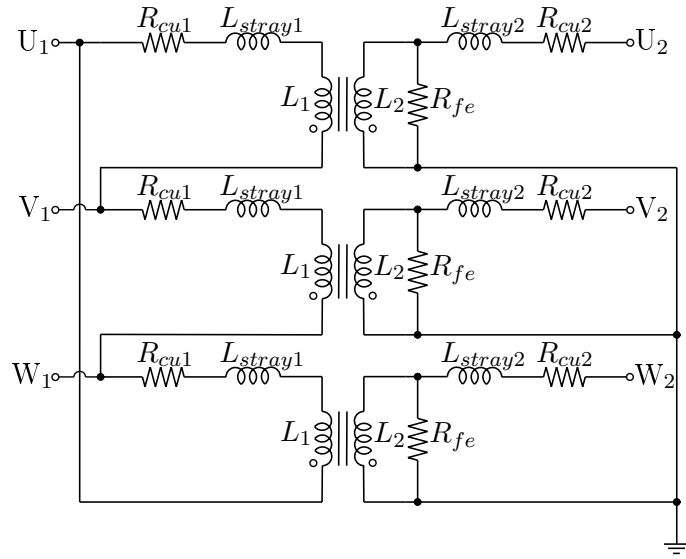
FIGURE 3.1: Steinmetz equivalent circuit diagram used to model a real transformer [49]. An ideal transformer is modelled with two perfectly coupled inductors (L_1 and L_2) per phase. A resistor (R_{cu}) and inductor (L_{stray}) in series on both the primary and secondary side are modelled to account for the copper resistance and the stray losses of the transformer and a resistor in parallel (R_{fe} on the secondary side is used to model the iron losses of the transformer.
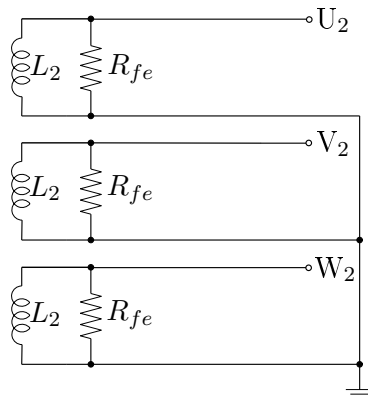
FIGURE 3.2: Transformer equivalent circuit diagram under the no-load losses test conditions [49].

$$L_2 = \frac{V_{oc}/I_{L2}}{2\pi f} \tag{3.2}$$

Where:

$$I_{L2} = \sqrt{I_{oc}^2 - \left(\frac{V_{oc}}{R_{fe}}\right)^2} \tag{3.3}$$

Also with knowledge of the rated transformer ratio a the primary winding inductance L_1 can be determined using Equation 3.4.

$$L_1 = a^2 L_2 \tag{3.4}$$

The load losses test is conducted on the transformer with the secondary side short-circuited and a voltage V_{sc} applied to the primary side in order to excite the transformer rated primary side current I_{sc} [50]. The power drawn under these conditions P_{sc} equals the load losses caused by stray flux and copper resistance on both sides of the transformer [49]. Also the winding inductances and the ferritic resistance can be assumed to be small in comparison to the losses, hence the equivalent circuit diagram show in Figure 3.3 can be drawn [49].
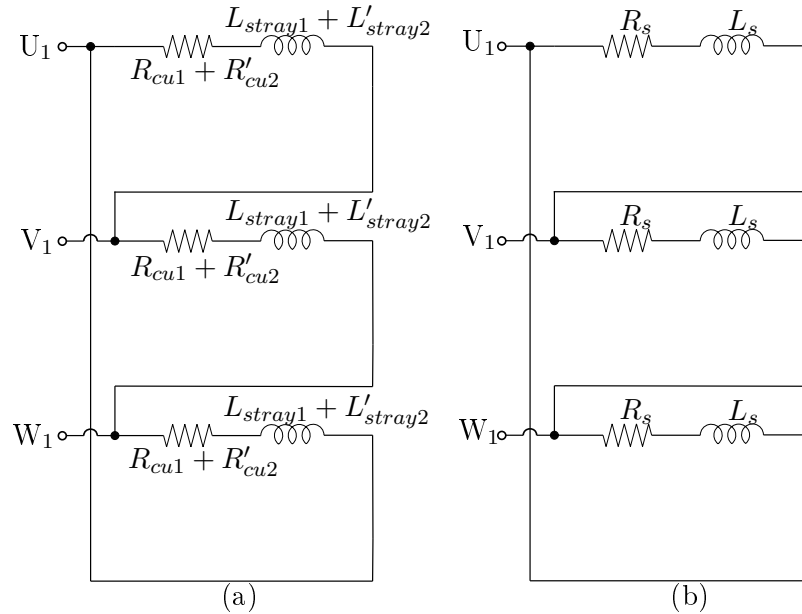
FIGURE 3.3: Transformer equivalent circuit diagram under load losses test conditions [49], figure (a) and (b) are identical except that the symbols for the circuit components are simplified in figure (b).

Using the results from the load losses test the unknown values in Figure 3.3 (b) can be determined using Equations 3.5 and 3.6 and the unknown values in Figure 3.3 (a) can be determined using Equations 3.7 and 3.8 and the remaining unknown values from Figure 3.1 can be determined with Equations 3.9 and 3.10.

$$R_s = \frac{P_{sc}}{3I_{sc}^2} \tag{3.5}$$

$$L_s = \frac{\sqrt{V_{sc}^2 - (I_{sc}R_s)^2}}{2\pi f I_{sc}} \tag{3.6}$$

$$L_{stray1} = L'_{stray2} = \frac{L_s}{2} \tag{3.7}$$

$$R_{cu1} = R'_{cu2} = \frac{R_s}{2} \tag{3.8}$$

$$L_{stray2} = \frac{L'_{stray2}}{a^2} \tag{3.9}$$

$$R_{cu2} = \frac{R'_{cu2}}{a^2} \tag{3.10}$$

The sub-circuit capability of LTspice was once again used to model the transformer using the equivalent circuit from Figure 3.1 and programming the equations for all of the unknowns. The values of operating frequency, no-load losses current, voltage and power, load losses voltage, current and power and transformer ratio are required inputs.

3.3.3 MV Cables

The next component to be modelled in a solar PV plant are the three phase medium voltage cables connecting the medium voltage side of the transformer station with the grid connection station. For this a six wire model was used whereby three wires represent each of the three conductors and the other three wires represent the copper sheaths of each conductor. The three conductors are connected to each of the three phases at the medium voltage side of the transformer station and also to the grid connection point and the three copper sheaths are wired to the solar plant earthing system at the transformer end and to the grid connection station earthing system at the grid end.

For the purposes of the following analysis the following notation shall be used, Z_s and Z_m refer to self and mutual impedance per unit length of wire, L_s and L_m refer to self and mutual inductance per unit length of wire, subscripts cu, cv and cw refer to the conductors of phases U, V and W, subscripts su, sv and sw refer to the sheaths of phases U, V and W respectively. For example $Z_{m,cv:sw}$ refers to the mutual impedance per unit length of the sheath from phase W on the conductor from phase V.

To model the cables each wire requires 7 individual components, 1 resistor for the total resistance of the wire, 1 inductor for the self inductance of the wire and 5 inductors for the mutual inductance of the wire with each of the other 5 wires in the system. The equivalent circuit diagram developed for this is shown in Figure 3.4.

To calculate the impedances Carson's theory of earth fault return path through the earth [51] was used. This method is based upon an overhead conductor, producing an electric field in the surrounding atmosphere and earth with a fictitious buried "image" conductor returning the current. Carson develops an analytical expression for the self and mutual impedances of the circuit in terms of two infinite integrals which can be solved for the Equations 3.11 and 3.12, see Appendix C for a detailed explanation of this derivation.
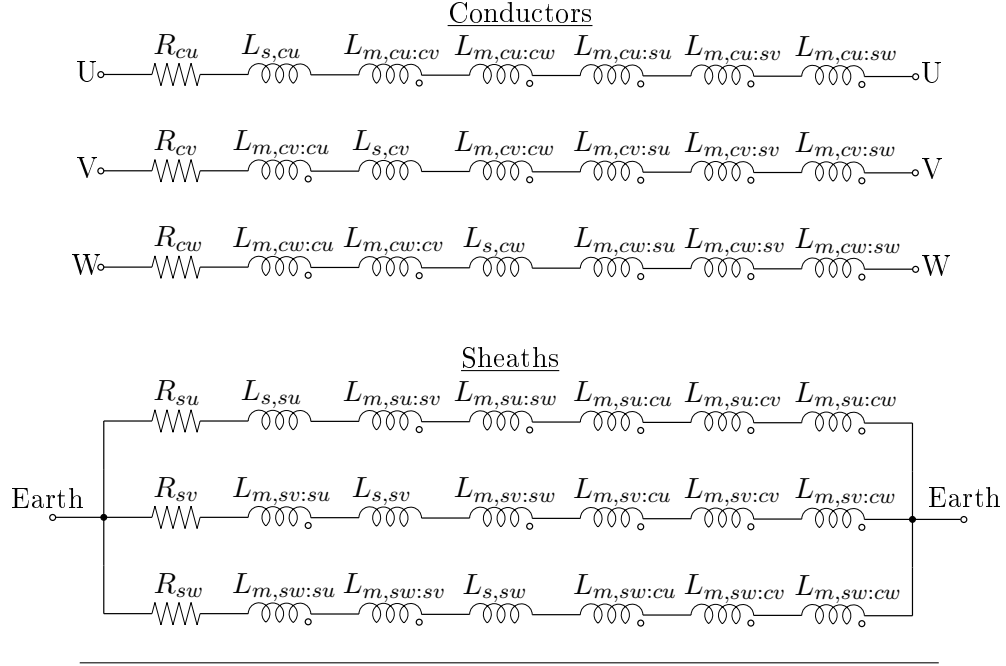
FIGURE 3.4: MV cables equivalent circuit diagram showing the internal resistance, self inductance and five mutual inductances per wire. The top three wires represent the three phase conductors and the bottom three wires represent the sheath of each phase conductor.

$$Z_{s,i} = R_i + \frac{\omega\mu_0}{8} + j\frac{\omega\mu_0}{2\pi}\ln\left(\frac{658}{r_i}\sqrt{\frac{\rho}{f}}\right) \tag{3.11}$$

$$Z_{m,i:k} = \frac{\omega\mu_0}{8} + j\frac{\omega\mu_0}{2\pi}\ln\left(\frac{658}{D_{ik}}\sqrt{\frac{\rho}{f}}\right) \tag{3.12}$$

Where:
R_i is resistance of wire i per unit length in Ω/m
ω is angular frequency of AC current in radians/s
μ_0 is vacuum permeability in H/m
r_i is the outer radius of wire i in m
ρ is soil resistivity in Ωm
f is frequency of AC current in Hz
D_{ik} is the distance between the centres of wires i and k in m (for concentric wires the outer radius of the larger wire is used)

It must be noted that these equations have been developed on the assumption of a homogeneous soil resistivity and for an overhead conductor. Carson however published a subsequent paper showing that when the equations developed for the overhead conductor are applied to a buried conductor close to the surface of the earth (≤ 1 m depth) the resultant error is negligible [52].

For the solar PV plants under study the medium voltage cables are laid in the trefoil formation leading to two configurations of self impedance 1) self impedance of a conductor and 2) self impedance of a sheath and four different configurations of mutual impedance 1) between a conductor and an adjacent conductor 2) between a sheath and an adjacent sheath 3) between a conductor and its corresponding sheath and 4) between a conductor and an adjacent sheath.

An LTspice sub-circuit was developed with the equivalent circuit diagram from Figure 3.4 incorporating Equations 3.11 and 3.12 covering each of the configurations of self and mutual impedance. The real parts of each impedance were lumped into one resistor for each wire and the inductors representing each of the mutual inductances were mutually coupled. The coupling coefficient for each pair of coupled inductors was programmed into the LTspice model using Equation 3.13.

$$K_{ik} = \frac{L_{m,i:k}}{\sqrt{L_{s,i}L_{s,k}}} \tag{3.13}$$

3.3.4 Grid Connection

Finally a model to simulate the grid was developed. From the point of view of the grid connection point of the solar plant the grid behaves as a constant voltage source with an internal impedance. Hence the grid is modelled as three constant voltage sources set with a 120° phase shift from each other with a resistor and inductor in series as seen in Figure 3.5.
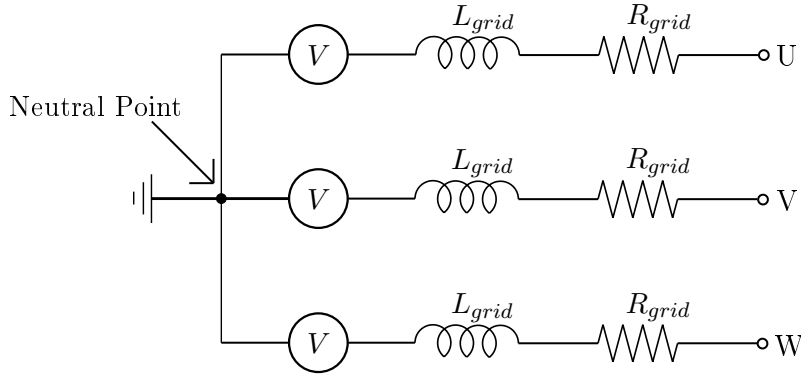
FIGURE 3.5: Grid connection point equivalent circuit diagram showing a three phase constant voltage source with internal impedance.

The nominal operating voltage V_n and frequency f are required inputs, a trivial task simply the set values by the grid operator. A less trivial task however is the determination of the grid internal resistance R_{grid} and inductance L_{grid}, these are calculated from the short circuit power S_{sc} and phase angle ϕ at the grid connection point provided by the grid operator as per Equations 3.14 and 3.15.

$$R_{grid} = Z_{grid}\cos(\phi) \tag{3.14}$$

$$L_{grid} = \frac{Z_{grid}\sin(\phi)}{2\pi f} \tag{3.15}$$

Where:

$$Z_{grid} = \frac{V_n^2}{S_{sc}} \tag{3.16}$$

Once again a sub-circuit component for the grid was developed in LTspice with required input for short circuit power, phase angle, nominal voltage and frequency.

3.3.5   Complete Plant

To model an entire solar plant it is a simple matter of examining the single line diagram of the plant and selecting and dropping the required components into an LTspice circuit and wiring them up. The datasheets for each component are then used to input the required data. To analyse the interaction between the solar plant and the earthing system it is a simple matter of copying the earthing system circuit into the soar plant circuit and connecting the earthing system to the neutral points of the transformers, a simple example of a two transformer solar plant is shown in Figure 3.6.
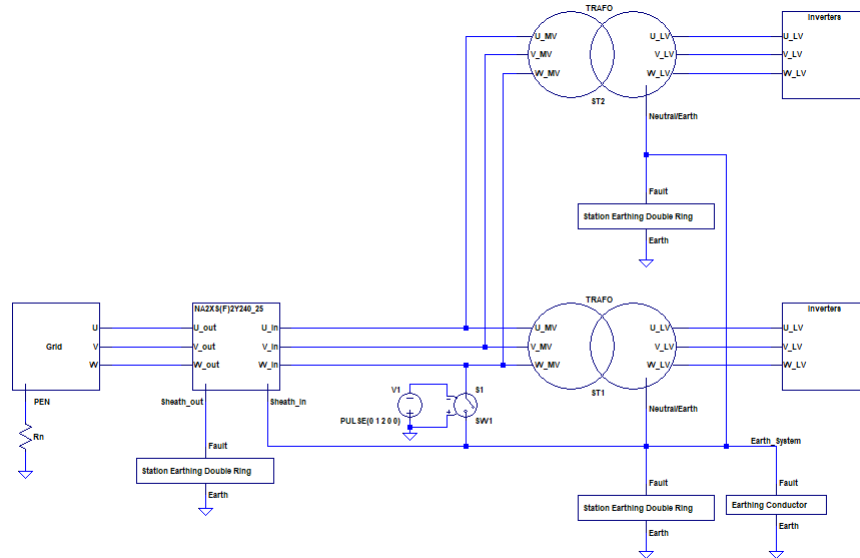
FIGURE 3.6: Two transformer solar plant model circuit showing the plant components for inverters feeding into two transformers. The transformers are connected to the grid connection point by the MV cables component. The earthing system is formed with three double ring station earthing components and a horizontal earthing conductor component. Lastly a voltage controlled switch (S1) is used to simulate a single phase to ground fault and the neural point is resistance earthed via resistor Rn.

3.4   Soil Resistivity Values

The accuracy of the model developed for the earthing system relies heavily on the accuracy of the soil resistivity measurement as the earthing resistance equations provided by both IEEE std. 80 and DIN EN 50522 are directly proportional to soil resistivity. As such the soil resistivity for each analysed solar plant must be measured using the Wenner method as described in section 2.5. A soil resistivity measurement protocol was produced to document the results, see Appendix D. Measurements are made with probe spacing starting at 3 m and stepping in 1 m increments up to a maximum of 15 m (maximum spacing distance is limited by cable length of the utilised measurement device the Gossen Metrawatt Geohm C battery powered earth tester). The measurement protocol also calls for the documentation of several other variables such as weather conditions and soil moisture content to ensure the measurements aren't being taken at a time of abnormally high soil moisture content (i.e. following

rainfall) leading to anomalous results. The highest reading of apparent soil resistivity from the protocol shall be used in the earthing system model in the interests of conservative results.

3.5 Verifying the Model

To verify the accuracy of the LTspice model the existing solar PV plant Drochtersen Stade, owned and operated by Enerparc AG, was studied. The site was visited and soil resistivity and earthing impedance measurements were taken immediately after one another to ensure the measured soil resistivity was valid when earthing impedance measurements were taken. The Wenner Method was used to measure the soil resistivity and the FOP method was used to measure the earthing impedance. The results were compared to the results delivered from the model when using the measured soil resistivity value.

The PV plant Drochtersen Stade is located in northern Germany (coordinates 53°40'48.2"N 9°27'47.4"E) close to the Elbe River on the river marshes. The plant has an installed peak power of 6,720 kW produced by 29,260 solar modules feeding current through 112 Sungrow 60 KTL solar inverters and 5 transformer stations, see Appendix E for a layout of the site and the transformer stations local earthing systems. Due to its close proximity to the river the soil is described as being fine silt sediment and a high moisture level of the soil is maintained due to the very shallow water table at approximately 0.5 m below mean soil surface level [53]. Due to the fine silt sedimentary soil with high moisture content a very low soil resistivity is expected, Figure 3.7 shows the results of the soil resistivity measurement.
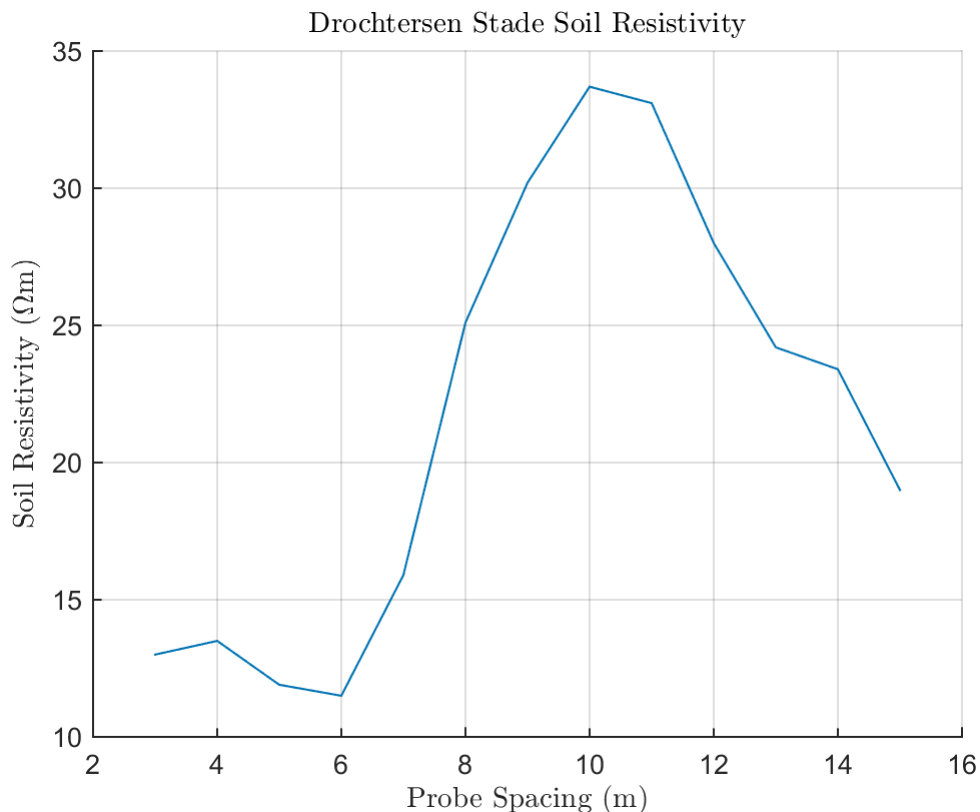
FIGURE 3.7: The soil resistivity profile at PV plant Drochtersen Stade produced by the Wenner Method.

As can be seen the soil resistivity is very low with a maximum value of 33.7 Ωm
and a minimum value of 11.5 Ωm, also it must be noted that the soil resistivity dis-
plays no obvious relationship to probe spacing (i.e. measurement depth) and a greatly
varying soil resistivity to probe spacing is observed. As discussed in section 3.4 for a
conservative estimate a homogeneous soil model is used for the LTspice model with
the soil resistivity set as the highest measured value, 33.7 Ωm.

3.5.1   Accuracy of the LTspice Model Earthing Impedance

After the soil resistivity measurement was made six separate earthing impedance
measurements were conducted with the aim to verify the earthing impedance values
given by the components developed for the LTspice model. Measurements were made
at two transformer stations (stations 1 and 4). At each station a measurement on the
station local earthing system (LES), the horizontal earthing conductor (HEC) and the
LES in parallel with the HEC were made. Note that the HEC is the buried horizontal
earthing electrode connecting all earthing components in the plant together.

The FOP curves for the three measurements at each transformer station are pre-
sented in Figures 3.8 and 3.9.

Fall of Potential Curves of Transformer Station 1 at Drochtersen Stade
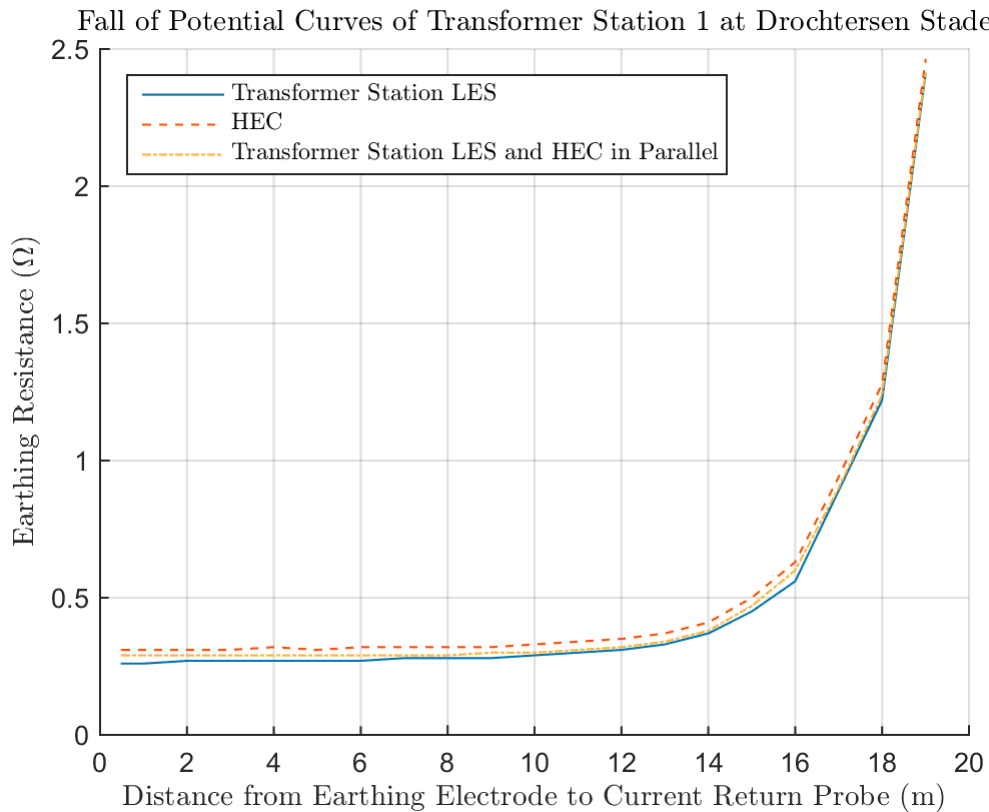
FIGURE 3.8: FOP curves measured at Drochtersen Stade transformer
station 1 showing the FOP curves for the transformer station LES, the
HEC and the LES and HEC in parallel.

Examining the curves in Figures 3.8 and 3.9 it is observed that the three curves
produced at each transformer station are extremely similar, this suggests that due
to the very low soil resistivity the LES and the HEC have become effectively electri-
cally connected via the soil hence when they are measured as separate systems the
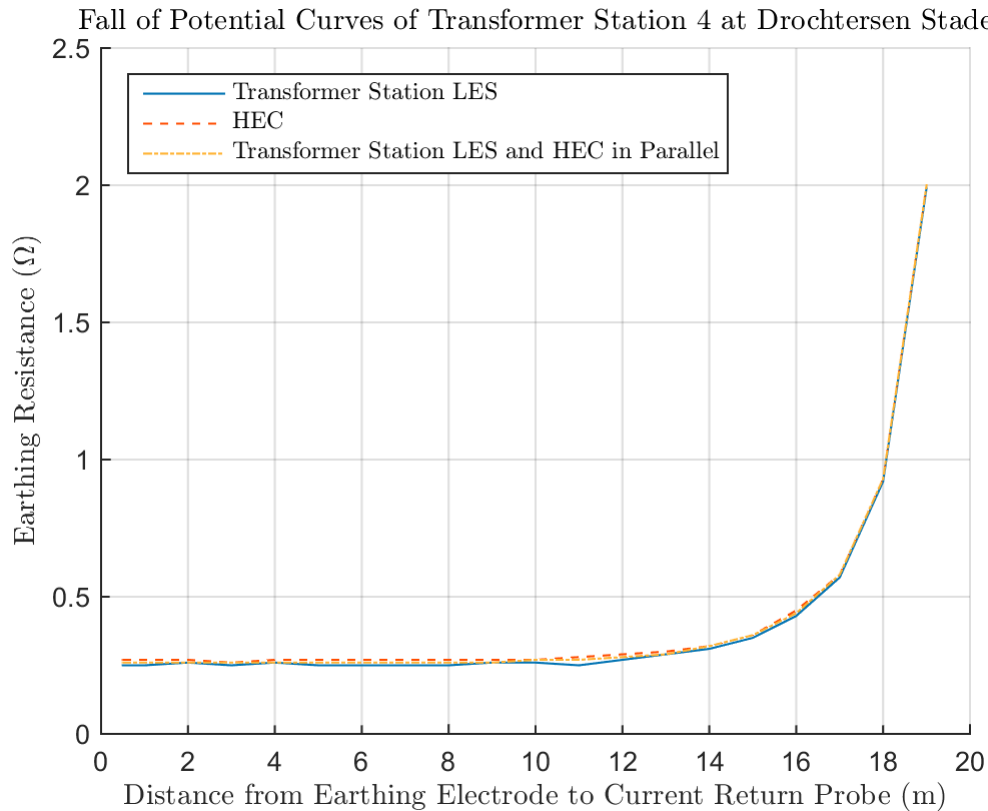
FIGURE 3.9: FOP curves measured at Drochtersen Stade transformer
station 4 showing the FOP curves for the transformer station LES, the
HEC and the LES and HEC in parallel.

returned figures are very similar to those obtained when they are measured connected
in parallel. Also it should be noted that measuring the HEC at different transformers
is actually measuring the same electrode from different locations, this is also the case
when measuring with the transformer station LEC and HEC in parallel as the HEC
connects all transformer LESs in the plant.

Also it is observed that all six FOP curves do not display the concave section
at small earthing electrode to current return probe distances that are typical of FOP
curves. The low soil resistivity can also explain this as the ESPR produced by earthing
electrodes in low resistivity soil decreases rapidly with distance from the earthing
electrode and in this case the ESPR produced by the earthing electrodes appears to
have decreased to a negligible amount at 0.5 m from the electrodes.

To read the earthing impedance from each FOP curve the mid-point technique was
used. The 0.618 rule was not used as the assumptions of the 0.618 rule do not apply
in this case. The earthing impedance values of the six measurements are displayed in
table 3.1 along with the values of earthing impedance given by the LTspice model for
the corresponding components.

Examining the values for the transformer station LES earthing impedance it is
obvious that the model returns values far higher than the measured values. The
reason for this is due to the low soil resistivity causing the LES to be electrically
connected via the soil to the HEC meaning that the measured values for the LES do
not reflect the true value of the LES earthing impedance as a stand alone component.

Examining the values for the HEC earthing impedance and the transformer sta-
tion LES and HEC in parallel earthing impedance it is noted that the model (for both

	LES R_E	**HEC R_E**	**LES and HEC R_E**
Transformer Station 1	0.29 Ω	0.33 Ω	0.30 Ω
Transformer Station 4	0.26 Ω	0.27 Ω	0.27 Ω
LTspice DIN EN 50522	2.25 Ω	0.16 Ω	0.12 Ω
LTspice IEEE std. 80	2.18 Ω	0.22 Ω	0.14 Ω

TABLE 3.1: Comparison of the measured earthing impedance values of the transformer station LES, the HEC and the transformer station LES and HEC in parallel at Drochtersen Stade transformer stations 1 and 4 with the values produced by the LTspice model conforming to standards DIN EN 50522 and IEEE std. 80.

DIN EN 50522 and IEEE std. 80) return values significantly lower than the measured values. To explain this an investigation into the errors and assumptions associated with the measurement technique and the LTspice model must be made.

First we know that reading the earthing resistance from the FOP curve using the mid-point technique delivers values lower than the true value but we are unable to quantify the magnitude of this error for the case of Drochtersen Stade as the soil is not homogeneous and the earthing electrode and current return probe have different geometries. We can however conclude that the error is negligible by examining the FOP curves. It is noted that an extensive horizontal section exists on each of the six curves in Figures 3.8 and 3.9 which indicates that the area of appreciable ESPR caused by the earthing electrode is not effecting the measurements and the true earthing impedance can be read from the FOP curve anywhere along the horizontal section of the curve.

Another source of error to consider is the homogeneous soil assumption used in the LTspice model. As stated previously the maximum measured value of soil resistivity is used in the LTspice model which is a conservative assumption leading to erroneously high earthing impedance values being returned. Unfortunately it is analytically impossible to quantify the magnitude of the error stemming from this assumption however work done by Nahman and Paunovic [54] have compared the results given by computer simulation utilising the finite element method with the analytical expressions given by IEEE std. 80 and DIN EN 50522. The comparison was done for 13 geometrically different earthing electrodes and it was shown for the IEEE std. 80 expression the values ranged from 108% to 123% and for the DIN EN 50522 expressions the values ranged from 108% to 130% of the values returned by the computer simulation. An error of this magnitude is significant but it errs on the side of safety and so is acceptable.

Finally a major source of error is the time of measurement being conducted within a few days of construction of the earthing system being constructed. IEEE std. 81 notes that after installation of an earthing electrode " the settling of the earth with annual cyclical weather changes tends to reduce the ground impedance substantially during the first year or two" [18]. As the earthing impedance measurements were conducted with freshly disturbed earth surrounding the earthing electrodes a poor connection between the electrodes and the soil is expected leading to erroneously high readings being taken. Once again it is not possible to analytically quantify this error but the measurements could be repeated after one to two years of operation of the earthing system to gain further insight. Due to time constraints of this study it was not possible to undertake this further set of measurements.

In summary the numerical discrepancy in the results produced by the LTspice

model and the measured values is acceptable. The observed discrepancy is due to the poor soil contact achieved by the newly installed earthing electrodes and the measured values are expected to decrease over time. Furthermore the other sources of error contribute to conservative results, something extremely important in the design of critical safety equipment such as an earthing system.

3.5.2   Auxiliary Earthing Electrodes

One further assumption made in the development of the LTspice model requires discussion. The metallic structures supporting the PV modules of a solar plant (herein referred to as the module tables) act as axillary earthing electrodes and their contribution to the earthing system has been ignored by the LTspice model. This assumption was made in the interests of simplicity of the model as the module tables display complex geometry which varies from solar plant to solar plant, also this is a conservative assumption. To check the validity of this assumption the earthing impedance of two module tables was measured at Drochtersen Stade during the same visit the earthing impedance of the other components was measured. The FOP curves of the two measured tables are shown in Figure 3.10.
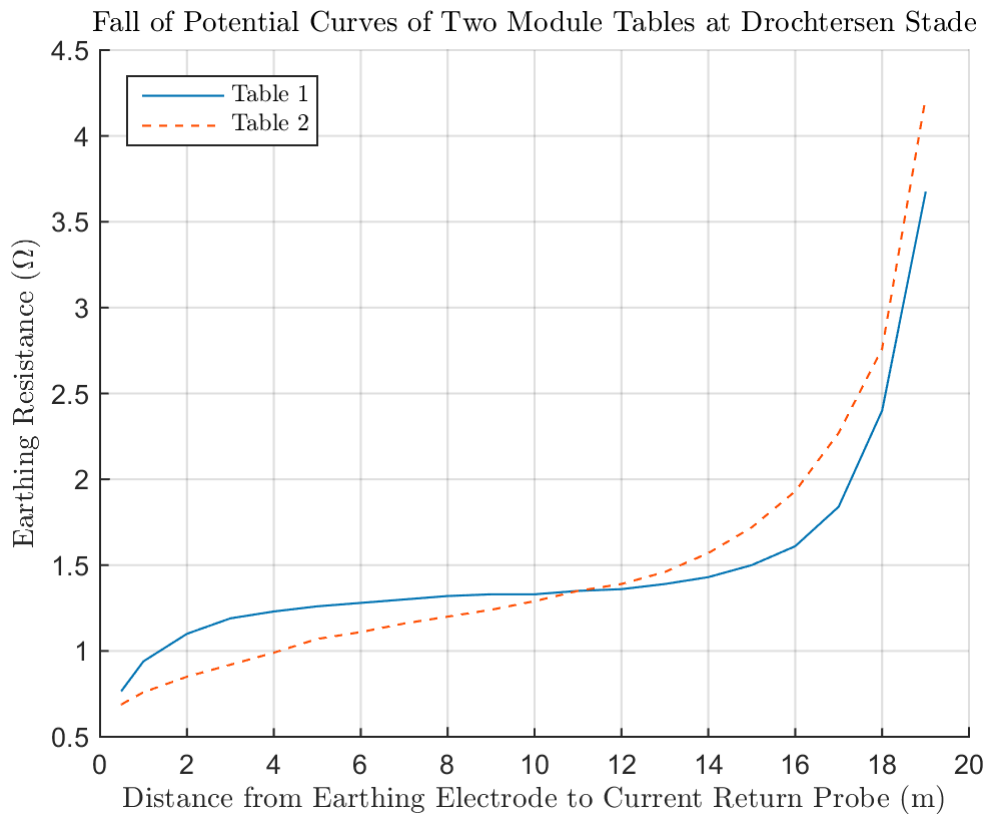
FIGURE 3.10:   FOP curves for 2 module tables measured at Drochtersen Stade.

As can be seen from the curves the concave section of increasing earthing impedance is clearly seen for small earthing electrode to current return probe distances, something not seen on the FOP curves for the other components, suggesting that the area of ESPR produced by the tables is much larger. Also using the mid-point method to find the earthing impedance values gives 1.33 and 1.29 Ω, values far higher than the

other components investigated. From these two results and noting that the assumption is conservative it can be argued that the assumption is valid, although this is a simple analysis and more work needs to be completed to obtain further data for a more detailed study.

3.5.3   Other Components of the LTspice Model

Finally all other components of the LTspice model were examined to ensure correct operation. Manual calculations were completed where possible to ensure programming of all equations was correct and short circuit calculations in line with Section 2.7 were compared with short circuit currents provided by LTspice confirming the correct operation of the program.

3.6   Utilising the Model

The functionality of LTspice is used primarily to calculate the EPR of the earthing system and the fault and earth currents during single phase to earth and double phase to earth faults. A switch is used to form a short circuit between either one or two of the phases from the medium voltage side of the transformers to the earthing system and a measure statement can be used to calculate the EPR and the fault and earth currents.

4 Results

4.1 Scenarios Under Investigation

In order to obtain an overview of the behaviour of a wide range of solar plants two plants of different sizes enveloping the expected range of solar park sizes installed by Enerparc AG will be investigated. The small plant consists of one 1.6 MVA transformer with 24 Sungrow 60 KTL inverters at maximum output associated with it. A 250 m three phase NA2XS(F)2Y240 RM/25 medium voltage cable connects the transformer to the grid as seen in Figure 4.1.

FIGURE 4.1: LTspice Model of the small plant used for investigating earthing system behaviour with resistance earthed neutral point.

The large plant consists of ten 1.6MVA transformers with 24 Sungrow 60 KTL inverters at maximum output associated with each. A 250 m three phase NA2XS(F)2Y240 RM/25 medium voltage cable connects each transformer to the next and the last transformer to the grid as seen in Figure 4.2.
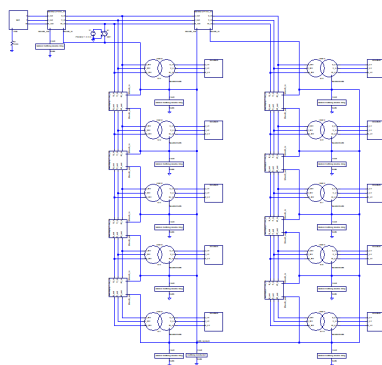
FIGURE 4.2: LTspice Model of the large plant used for investigating earthing system behaviour with resistance earthed neutral point.

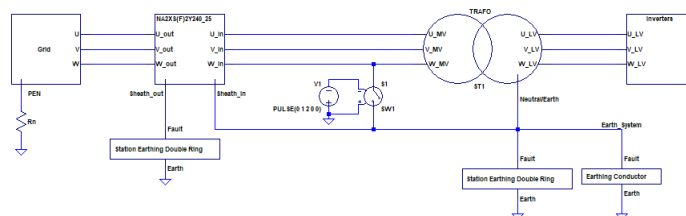All other parameters of the two plants remain unchanged to ensure the comparison between the two remains unbiased, the base case parameters are presented in Table 4.1.

Component	Parameter	Small Plant	Large Plant
Inverters	Max AC Current	96 A	96 A
	Quantity per Transformer	24	24
Transformers	Quantity	1	10
	Load Losses Power	13536 W	13536 W
	Load Losses Voltage	636.58 V	636.58 V
	Load Losses Current	23.13 A	23.13 A
	No-Load Losses Power	1122 W	1122 W
	No-Load Losses Voltage	400 V	400 V
	No-Load Losses Current	1.78 A	1.78 A
	Transformer Ratio	50	50
MV Cables	Length	250 m	250 m
	Conductor Radius	0.0096 m	0.0096 m
	Sheath Radius	0.0175 m	0.0175 m
	Cable Diameter	0.04 m	0.04 m
	Conductor Resistance	0.000125 Ω/m	0.000125 Ω/m
	Sheath Resistance	0.000714 Ω/m	0.000714 Ω/m
Grid Connection	Short Circuit Power	88,340,000 W	88,340,000 W
	Phase Angle	65.75 °	65.75 °
	Nominal Voltage	20,000 V	20,000 V
Transformer LES	Type	Double Ring	Double Ring
	Length	6.56 m	6.56 m
	Width	3.06 m	3.06 m
	Number of rods	4	4
HEC	Length	200 m	2,000 m
	PV Array Area	10,000 m^2	100,000 m^2
General	Frequency	50 Hz	50 Hz
	Soil Resistivity	50 Ωm	50 Ωm

TABLE 4.1: The base case parameters for the small and large solar plants under investigation. Note that the two plants only differ in size.

4.2   Neutral Point Treatment

As discussed in Section 2.3 the treatment of the neutral point (NP) significantly effects earthing system behaviour. To gain a quantitative understanding of the relationship between neutral point treatment and earthing system behaviour each of the two investigated plants were simulated separately with a resistance earthed neutral point and a resonant earthed neutral point. Figure 4.3 shows how the resistance earthed and resonant earthed neutral points are wired in LTspice.

To set the value of the neutral point resistor, R_N, for the resistance earthed scenario an experiment was conducted stepping the neutral point resistance from 1 Ω to 150 Ω and the value corresponding to a single phase fault current of 1 kA was selected. For the small plant using the DIN EN 50522 standard this was 15.93 Ω and the large plant using the DIN EN 50522 standard it was 15.82 Ω. The results of these two experiments are presented in Figures 4.4 and 4.5 respectively.

FIGURE 4.3: LTspice neutral point earthing methods showing resistance earthing on the left and resonant earthing on the right.
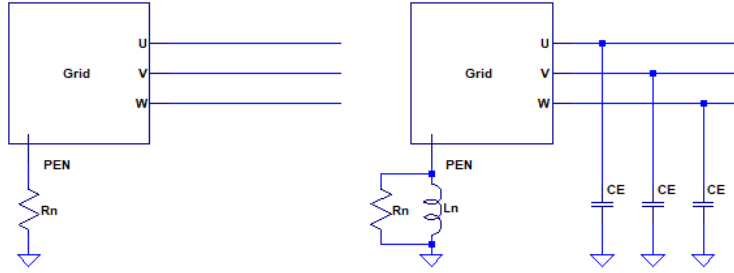
Also an isolated neutral point plant was simulated by setting the neutral point resistance to an extremely high value (99,999 kΩ) and setting line to earth capacitances on the three phases with an arbitrarily chosen value of 0.1 μF.

To set the value of the unknowns, namely neutral point inductance, L_N, and line to earth capacitance, C_E, in the resonant earthed neutral point scenario in reality requires either the in field measurement or calculation of the line to earth capacitance. Then using Equation 4.1 the neutral point inductance value is calculated to achieve a balanced system where only the residual fault current will flow during a fault.

$$L_N = \frac{1}{3 * \omega^2 * C_E} \tag{4.1}$$

Where:
ω is the AC current frequency in rad/s

In the model however the line to earth capacitance can not be measured or calculated as the characteristics of the system downstream of the grid connection point are not known. So for the LTspice model the value of C_E is arbitrarily set as 0.1 μF and using Equation 4.1 L_N is set at 33.77 H.

Now as LTspice does not model the losses leading to residual fault curent as discussed in section 2.3 a resistor is connected in parallel to the neutral point inductor to facilitate this as shown in Figure 4.3. To set the value of this resistor the capacitive earth current limits for self extinguishing single phase arcing faults are used as provided by DIN VDE 0845 Influence of High Voltage Systems on Telecommunication Systems [55]. The recommended maximum capacitative earth current (the current returning to the system via the line to earth capacitances of the phases) for a 20 kV resonant earthed system in order to obtain a self extinguishing arc is 60 A. Now DIN EN 50522 provides a table which details the value of fault currents to be taken into account for earthing system design and states that for a resonant earthed system the maximum residual fault current to be considered is 10% of the capacitative earth current i.e. 6 A for a 20 kV system.

So to find the value of the neutral point resistor an experiment was conducted where the value of the resistor was ranged from 500 Ω to 5000 Ω and the value that resulted in a 6 A steady state current was selected.

These values were 3373 Ω and 3266 Ω for the small and large plants respectively using DIN EN 50522 LTspice model. The results of these two experiments are presented in Figures 4.6 and 4.7.

Earthing System Variables vs Neutral Point Earthing Resistance
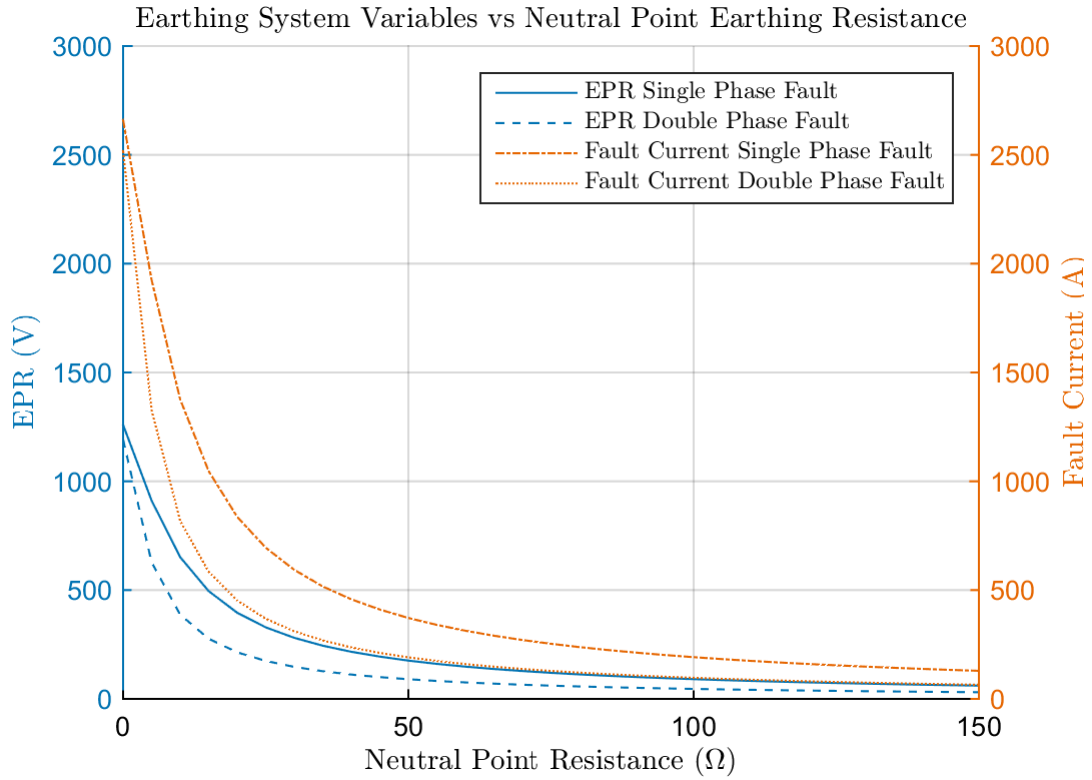
FIGURE 4.4: Earthing system variables vs neutral point earthing resistance for the small plant, resistance earthed.

Earthing System Variables vs Neutral Point Earthing Resistance
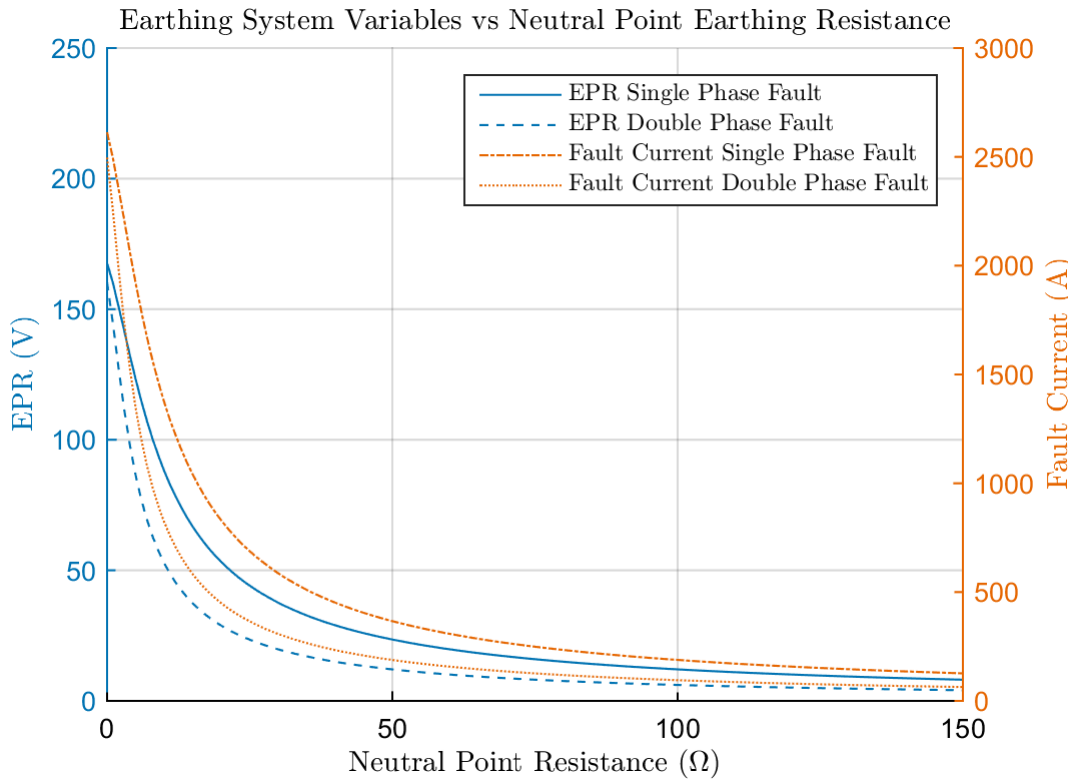
FIGURE 4.5: Earthing system variables vs neutral point earthing resistance for the large plant, resistance earthed.
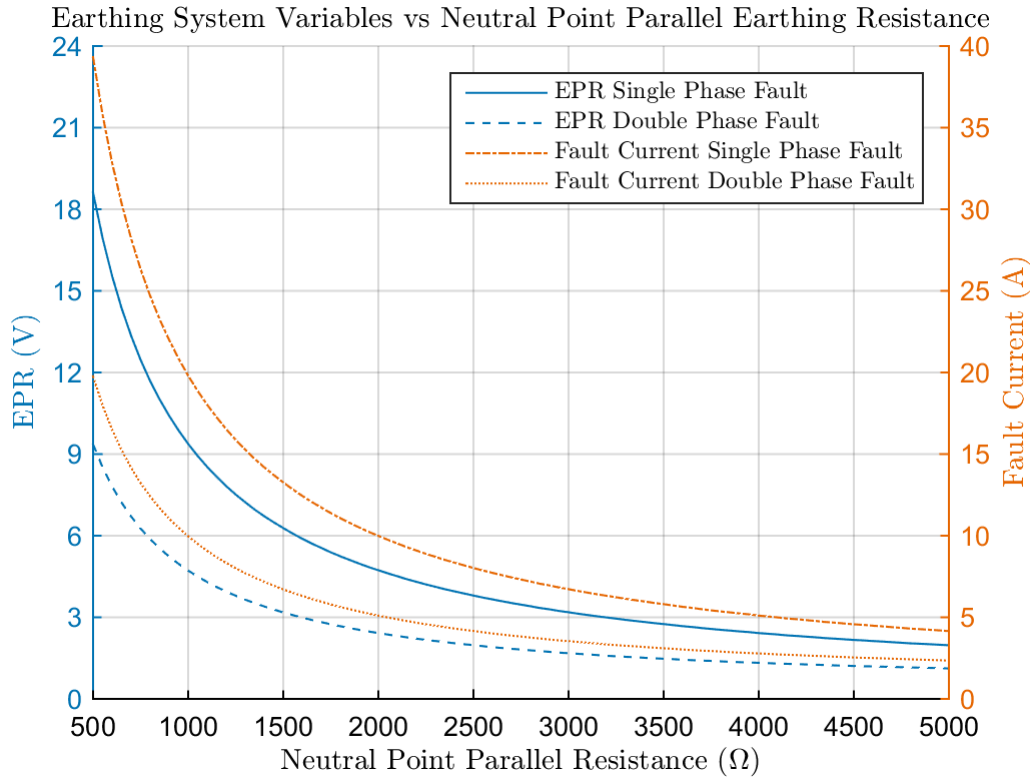
FIGURE 4.6: Earthing system variables vs neutral point parallel earth-
ing resistance for the small plant, resonant earthed.
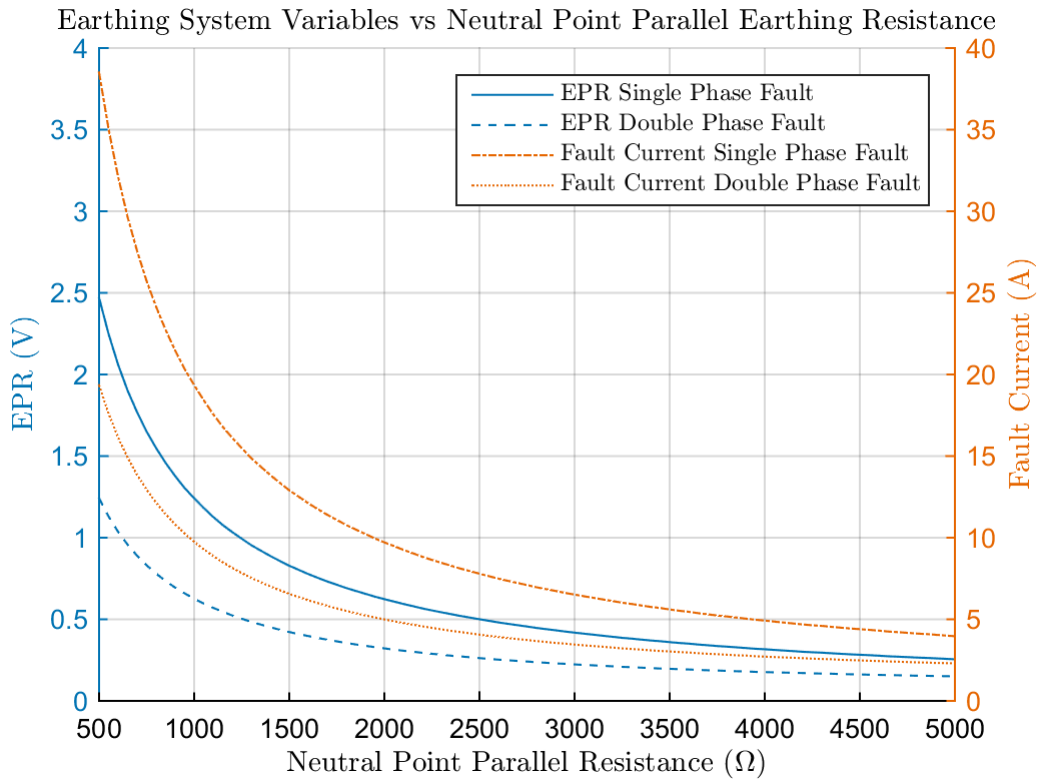
FIGURE 4.7: Earthing system variables vs neutral point parallel earth-
ing resistance for the large plant, resonant earthed.

4.3   Soil Resistivity Investigation

The resistivity of the soil has a significant effect on the behaviour of the earthing system as the resistance of the earthing electrodes is directly proportional to soil resistivity as discussed in Section 3.2. For this reason it was decided to undertake experiments using the LTspice model and a step command allowing the soil resistivity to be varied. A range of soil resistivity values was selected by consulting the literature and finding typical maximum and minimum soil resistivity values expected to be encountered for the soils in which Enerparc AG constructs solar plants. A range of 10 to 300 Ωm was selected and the values were stepped through in increments of 10 Ωm. This experiment was conducted for the small plant with resistance earthed neutral point, the small plant with resonant earthed neutral point, the large plant with resistance earthed neutral point and the large plant with resonant earthed neutral point. The results are presented in Figures 4.8, 4.9, 4.10 and 4.11 respectively showing EPR and fault current for single and double phase faults. All four experiments were conducted using the DIN EN 50522 LTspice model.

FIGURE 4.8: Earthing system variables vs soil resistivity for the small plant with resistance earthed neutral point.
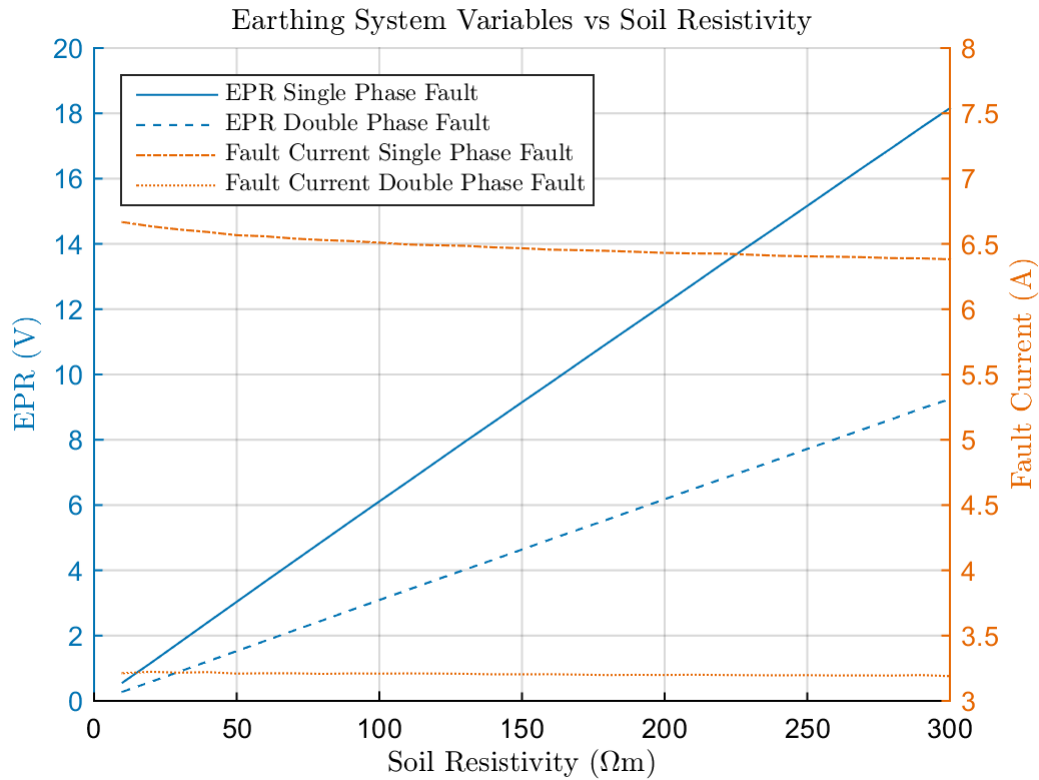
FIGURE 4.9: Earthing system variables vs soil resistivity for the small plant with resonant earthed neutral point.
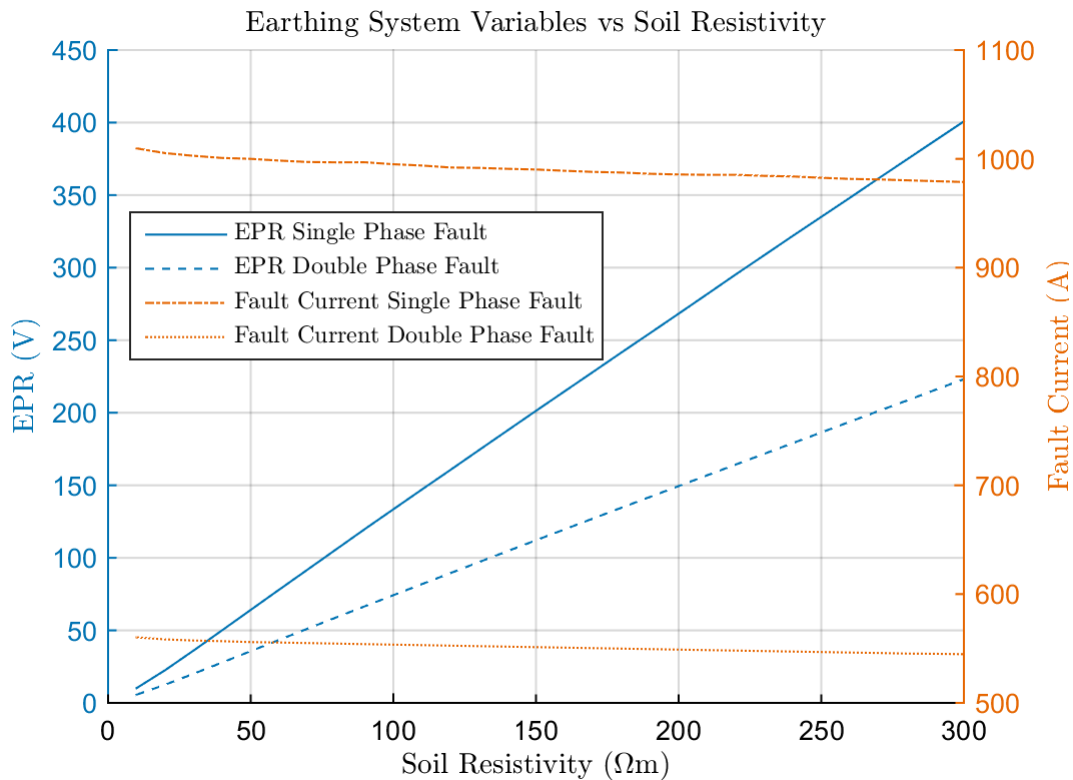
FIGURE 4.10: Earthing system variables vs soil resistivity for the large plant with resistance earthed neutral point.
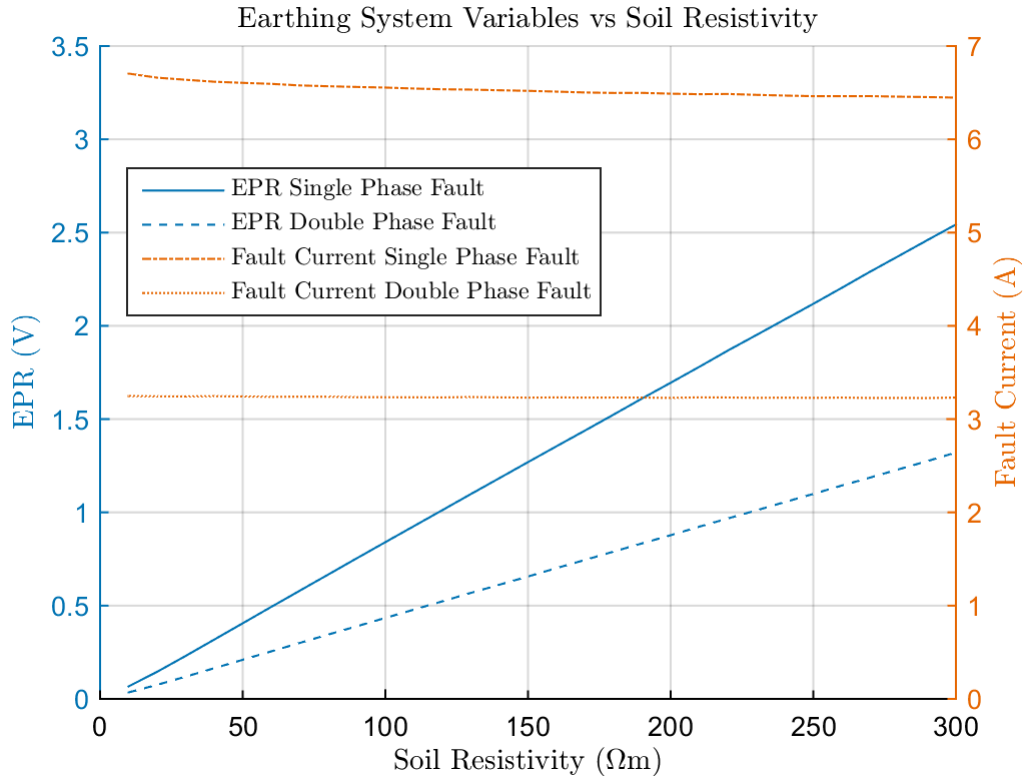
FIGURE 4.11: Earthing system variables vs soil resistivity for the large plant with resonant earthed neutral point.

4.4   MV Cable Length Investigation

The length of the MV cables connecting the last transformer to the grid connection station has a significant effect on the behaviour of the earthing system as the cables have an internal impedance associated with them causing the voltage level at the medium voltage side of the last transformer to drop for long cable lengths as discussed in Section 3.3.3. For this reason it was decided to undertake experiments using the LTspice model and a step command allowing the MV cable length to be varied. A range of MV cable lengths was selected by investigating currently installed Enerparc AG solar plants and determining the range of typical MV cable lengths installed. A range of 100 to 10,000 m was selected and the values were stepped through in increments of 100 m. This experiment was conducted for the small plant with resistance earthed neutral point, the small plant with resonant earthed neutral point, the large plant with resistance earthed neutral point and the large plant with resonant earthed neutral point. The results are presented in Figures 4.12, 4.13, 4.14 and 4.15 respectively showing EPR and fault current for single and double phase faults. All four experiments were conducted using the DIN EN 50522 LTspice model.

Earthing System Variables vs MV Cable Length

FIGURE 4.12: Earthing system variables vs MV cable length for the small plant with resistance earthed neutral point.

Earthing System Variables vs MV Cable Length

FIGURE 4.13: Earthing system variables vs MV cable length for the small plant with resonant earthed neutral point.

Earthing System Variables vs MV Cable Length

FIGURE 4.14: Earthing system variables vs MV cable length for the large plant with resistance earthed neutral point.

Earthing System Variables vs MV Cable Length

FIGURE 4.15: Earthing system variables vs MV cable length for the large plant with resonant earthed neutral point.

4.5 Grid Short Circuit Power Investigation

The short circuit power at the grid connection location has a significant effect on the behaviour of the earthing system as the internal impedance of the grid connection component is inversely proportional to short circuit power as discussed in section 3.3.4. For this reason it was decided to undertake experiments using the LTspice model and a step command allowing the grid connection short circuit power to be varied. A range of grid connection short circuit power values was selected by investigating currently installed Enerparc AG solar plants and determining the range of typical grid connection short circuit power values as reported by the grid operators. A range of 50 to 400 MW was selected and the values were stepped through in increments of 2 MW. This experiment was conducted for the small plant with resistance earthed neutral point, the small plant with resonant earthed neutral point, the large plant with resistance earthed neutral point and the large plant with resonant earthed neutral point. The results are presented in Figures 4.16, 4.17, 4.18 and 4.19 respectively showing EPR and fault current for single and double phase faults. All four experiments were conducted using the DIN EN 50522 LTspice model.
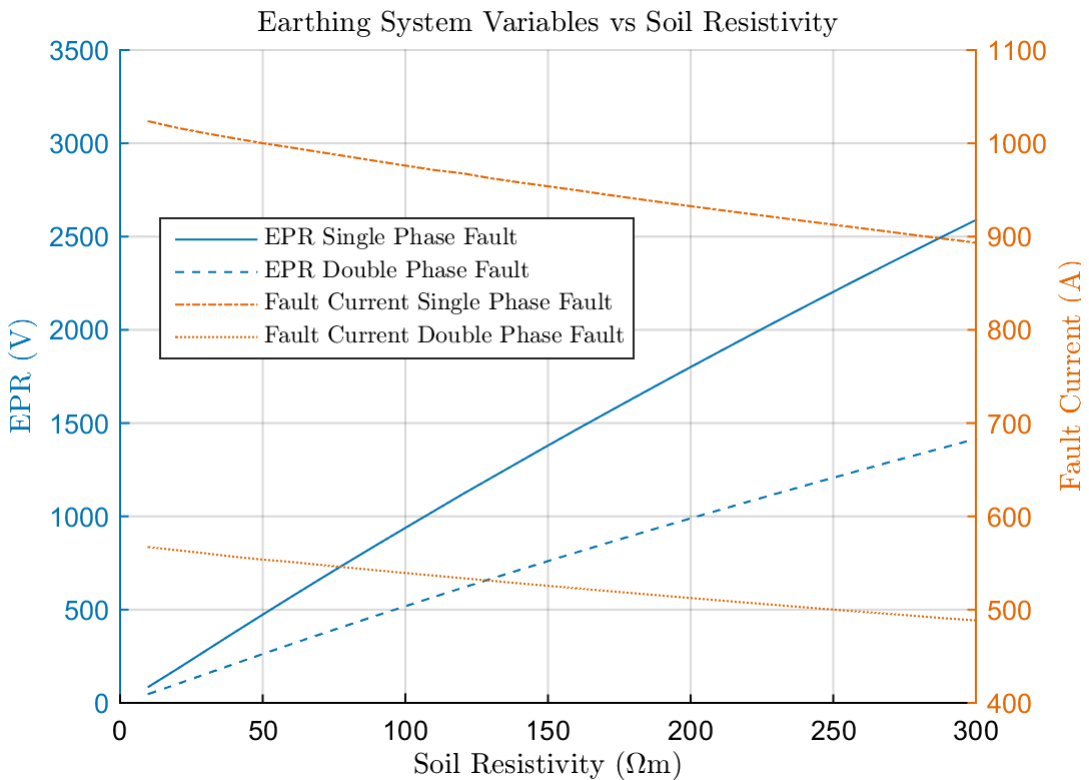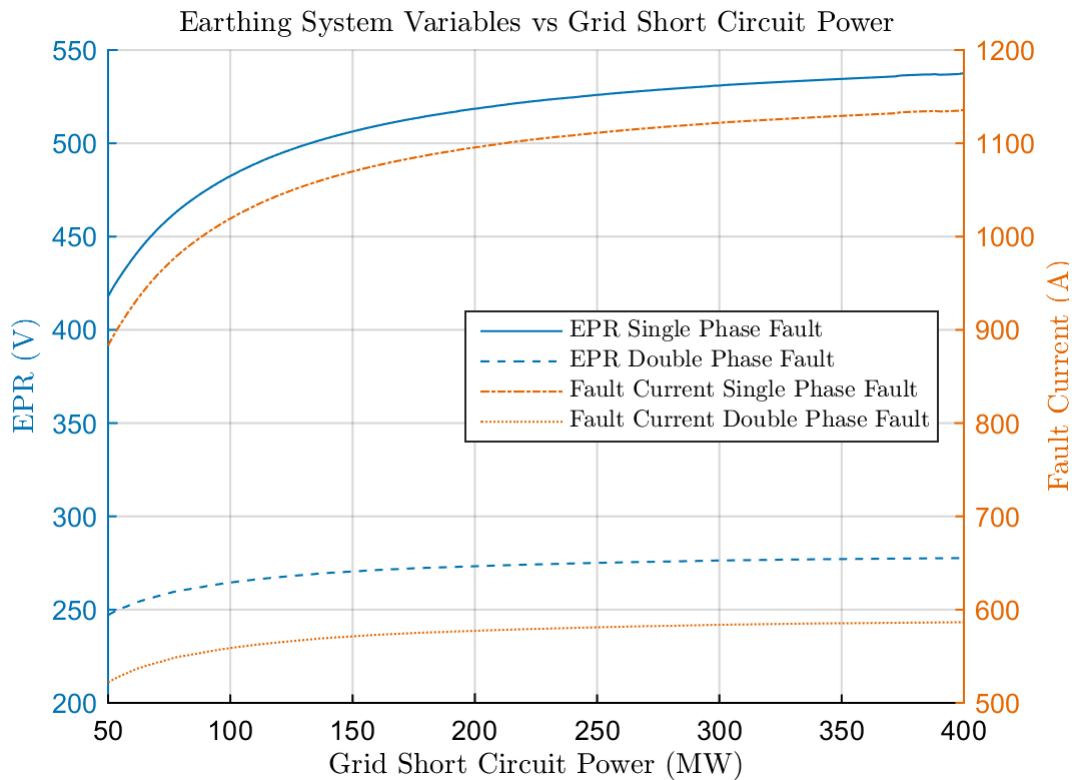

FIGURE 4.16: Earthing system variables vs grid connection short circuit power for the small plant with resistance earthed neutral point.
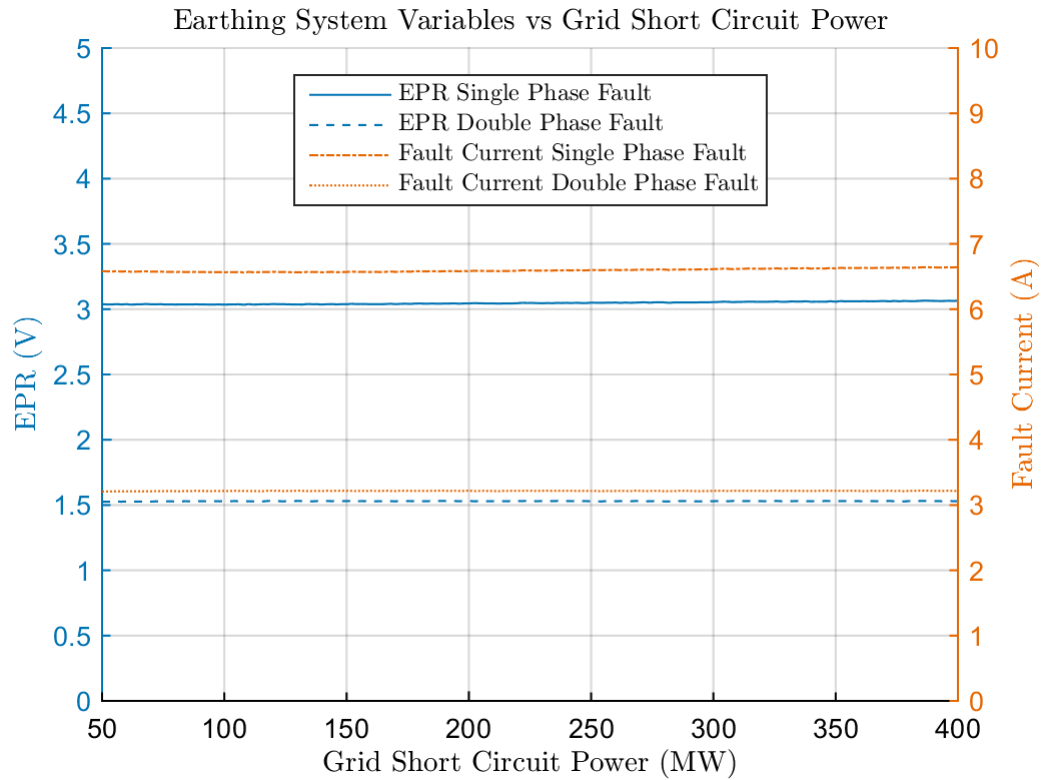
FIGURE 4.17: Earthing system variables vs grid connection short circuit power for the small plant with resonant earthed neutral point.
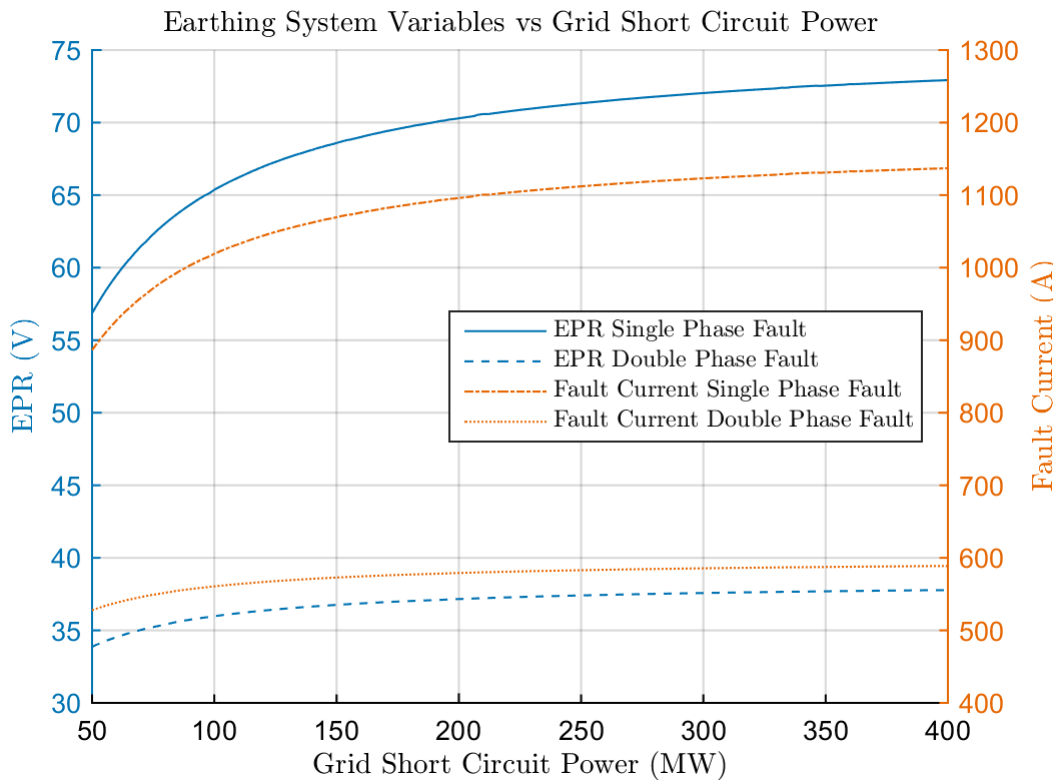
FIGURE 4.18: Earthing system variables vs grid connection short circuit power for the large plant with resistance earthed neutral point.
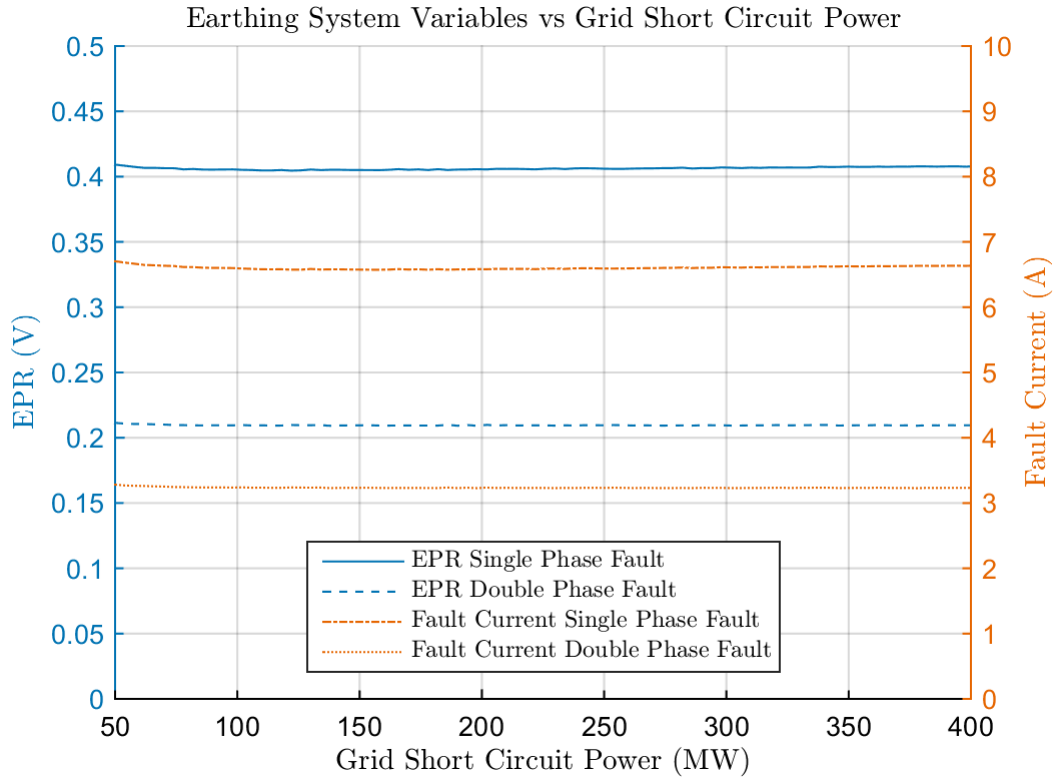
FIGURE 4.19: Earthing system variables vs grid connection short circuit power for the large plant with resonant earthed neutral point.

4.6 Grid Phase Angle Investigation

The phase angle at the gird connection point has a significant effect on the behaviour of the earthing system as the internal resistance of the grid connection component is directly proportional to the cosine of the grid phase angle and the internal inductance of the grid connection component is directly proportional to the sine of the grid phase angle as discussed in section 3.3.4. For this reason it was decided to undertake experiments using the LTspice model and a step command allowing the grid phase angle to be varied. The total possible range of grid phase angle is from 1 to 89 ° as LTspice can not analyse circuits with resistors or inductors of 0 Ω and this range was simulated in steps of 1 °. This experiment was conducted for the small plant with resistance earthed neutral point, the small plant with resonant earthed neutral point, the large plant with resistance earthed neutral point and the large plant with resonant earthed neutral point. The results are presented in Figures 4.20, 4.21, 4.22 and 4.23 respectively showing EPR and fault current for single and double phase faults. All four experiments were conducted using the DIN EN 50522 LTspice model.
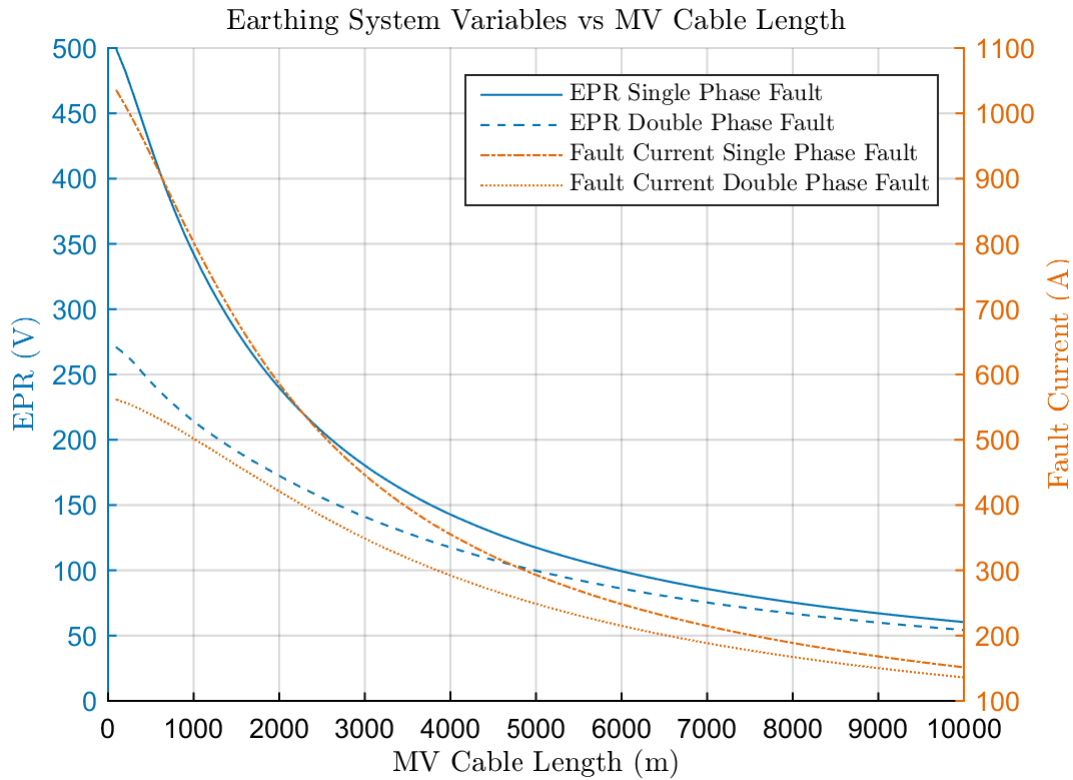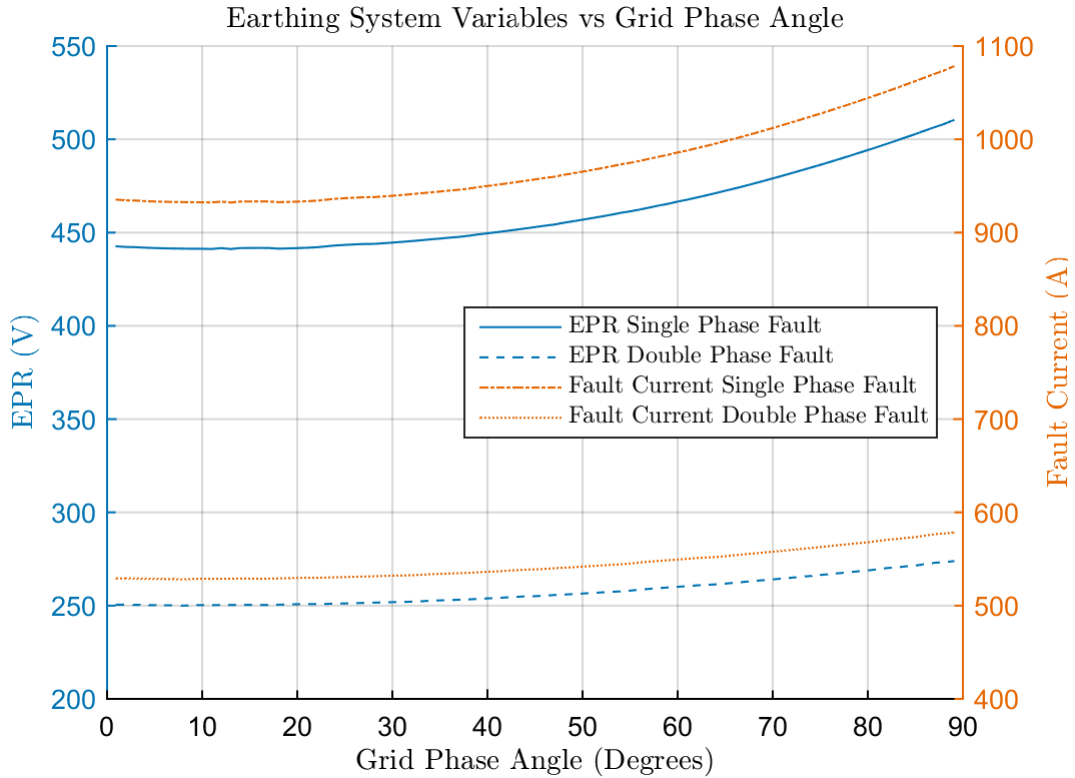
FIGURE 4.20: Earthing system variables vs grid phase angle for the
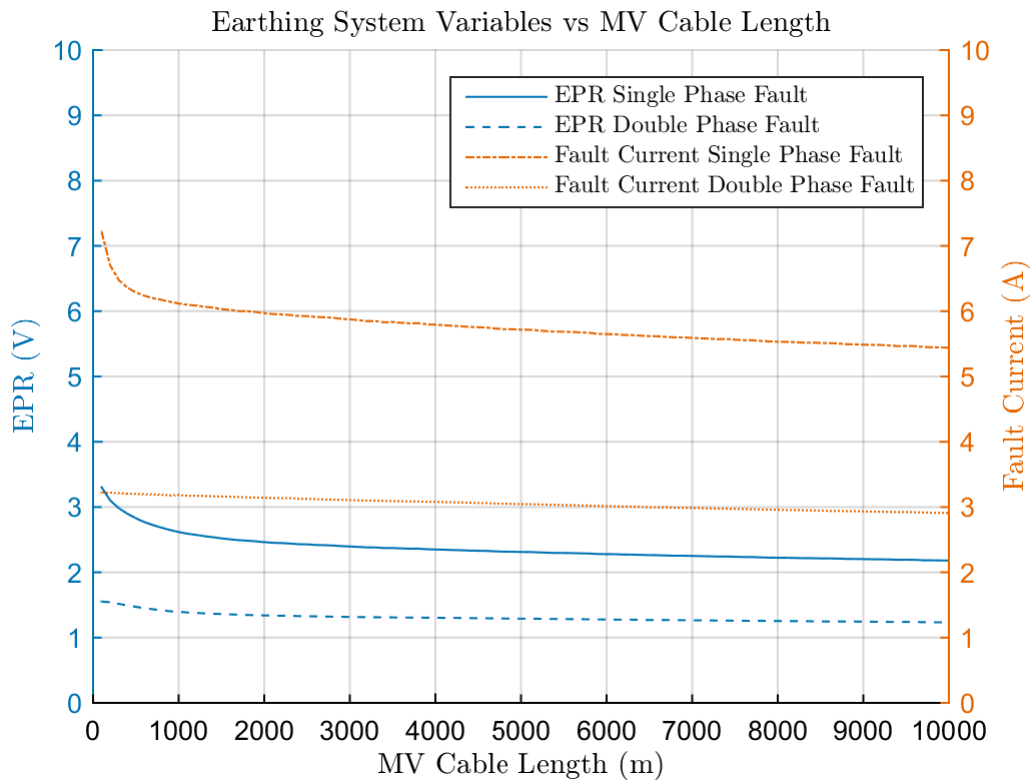small plant with resistance earthed neutral point.
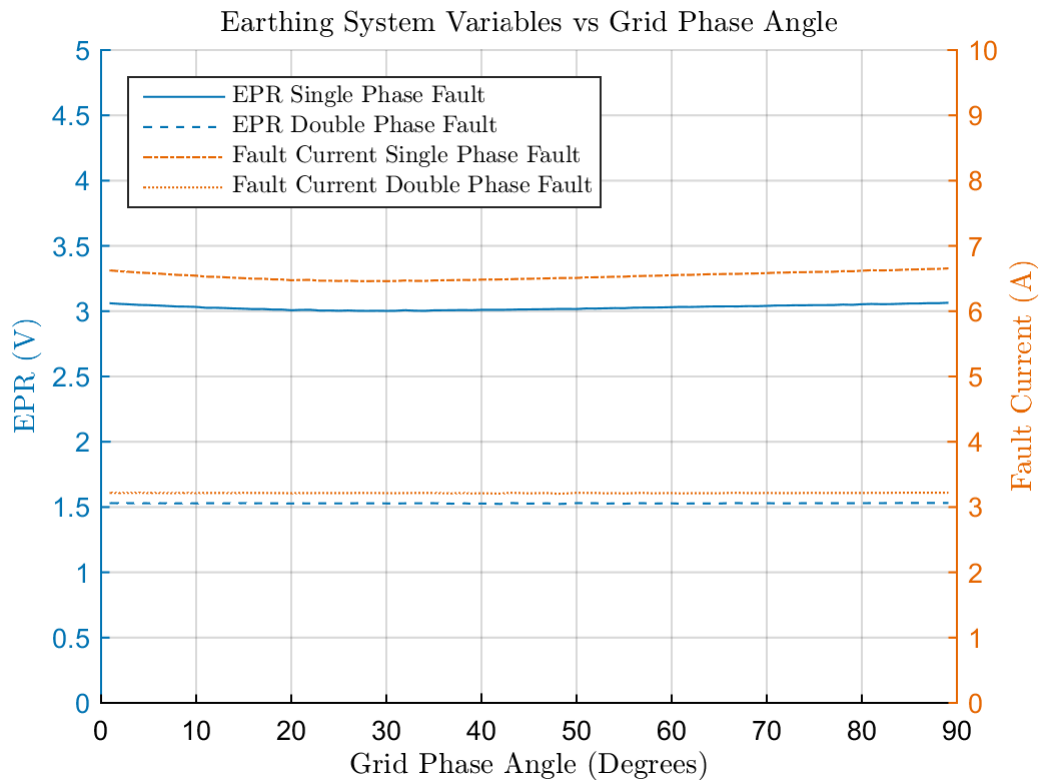
FIGURE 4.21: Earthing system variables vs grid phase angle for the
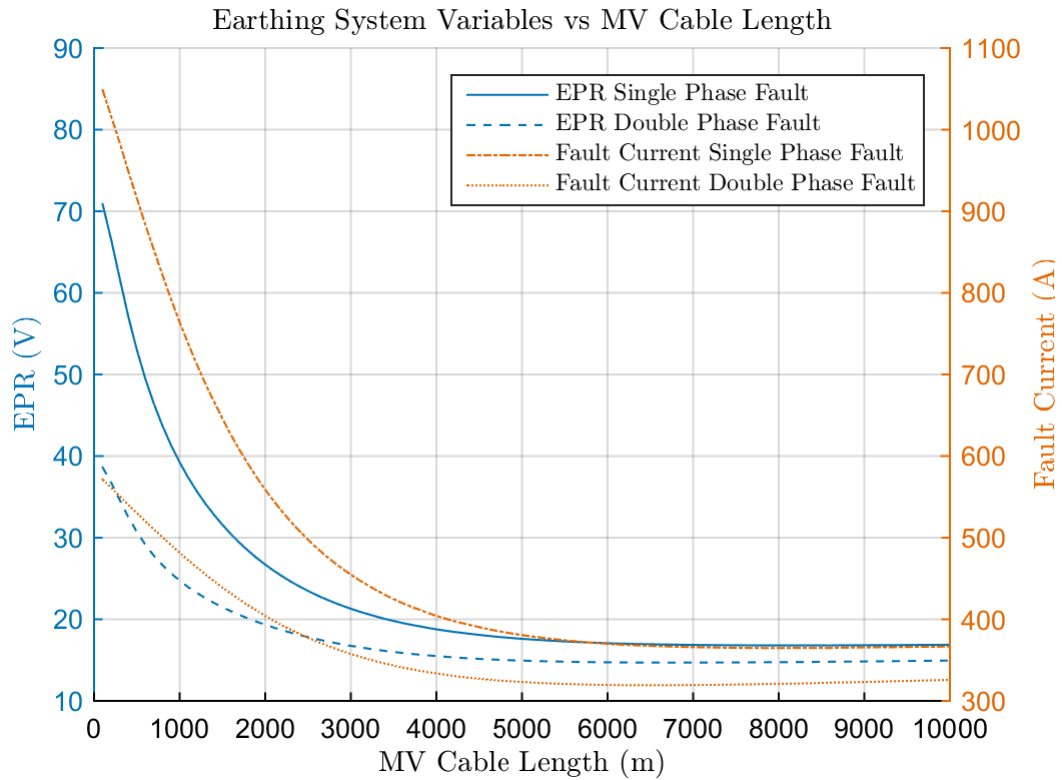small plant with resonant earthed neutral point.
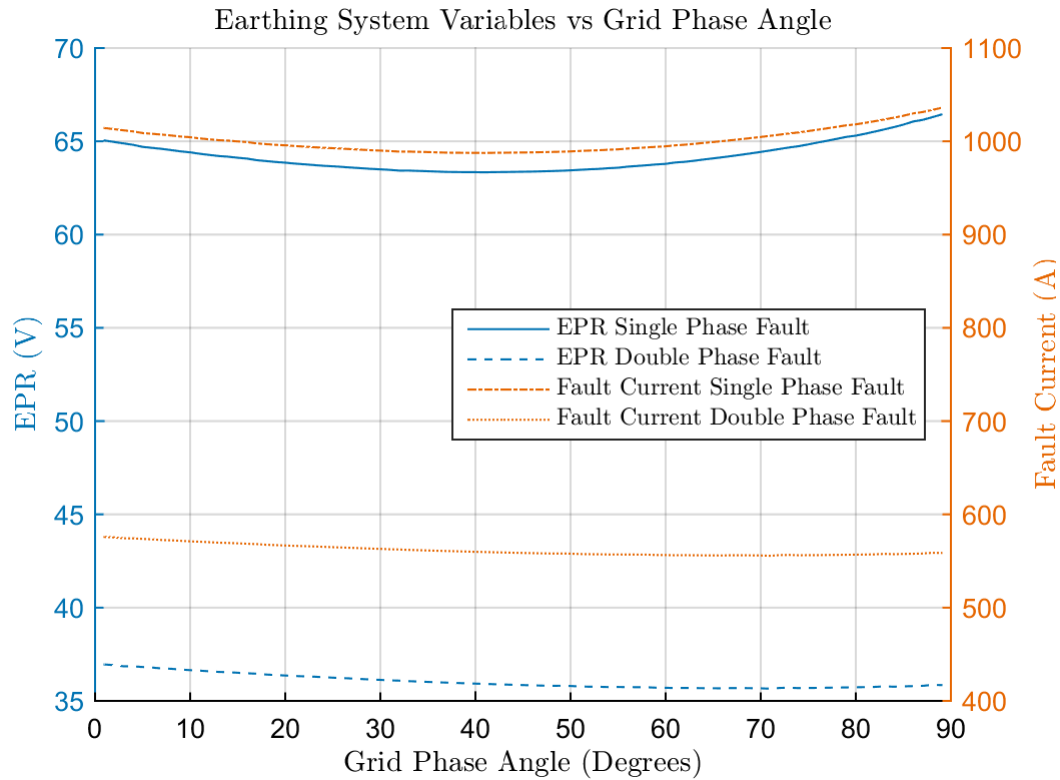
FIGURE 4.22: Earthing system variables vs grid phase angle for the
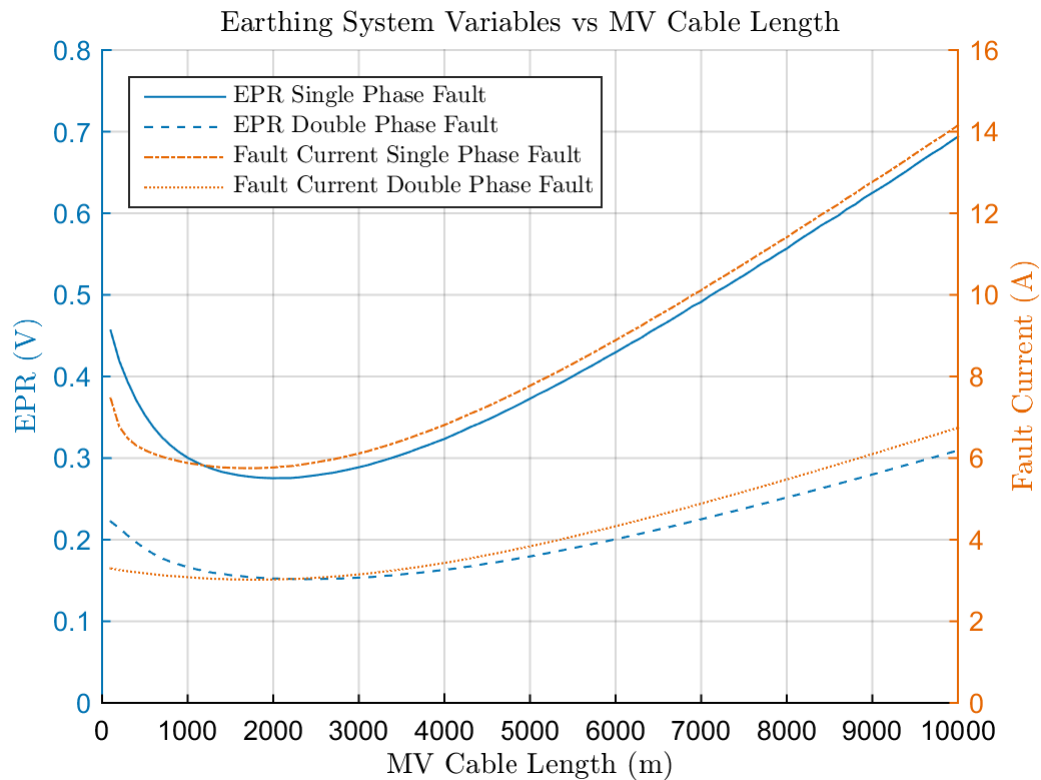large plant with resistance earthed neutral point.
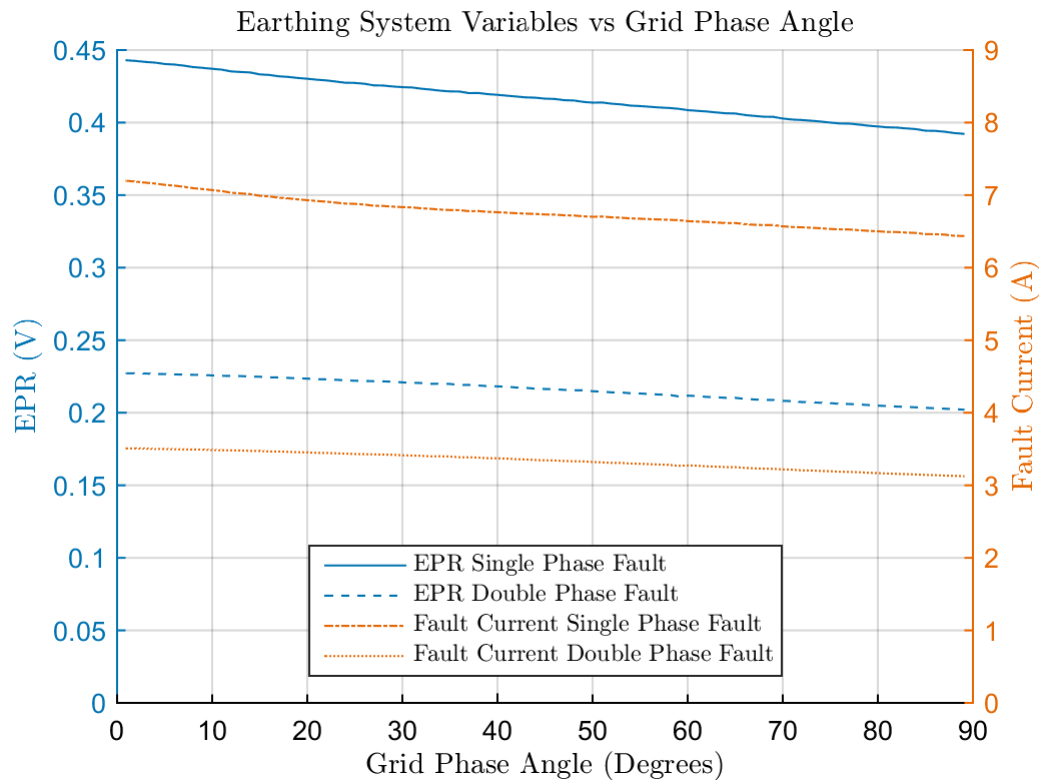
FIGURE 4.23: Earthing system variables vs grid phase angle for the
large plant with resonant earthed neutral point.

4.7   DIN EN 50522 and IEEE std. 80 Comparison

The results presented in Sections 4.2 - 4.6 are all produced using the DIN EN 50522
LTspice model. The difference between the IEEE std. 80 and DIN EN 50522 LTspice
models is only the value of resistance of the earthing system components and as such
the results for the IEEE std. 80 model are not presented as they exhibit similar
behaviour. However a comparison of the base case scenarios (as outlined in table 4.1)
between the two standards has been made. The neutral point treatment for both
resistance and resonant earthing remained identical to that previously used for the
DIN EN 50522 LTspice model. For the IEEE std. 80 the same values of neutral point
resistance and inductance that were used for the DIN EN 50522 model were used to
ensure the comparison between the two standards remained unbiased. However in a
situation where simply the characteristics of the IEEE std. 80 LTspice model were
being investigated the full methodology, as outlined in Section 4.2, for setting the
neutral point resistance or inductance values would be conducted.

Figure 4.24 displays the results for the resistance earthed neutral point and Figure
4.25 displays the results for the resonant earthed neutral point. Each figure plots the
EPR and the fault currents from the two standards against each other for a single
phase fault in the small plant, a double phase fault in the small plant, a single phase
fault in the large plant and a double phase fault in the large plant.

FIGURE 4.24: Comparison of DIN EN 50522 and IEEE std. 80 with
a resistance earthed neutral point.

DIN EN 50522 vs IEEE std. 80, Resonant Earthed Neutral Point
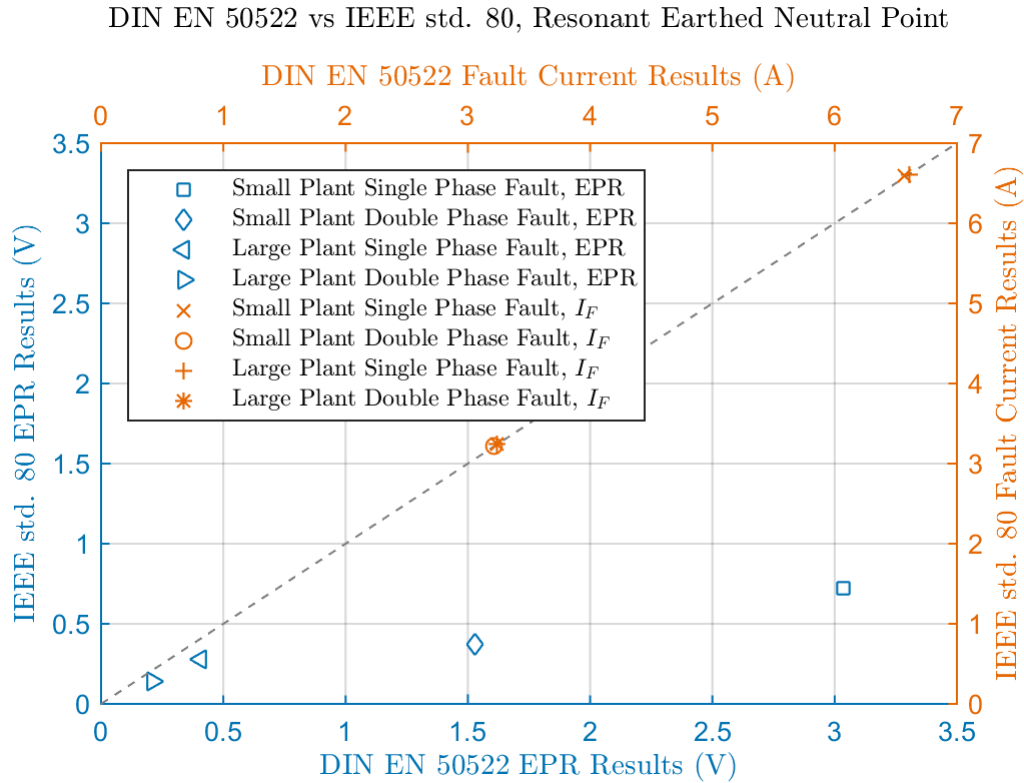
FIGURE 4.25: Comparison of DIN EN 50522 and IEEE std. 80 with a resonant earthed neutral point.

4.8 Short Fault Durations

As discussed in section 2.7.1 for resonant earthed neutral point systems the transient response can cause over voltages for short fault durations and for this reason the shortest possible fault durations are investigated here. The shortest possible fault duration for Enerparc Solar plants is 0.1 seconds due to the nature of the protection systems installed. The LTspice model was used to calculate the EPR for 0.1 second fault duration and the results are presented in Table 4.2.

	Small Plant	Large Plant
Single Phase Fault EPR (V)	10.3	10.6
Double Phase Fault EPR (V)	3.2	3.4

TABLE 4.2: The EPR caused by a 0.1 second fault duration for the resonant earthed neutral point plants.

5 Discussion

The results presented in Chapter 4 show the EPR and fault currents for both single and double phase faults for two different sized plants under a variety of different conditions. To understand the meaning of these results a closer look at the data shall be undertaken, beginning with an investigation into the allowable voltage limits and continuing by comparing those to the observed voltages returned from the simulations in Chapter 4. A discussion about using the developed model to identify a Global Earthing System will ensue and the chapter will be concluded by examining the limits of this study.

5.1 Allowable Voltage Limits

Section 2.6 details how the safe voltage limits for both DIN EN 50522 and IEEE std. 80 are calculated and here these techniques have been used to calculate the maximum allowable touch voltage. Touch voltage was investigated as it is inherently more dangerous than step voltage. Also for IEEE std. 80 the more stringent condition of a 50 kg person will be used to maintain conservativeness. The calculations have been executed for a current duration of 1 second and for the IEEE std. 80 case a soil resistivity of 50 Ωm and a surface layer derating factor of 1 is used. Table 5.1 summarises the allowable limits.

	Maximum Allowable Touch Voltage
DIN EN 50522	110 V
IEEE std. 80	124.7 V

TABLE 5.1: Maximum allowable touch voltage limits according to DIN EN 50522 and IEEE std. 80 for the base case scenario of a one second current duration, 50 Ωm soil resistivity and a surface layer derating factor of 1.

Now as the LTspice model does not calculate touch voltage the comparison to check the safety of the system shall be made with the returned EPR from the simulations and the voltage limits in Table 5.1. Once again this represents a conservative decision as EPR is greater than or equal to touch voltage under all conditions.

5.2 Neutral Point Treatment

The investigation into the effect of neutral point treatment on earthing system variables presented in Section 4.2 shows that the neutral point earthing method significantly effects earthing system behaviour. As well as this the methodology to determine the values of the neutral point earthing components has a significant effect.

Examining the graphs in Figures 4.4 to 4.7 a general shape in the curves is observed where initially a sharp decrease of Fault Current/EPR occurs which gradually flattens

out and asymptotes parallel with the y-axis. The x-axis intercept for the resistance earthed neutral point scenario represents the case of a directly earthed neutral point.

A directly earthed neutral point causes very high Fault Currents and consequently very high EPR due to the low impedance return pathway, these figures for a single phase fault are summarised in Table 5.2.

	Small Plant	Large Plant
Single Phase Fault Current	2660.6 A	2612.7 A
Single Phase Fault EPR	1259.4 V	167.7 V

TABLE 5.2: The Fault Current and EPR caused by a single phase fault for a directly earthed neutral point for the small and large plants.

Quite clearly the EPR values produced under the directly earthed neutral point scenario are far higher than the allowable limits for both DIN EN 50522 and IEEE std. 80 and so from the point of view of earthing system design this type of neutral point treatment is not recommended. Also it is interesting to note that the Fault Currents differ very little from the small plant to the large plant however the EPR differs significantly due to there being 10 times as much earthing electrode material in the large plant than the small plant.

An isolated neutral point system causes very small Fault Currents and consequently EPR as the return pathway for the fault current is via the line to earth capacitances of the healthy phases. These figures are summarised in Table 5.3

	Small Plant	Large Plant
Single Phase Fault Current	6.3 A	6.4 A
Single Phase Fault EPR	2.6 V	0.3 V

TABLE 5.3: The Fault Current and EPR caused by a single phase fault for an isolated neutral point for the small and large plants.

Obviously the plants with an isolated neutral point return EPR well below the allowable limits from both DIN EN 50522 and IEEE std. 80 and so from the point of view of earthing system design this type of neutral point treatment delivers a safe plant. However it must be noted that the Fault Current and EPR values for the isolated neutral point case depend on the line to earth capacitances of the system which are unique to each system and also each fault because fault location effects the value of line to earth capacitance.

Now looking into the resistance earthed scenario, for equipment protection reasons the value of resistance is that which produces a 1 kA Fault Current, in the case of the solar plants investigated that is a single phase fault. Table 5.4 summarises the earthing system variables for the resistance earthed neutral point systems.

As can be seen the large plant produces an EPR below the allowable limits while the small plant produces an EPR above the allowable limits. In the case of the small plant it is thus recommended to conduct further design work and extend the size of the earthing system to decrease the earthing resistance and bring the EPR below the allowable limits.

	Small Plant	**Large Plant**
Single Phase Fault Current	1000.1 A	999.9 A
Single Phase Fault EPR	473.3 V	64.1 V

TABLE 5.4: The Fault Current and EPR caused by a single phase fault for a resistance earthed neutral point for the small and large plants.

Now looking into the resonant earthed scenario where the value of parallel resistance chosen is that which produces a 6 A maximum residual Fault Current (steady state), in the case of the solar plants investigated here that is the single phase Fault Current. Table 5.5 summarises the earthing system variables for the resistance earthed neutral point systems.

	Small Plant	**Large Plant**
Single Phase Fault Current	6.5 A	6.6 A
Single Phase Fault EPR	3.0 V	0.4 V

TABLE 5.5: The Fault Current and EPR caused by a single phase fault for a resonant earthed neutral point for both the small and large plants.

Investigating the EPR produced from the resonant earthed neutral point plants it is clear that they are far below the allowable limits and it is concluded that these plants are safe and no further design work is required. It is also interesting to note that the fault currents are above the 6 A design value, this is due to the transient response occurring before steady state residual fault current is reached pushing the RMS fault current above 6 A.

Also the allowable current limits of the earthing system as presented in Table 2.3 need to be checked to ensure they are not exceeded. As the largest occurring fault current is 2660.6 A for the small plant with a directly earthed neutral point is well below the lowest allowable limit of 5.566 kA it can be concluded that from a current carrying perspective the earthing system is safe under all fault scenarios.

To conclude it has been shown that a solar plant with a directly earth neutral point will deliver an unsafe earthing system and further design work must be completed to decrease the earthing resistance of such a plant. For a solar plant with a resistance earthed neutral point the EPR depends on the size of the plant and larger plants are more safe than smaller plants. For a solar plant with an isolated or resonant earthed neutral point the EPR produced is very low and it can be argued that no dangerous touch or step voltages will arise in the majority of practical situations.

5.3 Soil Resistivity

The investigation into the effect of soil resistivity on earthing system variables presented in Section 4.3 at first glance demonstrates an intuitive relationship but with further analysis presents more complex behaviour.

The resistance of the earthing electrodes is directly proportional to soil resistivity, so as soil resistivity increases it is expected that EPR will increase and the Fault Current will decrease linearly. However in Figures 4.8 to 4.11 linear behaviour is not

observed. ERP demonstrates a decreasing increase and Fault Current demonstrates a decreasing decrease with increasing soil resistivity, it must be noted that this off-linearity is very slight and in some cases (particularly the large plant) is close to negligible.

To explain the off linearity of the observed results we need to look at the MV cables connecting the last transformer to the grid. The inductance of the cables and their sheaths are directly dependent on the natural logarithm of the square root of soil resistivity as seen in Equations 3.11 and 3.12. Although this is a complex relationship it can be said generally that as soil resistivity increases the impedance of the MV cables increases and so the voltage on the MV side of the transformer, the fault location, decreases leading to the observed results.

In light of this finding it must however be realised that the effect of the MV cables varying inductance is far smaller than the effect of the earthing electrode varying resistance.

Now looking to the allowable touch voltage limits Table 5.6 presents the limits of soil resistivity below which the EPR caused by a single phase fault does not exceed the allowable limits calculated in Section 5.1.

Plant Scenario	Soil Resistivity Limits (DIN)	Soil Resistivity Limits (IEEE)
Small Plant, Resistance Earthed NP	13 Ωm	15 Ωm
Small Plant, Resonant Earthed NP	1873 Ωm	2118 Ωm
Large Plant, Resistance Earthed NP	84 Ωm	95 Ωm
Large Plant, Resonant Earthed NP	13200 Ωm	14950 Ωm

TABLE 5.6: Soil resistivity values below which the EPR caused by a single phase fault does not exceed the allowable touch voltage limits.

From Table 5.6 we see that resonant earthing of the neutral point leads to a safer solar plant due to the far lower fault currents that this type of neutral point treatment leads too, it is also worth noting that for the large plant the allowable limits of soil resistivity are far beyond the maximum reported soil resistivities in the literature and it can be said that this plant is safe under all soil conditions. For plants with a resistance earthed neutral point the design engineer must examine each plant and its soil conditions individually to decide if the plant is safe or not.

5.4   MV Cable Length

The MV cable length investigation on earthing system variables presented in Section 4.4 provides insightful results as the effects of MV cable length on the operation of the earthing system are complex.

The impedance of both the sheaths and the conductors of the MV cables are directly proportional to the length of the MV cables. This leads to a linearly decreasing voltage at the fault location with increasing MV cable length. Also an increase of the earthing system total impedance with increasing MV cable length occurs as a portion of the total earth fault current flows via the MV cable sheaths before flowing into the earth through the local earthing system of the grid connection station.

In terms Fault Current these two outcomes manifest in additive manners as decreasing fault location voltage causes decreasing Fault Current and increasing earthing system total impedance also causes Fault Current to decrease.

In terms of EPR these two outcomes manifest in opposing manners as decreasing fault location voltage causes decreasing Fault Current and therefore decreasing EPR however increasing earthing system total impedance causes EPR to increase.

Furthermore the mutual inductance effects of the MV cables must be considered. For a resistance earthed neutral point system, upon fault initiation the currents in the healthy phase(s) remain constant but the current in the faulted phase(s) will increase to the value of the fault current. This increase in current increases the mutual inductance values of the other components of the MV cables namely the sheaths and the unfaulted conductors adding to the effects described above.

Looking to Figures 4.12 and 4.14 it is observed that Fault Current and EPR are decreasing with increasing MV cable length. For Fault current this is in line with expectations. For EPR this is mostly in line with expectations and shows that the effect of increasing MV cable sheath impedance is inferior to the effect of decreasing voltage at the fault location.

Now if we consider the case of a resonant earthed neutral point system there are different effects to consider when discussing the mutual inductance of the MV cables. For a single phase fault upon fault initiation the current in the faulted phase will remain almost at its pre-fault value dropping by just 6 A (albeit with an exponentially decaying transient component initially) and so very little change in the mutual inductance values is expected. When Figure 4.13 is examined we see that for a single phase fault the Fault Current and EPR decrease with increasing MV cable length as expected.

For a double phase fault a decreasing Fault Current and EPR are observed however with less gradient than a single phase fault. This is due to the high impedance return pathway causing the short circuit current to flow between the two phases and not via the earth return pathway. Effectively a phase to phase fault clear of earth has formed with some residual current flowing via the earthing system leading to a slowly decreasing Fault Current and EPR in regards to MV cable length.

Finally examining Figure 4.15 we see initially decreasing Fault Current and EPR for both single and double phase faults but the Fault Current and EPR increase at MV cable lengths greater than approximately 2000 m. This is attributable to the far greater current output of the large plant as opposed to the small plant. At maximum production the solar inverters are producing 460 A of current on the MV side of the transformers. This current will cause a voltage rise on the solar plant side of the MV cables (the fault location) as their length increases leading to the increasing Fault Current and EPR for longer cable lengths. This effect is not observed in the small plant as it produces only 46 A of current on the MV side of the transformers which is not enough to produce an observable effect.

To sum up the length of the MV cables in a grid connected solar plant has significant effects on the behaviour of the earthing system. To understand the details of these effects the design engineer must consider the neutral point treatment of the grid and the size of the pant. For resistance earthed neutral point solar plants increasing MV cable length will cause the Fault Current and EPR produced from single and double phase faults to decrease. For resonant earthed systems the size of the plant must also be considered. For small plants the Fault Current and EPR of single and double phase faults will decrease with increasing MV cable lengths. With large plants the solar production will cause an increasing voltage at the fault location. As such the Fault Current and EPR will initially decrease with increasing MV cable length and then begin to increase after a critical MV cable length has been reached, this length

being dependant on the characteristics of the plant and the rate of solar production at the time of the fault.

5.5   Grid Short Circuit Power

The investigation into the grid short circuit power presented in Section 4.5 shows a mostly intuitive result. Simply it is expected that as short circuit power increases the fault variables (Fault Current and EPR) shall increase.

For the resistance earthed neutral point scenario the observed Fault Current and EPR curves match with expectations. Investigating Equation 3.16 we see that grid internal impedance is inversely proportional to grid short circuit power so with increasing short circuit power we expect inversely increasing voltage at the fault location asymptoting to the nominal grid voltage. In line with this relationship we see the Fault Current and EPR curves from Figures 4.16 and 4.18 increasing to an asymptote the value of which corresponds to the Fault Current and EPR produced from a grid connection point with zero internal impedance.

For the resonant earthed neutral point plants negligible changes in Fault Current and EPR for both single and double phase faults are observed in both the small and large plants. This can be attributed to the very high impedance return pathway for the fault current causing the Fault Current and hence EPR to vary little with changes in voltage at the fault location.

In conclusion the observed results match very closely with expectation as in general increasing grid short circuit power leads to increasing Fault Currents and EPR. However for the resonant earthed neutral point plants the high impedance return pathway leads to negligible changes in Fault Current and EPR.

5.6   Grid Phase Angle

The investigation into the effects of grid phase angle on earthing system behaviour presented in Section 4.6 shows that Fault Current and EPR have a slight dependence on grid phase angle.

This is an intuitive result as grid phase angle does not effect the magnitude of the grids internal impedance simply just the phase difference between the voltage and current wave forms. What this does lead to however is a varying voltage at the fault location caused by the varying vectorial sum of the voltage waveforms produced by the grid (varying) and the solar plant (constant).

From Figures 4.20 to 4.22 we see for single phase faults a general shape to the Fault Current and EPR curves of initially decreasing to a minimum and then increasing until the maximum grid phase angle is reached telling us that the maximum fault location voltage occurs at maximum grid phase angle. However for Figure 4.23 we observed steadily decreasing Fault Current and EPR with increasing grid phase angle telling us that the greater solar production in the large plant causes the voltage at the fault location to decrease with increasing grid phase angle.

In conclusion the grid phase angle has a very small effect on earthing system behaviour and the earthing system designer can safely ignore these effects when designing a new system.

5.7 DIN EN 50522 and IEEE std. 80 Comparison

A comparative investigation between the two major international earthing system design standards, DIN EN 50522 and IEEE std. 80, was conducted in Section 4.7. To understand the meaning of the presented results let us first analyse the differences in the LTspice models developed under each of the two standards. The components forming the production system of the solar plant, namely the inverters, the transformers, the MV cables and the grid connection point are identical in both models as they do not fall under the remit of earthing system design. The only components where differences occur are the earthing system components namely the local station earthing components (single and double ring) and the horizontal earthing component. As we saw in Chapter 3 all of the components of the earthing system are simply constructed of resistors whose values are determined with Equations 2.24, 2.25 and 2.26 for the DIN EN 50522 standard and Equation 2.23 for the IEEE std. 80 standard. So in essence the only difference between the DIN EN 50522 and the IEEE std. 80 LTspice models is the total earthing system resistance.

Now looking at Figures 4.24 and 4.25 we see the Fault Current and EPR produced from single and double phase faults from the small and large plants. Figure 4.24 showing results from the resistance earthed neutral point plants and Figure 4.25 the resonant earthed neutral point plants.

The Figures plot the results returned from the two design standards against each other so any points lying on the oblique dashed line indicate the standards return the same values, points below the oblique line indicate that the DIN standard produces higher values and points above the oblique line indicate that the IEEE standard produces higher values. Note that higher returned values leads to more conservative design.

Analysing the results we see that for Fault Current the two standards are in very close agreement, a small deviation from the oblique dashed line is observed for a single phase fault in the small plant for the resistance earthed neutral point scenario. On average the IEEE standard returns results 100.9 % higher values for the small plant and 100.1 % higher values for the large plant than the DIN standard.

Looking into EPR we see that for all eight situations the DIN standard returns higher values with an average of 411.6 % higher for the small plant and 146.5 % higher for the large plant than the values returned by the IEEE standard.

Both the results for Fault Current and EPR show that for the earthing electrodes used in this study the DIN EN 50522 estimates a higher earthing resistance than the IEEE std. 80 and is therefore more conservative. Furthermore the DIN EN 50522 estimate for the allowable limits of touch and step voltage are lower than the IEEE std. 80 limits, another point of conservatism for the DIN standards leading to a higher safety factor for plants designed under the DIN standard than those designed under the IEEE standard.

5.8 Short Fault Durations

Using the methods described in Section 2.6 the safe touch voltage limits for a 0.1 second current duration are 660 V and 394 V according to DIN EN 50522 and IEEE std. 80 respectively, clearly the results presented in Section 4.8 are far below this and so are safe.

5.9   Global Earthing System

As discussed in Section 2.10 the identification of an earthing system as a GES has various benefits but there does not yet exist an officially approved method of identifying a system as a GES. To be considered a GES there are several requirements an earthing system must meet. Firstly a GES must be "created by interconnecting local grounding systems" [6] which a solar plant earthing system is as each local transformer earthing system is interconnected with the horizontal earthing electrode. Secondly a GES must "permit the division of the ground fault current in a way that results in a reduction of the ground potential rise at the fault location. Such a system could be said to form a quasi-equipotential surface" [6] which a solar plant earthing system also does as any fault current flowing into the earthing system will be divided amongst each of the local earthing systems at the transformer stations via the horizontal earthing conductor leading to a reduction in EPR at the fault location and the forming of a quasi-equipotential total earthing system. Finally a GES must ensure "that there are no dangerous touch and step voltages" [6] which not all solar earthing systems do as seen in Chapter 4 leading to the difficulty in identifying a solar plant earthing system as a GES.

The developed LTspice models can be used to identify any solar plant earthing system as a GES as the models are capable of calculating the EPR under the worst case fault current and hence capable of proving the EPR is below the allowable limits of step and touch voltage and therefore not developing any dangerous step and touch voltages. The major strength of the LTspice model is that it can be applied to any grid connected solar plant and is user friendly as the user simply drags and drops the required components from the developed component library, inputs the required parameters and the system is ready to analyse. This method of identifying a GES is in essence identical to the Campoccia method [45] but the circuit calculations are automated and it is only valid for grid connected solar plant earthing systems.

5.10   Comparison to Similar Studies

In the literature there exist two studies comparable to this thesis. The earliest by Dawalibi and Ma in 2010 titled 'Grounding Analysis of a Solar Power Generation Facility' [4] and the latest by Datsios and Mikropoulos titled 'Safe Grounding System Design for a Photovoltaic Power Station' published in 2012 [15].

The paper by Dawalibi and Ma conducts an earthing study of a 10 MW solar power plant feeding power to an existing 220 kV power station located adjacent to the solar plant. Soil resistivity measurements were made at the site and a three layer soil resistivity model was used for analysis of the earthing system.

The earthing system was modelled using the commercially available CDEGS software package and this was used to conduct the performance analysis. A maximum Fault Current of 21.4 kA was injected into the earthing system which produced an EPR of 1.91 kV and a maximum touch voltage of 238.4 V at the solar plant. The IEEE std. 80 method was used to calculate an allowable touch voltage of 258.8 V and as such the earthing system was deemed safe.

The paper presents the method of conducting a solar plant earthing system analysis based on one example and offers no insight into the behaviour of the earthing system under various conditions and plant configurations. Also specialised earthing analysis software was used for the performance analysis of the system. Drawing comparisons between this thesis and the paper by Dawalibi and Ma is therefore difficult. The basic

method between the two is identical but this thesis is focused on understanding how earthing systems behave under different conditions rather than analysing one specific example.

The work done by Datsios and Mikropoulos is very similar to that by Dawalibi and Ma in that the procedure for the earthing analysis of a solar plant is demonstrated by completing the analysis for a single plant. Once again the IEEE std. 80 method is used to calculate the allowable touch voltage and soil resistivity measurements are taken in the field and a two layer soil model was developed. Fault current calculations were conducted and the commercially available earthing analysis software CYMGRD was used to conduct the performance analysis. The plant was located on an area of very high soil resistivity (approximately 2900 - 6400 Ωm)and as such the EPR under a 1012.7 A fault was found to be 12kV with maximum touch voltage of approximately 1120 V which is below the allowable limit of 1153 V and so the plant was deemed safe in one area of the plant. However in another area of the plant the maximum touch voltage was found to be 1486 V and so it is suggested that a high resistivity surface layer is spread to increase the allowable touch voltage limits in this area.

Once again comparisons between the Datsios and Mikropoulos paper and this thesis are limited but the basic method of analysis is identical to that used in this thesis. Unfortunately no investigation into the behaviour of the earthing system under different conditions was conducted in the Datsios and Mikropoulos paper unlike this thesis.

5.11   Limitations and Important Considerations

The solar plant earthing system study has investigated the behaviour of an earthing system of various solar plant configurations and presented the findings. To interpret and use the findings in a safe and prudent manner it is important the limitations of the study are understood. Also there exist some important considerations that must be made clear so that incorrect conclusions are not drawn from the data.

Firstly from the results it appears as though under all cases a single phase fault causes higher Fault Current and EPR however this is not the case. Whether a single or double phase fault causes the highest Fault Current and EPR depends of the sequence impedances of the system, as discussed in Section 2.7. For the systems under study in this thesis a single phase fault always resulted in the higher Fault Current and EPR. This is not always the case and each system must be analysed on its own merits and both double phase and single phase faults should always be investigated.

The next limitation to be considered is how the values of the neutral point earthing components were set. The resistance of the resistance earthed neutral point was chosen so a maximum earth current of 1 kA would flow. Similarly the parallel resistance of the resonant earthed neutral point was chosen so that a maximum residual steady state fault current of 6 A would flow. The 1 kA value was chosen as this is the maximum allowable fault current for equipment protection reasons. The 6 A value was calculated as being 10 % of the maximum capacitative earth current to obtain a self extinguishing arc according to DIN VDE 0845 and DIN EN 50522.

The neutral point components values are not always calculated using these methods and should not be considered all encompassing values. Each solar plant under investigation must be analysed using the methods chosen to determine the treatment

of the neutral point by whatever means that is.

Another important consideration to make is that this study has only presented results for a solar plant connected to the medium voltage grid in Germany with a nominal voltage level of 20 kV. If however the analysed plant was connected to a higher voltage level then it is expected that higher Fault Current and EPR values would be returned. This is the case in other similar studies such as the one conducted by Dawalibi and Ma [4] whom investigate a plant connected to a 220 kV existing power plant. In such cases the high EPR that may occur will require design modifications beyond the standard earthing system design and often include the spreading of a high resistivity soil covering such as crushed rock.

Furthermore grid nominal voltage fluctuations have not been considered as this study is focused on understanding the behaviour of the earthing system rather than investigating if the studied system is safe. When analysing a true system it is recommended that the maximum grid voltage rather than the nominal voltage be used.

Finally it must be noted that the model is based on the assumption of homogeneous soil characteristics which does not accurately reflect the true soil characteristics. In order then to maintain conservativeness when using this model it is adamant that soil resistivity measurements are taken in the field and the highest measured value is used in the model.

Once all of the points discussed here are taken into account the developed model can be used to analyse and determine the safety of grid connected solar plant earthing systems with confidence.

6 Future Outlook

The work presented in this thesis has provided a model to investigate the behaviour of a grid connected solar plant earthing system and has quantitatively investigated the effects of varying various solar plant characteristics on the behaviour of the earthing system. However throughout the study several assumptions and simplifications were made, these assumptions and simplifications lead to overly conservative results and ultimately cause over engineering. Further work and investigation should be conducted into these assumptions and simplifications to quantify the effects they have on the study and in the best case remove the need to make them.

Section 3.5.1 discusses how the accuracy of the earthing components of the LTspice model were verified. This analysis was done with field measurements of two transformer stations from one solar plant. This is a very small sample size and statistical analysis to prove the accuracy of the model is not possible. It is recommended that field measurements are taken from a sample size large enough to allow a full statistical analysis and prove within a certain confidence limit the accuracy of the model. Also it is recommended that the sample contains a variety of solar plants with different soil conditions to ensure the collected data envelopes all possible future scenarios and it is recommended that the measurements are made one to two years after construction of the earthing system to ensure the disturbed soil has fully settled.

Ignoring the contribution to the earthing system of the metallic structures supporting the solar PV modules (module table) has been a notable simplification of this study. The module tables are connected to the earthing system via the horizontal earthing electrode and act as auxiliary earthing electrodes. The legs supporting the module tables are made of galvanised steel and are rammed directly into the soil providing a large contact surface area with the soil and hence acting as a parallel pathway for fault current to flow. Ignoring the contribution of these auxiliary electrodes leads to conservative design and over engineering of the earthing system and it is recommended that an earthing system component modelling the module tables is developed in the existing LTspice component library.

Finally the developed LTspice model currently operates on the assumption of homogeneous soil conditions and as such the highest measured soil resistivity value is used. This leads to the resistance of the earthing system being overestimated. It is recommended that the equations to calculate the resistance of the earthing system components are reviewed and equations capable of calculating the resistance of the earthing electrodes in a 2-layer soil model are developed and implemented. This will also require a 2-layer soil model to be used and the well known model as discussed in Section 2.5 can be used.

7 Conclusion

Over the course of this study the behaviour of grid connected solar plant earthing systems has been investigated using computer simulations with a model developed in LTspice. The model calculates the main earthing system variables, Fault Current and EPR, under various solar plant configurations, grid connection characteristics and soil conditions. The major design parameters that the design engineer must take into account have been identified and their effect on earthing system performance have been discussed.

A major finding of this thesis is that solar plants with an isolated or resonant earthed neutral point will have earthing systems meeting the equipment protection and human protection requirements under all plant configurations and all practical soil resistivity values. However for plants with a resistance or directly earthed neutral point this is rarely the case and dedicated studies must be made on any such plant to verify the behaviour of the earthing system.

Furthermore it has been shown that larger plants are inherently more safe than smaller plants due to the larger amount of earthing electrode material. As well as this it has been demonstrated that increasing soil resistivity leads to increasing EPR and decreasing Fault Current.

An investigation into the effect of MV cable length on earthing systems has shown that, in general, as MV cable length increases the EPR and Fault Current decreases, with the exception of large plants with a resonant earthed neutral point where the solar production can cause a rising EPR and Fault Current for long MV cable lengths. Also it has been found that increasing the Short Circuit Power at the grid connection location causes increasing EPR and Fault Current but for systems with a resonant earthed neutral point this effect is negligible. Furthermore it was shown that the phase angle at the grid connection point has a very small impact on the behaviour of the earthing system and this variable can be safely ignored by the design engineer.

Also the comparison made between the two major international earthing standards DIN EN 50522 and IEEE std. 80 has shown that for grid connected solar plants the DIN standard leads to the more conservative results.

Finally it has been shown that the LTspice model can be used to identify a particular solar plant earthing system as a GES by effectively using an automated version of the Campoccia method.

Bibliography

[1]   "IEEE Guide for Safety in AC Substation Grounding". In: *IEEE Std 80-2013 (Revision of IEEE Std 80-2000/ Incorporates IEEE Std 80-2013/Cor 1-2015)* (2015), pp. 1–226. DOI: 10.1109/IEEESTD.2015.7109078.

[2]   DIN VDE. *0101 Teil 2, auch DIN EN 50522: Erdung von Starkstromanlagen mit Nennwechselspannungen über 1 kV*. 2011.

[3]   Reinhold Rüdenberg. "Grounding principles and practice I—Fundamental considerations on ground currents". In: *Electrical Engineering* 64.1 (1945), pp. 1–13.

[4]   Jinxi Ma and Farid P Dawalibi. "Grounding analysis of a solar power generation facility". In: *Power and Energy Engineering Conference (APPEEC), 2010 Asia-Pacific*. IEEE. 2010, pp. 1–4.

[5]   *Enerarc AG Company Description*. http://www.enerparc.de/index.php/en/company. Accessed: 14-Aug-2017.

[6]   CENELEC. *HD 637 S1: Power installations exceeding 1kV ac*. Tech. rep. European Committee for Electrotechnical Standardization, 1999.

[7]   "IEEE Guide for Generating Station Grounding". In: *ANSI/IEEE Std 665-1987* (1987). DOI: 10.1109/IEEESTD.1987.122156.

[8]   Eugene J Fagan and Ralph H Lee. "The use of concrete-enclosed reinforcing rods as grounding electrodes". In: *IEEE Transactions on Industry and General Applications* 4 (1970), pp. 337–348.

[9]   Abdallah R Al-Zyoud et al. "Effect of Neutral Grounding Methods on the Earth Fault Characteristics". In: *Progress In Electromagnetics Research*. PIERS Proceedings. 2015, pp. 1144–1151.

[10] S Ravlić and A Marušić. "Simulation Models for Various Neutral Earthing Methods in Medium Voltage Systems". In: *Procedia Engineering* 100 (2015), pp. 1182–1191.

[11] Jeff Roberts, Hector J Altuve, and Daqing Hou. "Review of ground fault protection methods for grounded, ungrounded and compensated distribution systems". In: *28th Annual Western Protective Relay Conf*. Spokane, Washington. 2001, pp. 23–25.

[12] Renato Čučić, Vitomir Komen, and Marijana Živić Đurović. "Neutral point concept in distribution networks". In: *Engineering Review* 28.2 (2008).

[13] Erkki Lakervi and Edward J Holmes. *Electricity distribution network design*. 21. IET, 1995.

[14] Bystrik Dolnik and Juraj Kurimskỳ. "Contribution to earth fault current compensation in middle voltage distribution networks". In: *Przglad Electrotechniczny (Electrical Review)* (2011), pp. 0033–2097.

[15] Zacharias G Datsios and Pantelis N Mikropoulos. "Safe grounding system design for a photovoltaic power station". In: *8th Mediterranean Conference on Power Generation, Transmission, Distribution and Energy Conversion*. MEDPOWER. 2012, pp. 1–6.

[16] M Nassereddine, J Rizk, and A Hellany. "How to design an effective earthing system to ensure the safety of the people". In: *Advances in Computational Tools for Engineering Applications, 2009. ACTEA'09. International Conference on*. IEEE. 2009, pp. 416–421.

[17] Frank Wenner. "A method for measuring earth resistivity". In: *Journal of the Franklin Institute* 180.3 (1915), pp. 373–375.

[18] "IEEE Guide for Measuring Earth Resistivity, Ground Impedance, and Earth Surface Potentials of a Grounding System". In: *IEEE Std 81-2012 (Revision of IEEE Std 81-1983)* (2012), pp. 1–86. DOI: 10.1109/IEEESTD.2012.6392181.

[19] Mohamad Nassereddine, Jamal Rizk, and Ghalia Nasserddine. "Soil Resistivity Data Computations; Single and Two-Layer Soil Resistivity Structure and Its Implication on Earthing Design". In: *World Academy of Science, Engineering and Technology* 7 (2013), pp. 878–883.

[20] FP Dawalibi, Jinxi Ma, and RD Southey. "Behaviour of grounding systems in multilayer soils: a parametric analysis". In: *IEEE Transactions on Power Delivery* 9.1 (1994), pp. 334–342.

[21] Anatja Samouëlian et al. "Electrical resistivity survey in soil science: a review". In: *Soil and Tillage research* 83.2 (2005), pp. 173–193.

[22] JA Laver and H Griffiths. "The variability of soils in earthing measurements and earthing system performance". In: *Rev. Energ. Ren.: Power Engineering* (2001), pp. 57–61.

[23] Siow Chun Lim, Chandima Gomes, and Mohd Zainal Abidin Ab Kadir. "Electrical earthing in troubled environment". In: *International Journal of Electrical Power & Energy Systems* 47 (2013), pp. 117–128.

[24] Jinliang He et al. "Seasonal influences on safety of substation grounding system". In: *IEEE Transactions on Power Delivery* 18.3 (2003), pp. 788–795.

[25] Huiliang Zhao et al. "Safety-limit curves for earthing system designs: appraisal of standard recommendations". In: *IEE Proceedings-Generation, Transmission and Distribution* 152.6 (2005), pp. 871–879.

[26] Charles F Dalziel and Frank P Massoglia. "Let-go currents and voltages". In: *Transactions of the American Institute of Electrical Engineers, Part II: Applications and Industry* 75.2 (1956), pp. 49–56.

[27] Charles F Dalziel. "Electric shock hazard". In: *IEEE spectrum* 9.2 (1972), pp. 41–50.

[28] Charles F Dalziel and William R Lee. "Reevaluation of lethal electric currents". In: *IEEE Transactions on Industry and General Applications* 5 (1968), pp. 467–476.

[29] "Technical Standard 60479-1 Effects of current on human beings and livestock – Part 1: General aspects". In: *International Electrotechnical Commission* (2005), pp. 1–117.

[30] CH Lee and AP Sakis Meliopoulos. "Comparison of touch and step voltages between IEEE Std 80 and IEC 479-1". In: *IEE Proceedings-Generation, Transmission and Distribution* 146.6 (1999), pp. 593–601.

[31] Nasser Tleis. *Power systems modelling and fault analysis: theory and practice*. Newnes, 2007.

[32] Osmo Siirto et al. "Neutral point treatment and earth fault suppression". In: *Electric Power Quality and Supply Reliability Conference (PQ), 2012*. IEEE. 2012, pp. 1–6.

[33] JG Sverak. "Sizing of ground conductors against fusing". In: *IEEE Transactions on Power Apparatus and Systems* 1 (1981), pp. 51–59.

[34] JA Sullivan. "Alternative earthing calculations for grids and rods". In: *IEE Proceedings-Generation, Transmission and Distribution* 145.3 (1998), pp. 271–280.

[35] SJ Schwarz. "Analytical expressions for the resistance of grounding systems". In: *Transactions of the American Institute of Electrical Engineers. Part III: Power Apparatus and Systems* 73.2 (1954), pp. 1011–1016.

[36] EATON Corporation PLC. *CYMGRD Substation Grounding Program*. 2017. URL: http://cyme.com/software/cymgrd/ (visited on 04/11/2017).

[37] Safe Engineering Services and Technologies ltd. *CDEGS*. 2017. URL: http://www.sestech.com/Products/SoftPackages/CDEGS.htm (visited on 04/11/2017).

[38] Jinxi Ma and Farid P Dawalibi. "Extended analysis of ground impedance measurement using the fall-of-potential method". In: *IEEE Transactions on Power Delivery* 17.4 (2002), pp. 881–885.

[39] JR Alderton, PC Anderson, and RJ Cakebread. "Calculation and measurement of the earth impedance of an ehv substation". In: *Proceedings of the Institution of Electrical Engineers*. Vol. 125. 12. IET. 1978, pp. 1367–1375.

[40] GF Tagg. "Measurement of earth-electrode resistance with particular reference to earth-electrode systems covering a large area". In: *Proceedings of the Institution of Electrical Engineers*. Vol. 111. 12. IET. 1964, pp. 2118–2130.

[41] Gossen Metrawatt Gmbh. *GEOHM C-CB int. Datasheet*. online. 2014.

[42] Sonel S.A. *MRU-21 Datasheet*. online. 2017.

[43] Pietro Colella, Enrico Pons, and Riccardo Tommasini. "A Comparative Review of the Methodologies to Identify a Global Earthing System". In: *IEEE Transactions on Industry Applications* (2017).

[44] Pietro Colella, Enrico Pons, and Riccardo Tommasini. "The identification of global earthing systems: a review and comparison of methodologies". In: *Environment and Electrical Engineering (EEEIC), 2016 IEEE 16th International Conference on*. IEEE. 2016, pp. 1–6.

[45] A Campoccia and G Zizzo. "Simple circuit models for studying global earthing systems". In: *Power Tech, 2007 IEEE Lausanne*. IEEE. 2007, pp. 1947–1952.

[46] Linear Technology. *LTspice*. 2017. URL: http://www.linear.com/designtools/software/\#LTspice (visited on 04/24/2017).

[47] Laurence W Nagel and Omega Enterprises. "The life of SPICE". In: *1996 Bipolar Circuits and Technology Meeting*. 1996.

[48] Colin Warwick. "Everything you always wanted to know about SPICE*(* But were afraid to ask)(PDF)". In: *EMC Journal (Nutwood UK Limited)(82)* (2009), pp. 27–29.

[49] Maurice George Say. *Alternating current machines*. Halsted Press, 1976.

[50] "IEEE Standard Test Code for Liquid-Immersed Distribution, Power, and Regulating Transformers". In: *IEEE Std C57.12.90-2010 (Revision of IEEE Std C57.12.90-2006)* (2010), pp. 1–100. DOI: 10.1109/IEEESTD.2010.5610578.

[51] John R Carson. "Wave propagation in overhead wires with ground return". In: *Bell Labs Technical Journal* 5.4 (1926), pp. 539–554.

[52] John R Carson. "Ground return impedance: Underground wire with earth return". In: *The Bell System Technical Journal* 8.1 (1929), pp. 94–98.

[53] Büro für Hydrogeologie angewandte Geologie und Wasserwirtschaft. *Solarpark Drochtersen Stade: Gutachten zur Ermittlung der erforderlichen Rammtiefe für Stahlprofile als Gründungselemente*. Tech. rep. Enerparc AG, 2017.

[54] Jovan Nahman and Ivica Paunovic. "Resistance to earth of earthing grids buried in multi-layer soil". In: *Electrical Engineering* 88.4 (2006), pp. 281–287.

[55] DIN VDE 0845. *Influence of high voltage systems on telecommunication systems Part 1: General, limits, calculation and measurement methods*. 2013.

A IEC 479-1 Safe Voltage Limits Calculation

IEC 479-1 provides a graphical method to find the allowable touch and step voltages. First the allowable body current must be determined using Figure A.1, where the three curves C_1, C_2 and C_3 give the body current I_{body} in A for the left hand to feet current path, that leads to ventricular fibrillation (heart failure) with a probability of $\leq 5\%$, $\leq 50\%$ and $>50\%$ respectively [29], the zones AC-1, AC-2, AC-3 and AC-4 refer to the physical effects of the current with AC-1 being the zone of perception, AC-2 involuntary muscle contractions, AC-3 strong muscle contractions, breathing difficulties, heart disturbances but no organic damage and AC-4 involves cellular damage and possibility of ventricular fibrillation.
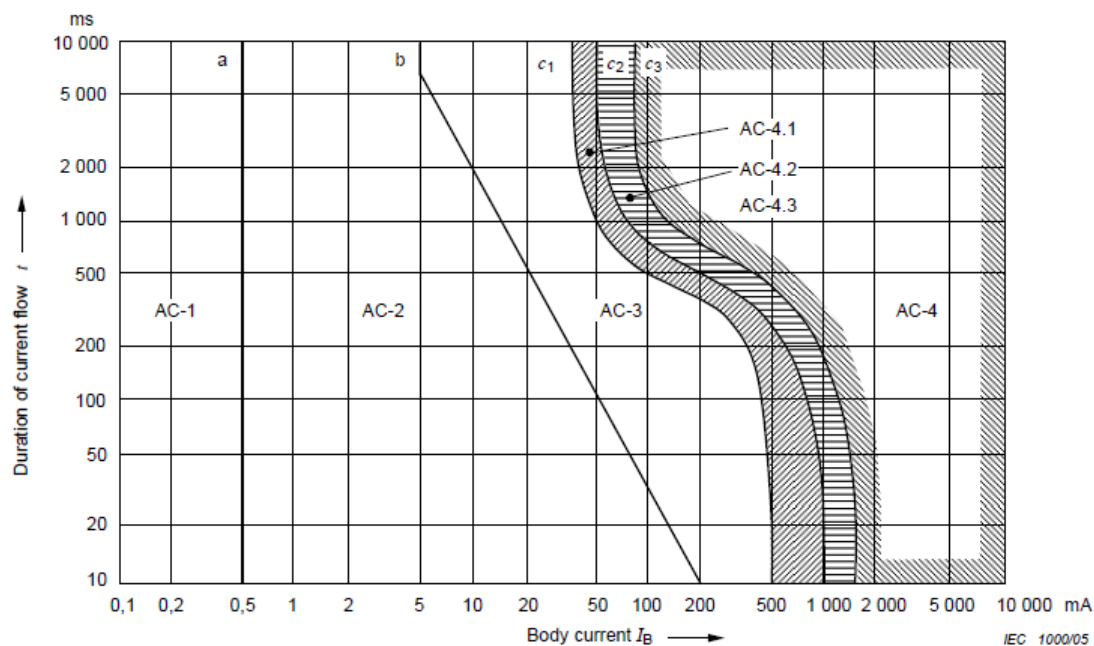
FIGURE A.1: Allowable body current as a function of shock duration [29].

Now the resistance of the electrical circuit must be estimated, IEC 479-1 provides tabulated data for the total human body impedance of the hand to hand current path, Z_T in Ω for nine cases covering dry, wet and saltwater wet contact conditions of small (100 mm^2), medium (1000 mm^2) and large (10000 mm^2) contact areas. Each table provides impedance data for values of Z_T not exceeded by 5%, 50% and 95% of the population. The tabulated data provided gives the resistance values as a function of touch voltage so this value must be calculated using the techniques outline in Section 2.9. The tables have not been included here to save space but can be found in the IEC 479-1 document.

Once a body resistance value for the hand to hand current path has been obtained Figure A.2 is used to determine the resistance of the particular current path of interest. For touch voltage the current path is from one hand to both feet hence we have the arm and torso in series and the legs in parallel, using the quantities provided in Figure A.2 we find that the resistance of the touch voltage path is 78.6% that of the hand to hand path. Similarly for step voltage we have both of the legs in series and we get the resistance of the step voltage path is 107.4% that of the hand to hand path.
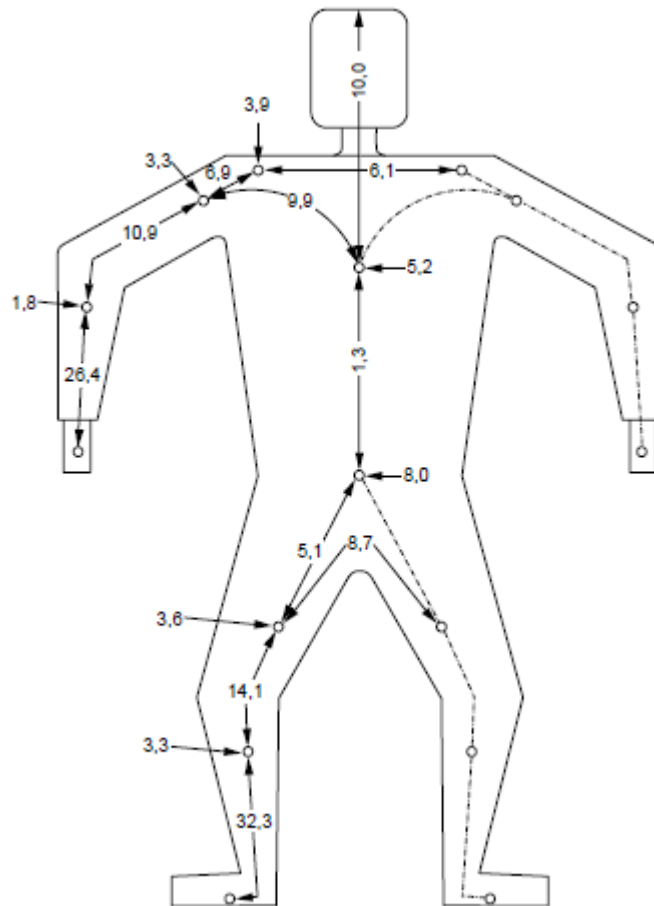

FIGURE A.2: Current path resistance to various body locations as a percent in relation to hand to foot resistance [29].

Now with the acquired data the allowable touch and step voltages can be calculated using Equations A.1 and A.2.

$$V_{touch,allow} = I_{body}(0.786Z_T) \tag{A.1}$$

$$V_{step,allow} = I_{body}(1.074Z_T) \tag{A.2}$$

B Derivation of Asymmetrical Current Decrement Factor

At the initiation of an earth fault the reactive component of a 3 phase AC system may be storing some energy depending on when in relation to the sinusoidal voltage wave the fault occurs. The stored energy will then lead to a constant polarity DC offset which decays exponentially with time and the rate of decay is dependent on the reactance to resistance ratio of the system, Figure B.1 displays an example of an asymmetrical earth current.

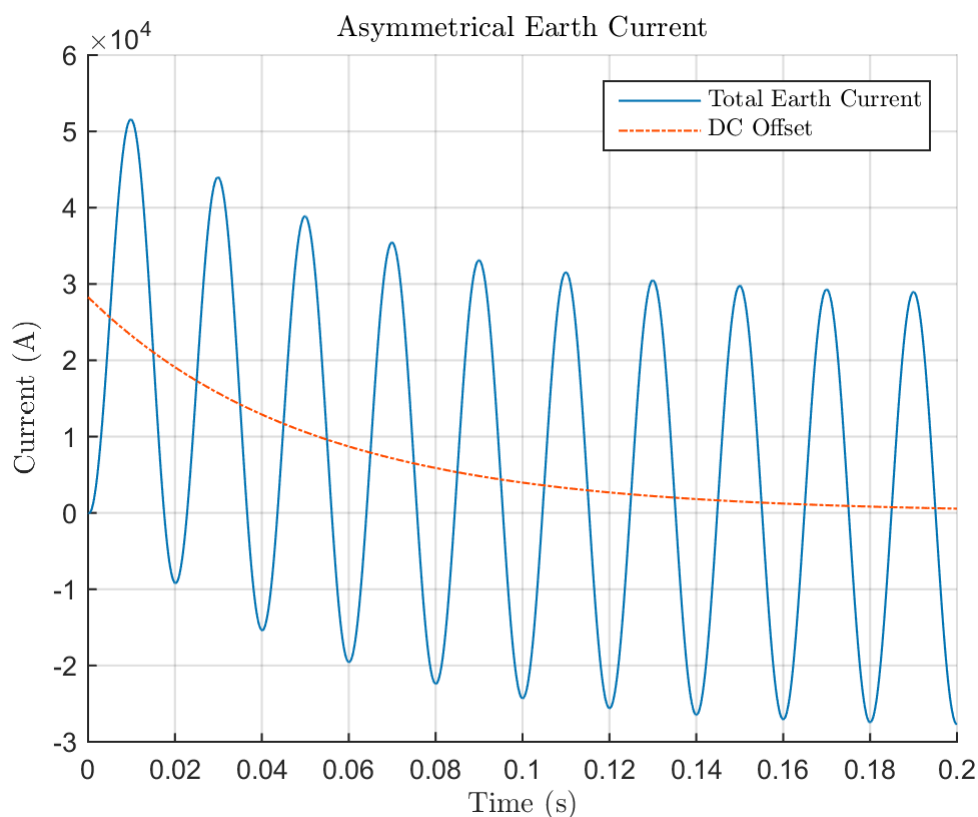FIGURE B.1: Asymmetrical current waveform, with DC offset displayed, over a 0.2 second period produced by a 20 kV 50 Hz voltage source with an X/R ratio of 8.

To quantify the contribution of this DC component to the fault current lets first consider the following R-L circuit shown in Figure B.2.

And accompanying the circuit we have the following equations for voltage and current.
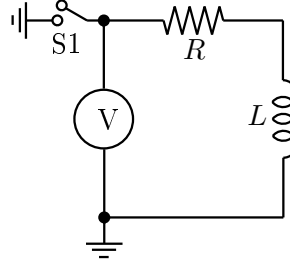
$$V = \sqrt{2}V_n \sin{(\omega t)} \tag{B.1}$$

FIGURE B.2: R-L circuit used for deriving the asymmetrical current decrement factor.

$$I = \sqrt{2}\frac{V_n}{Z}\sin\left(\omega t - \phi\right) \tag{B.2}$$

Where:
V_N is nominal voltage in V
ω is angular frequency in rad/s
t is time in s
Z is the impedance of the system in Ω
ϕ is the phase angle in rad

Now consider the initiation of an earth fault via switch S1 at $t = \frac{\alpha}{\omega}$, now we have an asymmetrical earth current equal to:

$$I_{E,asym} = \sqrt{2}\frac{V_n}{Z}\sin\left(\omega t + \alpha - \phi\right) + I_L \tag{B.3}$$

Where:
I_L is current contribution from the reactive component of the circuit in A

Now applying Kirchhoff's voltage law to the circuit in Figure B.2 we arrive at Equation B.4.

$$L\frac{dI_L}{dt} = -RI_L \tag{B.4}$$

And solving the first order linear differential equation we find:

$$I_L = Ce^{\frac{-Rt}{L}} \tag{B.5}$$

And using the boundary condition that at the initiation of the earth fault $I_L = \sqrt{2}\frac{V_n}{Z}\sin\left(\alpha - \phi\right)$ the constant C is found giving the current contribution from the reactive component of the circuit.

$$I_L = \sqrt{2}\frac{V_n}{Z}\sin\left(\alpha - \phi\right)e^{\frac{-Rt}{L}} \tag{B.6}$$

Also if we say $T_a = X/\omega R$ which is the DC offset time constant we come to the total asymmetrical earth current:

$$I_{E,asym} = \sqrt{2}\frac{V_n}{Z}[\sin\left(\omega t + \alpha - \phi\right) - e^{\frac{-t}{Ta}}\sin\left(\alpha - \phi\right)] \tag{B.7}$$

Now as we are concerned with the maximum contribution of the DC offset, which occurs at $\alpha - \phi = -\frac{\pi}{2}$, then Equation B.7 becomes:

$$I_{E,asym} = \sqrt{2}\frac{V_n}{Z}[e^{\frac{-t}{T_a}} - \cos{(\omega t)}] \tag{B.8}$$

Now to find the decrement factor we want to find the ratio of the RMS value of the asymmetrical and symmetrical fault currents for the entire fault duration, t_f, as in Equation B.9.

$$D_f = \frac{I_{E,asym,RMS}}{I_{E,sym,RMS}} \tag{B.9}$$

So to find $I_{E,asym,RMS}$ we need to integrate Equation B.8 as in Equation B.10.

$$I_{E,asym,RMS} = \sqrt{\frac{1}{t_f}\int_0^{t_f}[\sqrt{2}\frac{V_n}{Z}(e^{\frac{-t}{T_a}} - \cos{(\omega t)})]^2 dt} \tag{B.10}$$

Which becomes:

$$I_{E,asym,RMS} = \frac{V_n}{Z}\sqrt{\frac{2}{t_f}\int_0^{t_f}[e^{\frac{-t}{T_a}} - \cos{(\omega t)}]^2 dt} \tag{B.11}$$

Noting that $\frac{V_n}{Z} = I_n$ where I_n is the nominal current which is equivalent to the symmetrical earth current so we can rearrange Equation B.11 to:

$$\frac{I_{E,asym,RMS}}{I_{E,sym,RMS}} = D_f = \sqrt{\frac{2}{t_f}\int_0^{t_f}[e^{\frac{-t}{T_a}} - \cos{(\omega t)}]^2 dt} \tag{B.12}$$

And evaluating the integral we arrive at the final result.

$$D_f = \sqrt{1 + \frac{T_a}{t_f}\left(1 - e^{\frac{-2t_f}{T_a}}\right)} \tag{B.13}$$

C Carson's Ground Return Theory

This appendix details the derivation of the self and mutual impedance Equations 3.11 and 3.12.

First let us consider an overhead wire running parallel to the z-axis, intersecting the y-axis at a height h meters above the earth carrying an alternating current I of angular frequency ω. The surface of the earth is assumed flat and is coplanar with the xz-plane, the earth is modelled as having homogeneous resistivity of ρ and being infinite in proportion. There exists a fictitious mirror image of the overhead wire buried at a depth of h in the ground as shown in Figure C.1

FIGURE C.1: Overhead wire with buried wire image showing the distances D' and D" from the wire and the wire image, respectively, to a point (x, y) in space.

Carson's analysis begins with an analysis of the electric field strength E_z and the magnetic fields H_x and H_y produced by the alternating current in the overhead wire and results in Equation C.1 for the electric field strength in the air.

$$E_z = -\frac{\omega\mu_0 I}{\pi} \int_0^\infty (\sqrt{\mu^2 + j} - \mu)e^{-(h'+y')\mu} \cos(x'\mu)d\mu - \frac{j\omega\mu_0 I}{2\pi} \ln\left(\frac{D''}{D'}\right) + V\Gamma \qquad y \geq 0$$

(C.1)

Where:
μ_0 is the vacuum permeability
μ is the permeability at point (x, y)
$h' = h\sqrt{\alpha}$
$x' = x\sqrt{\alpha}$
$y' = y\sqrt{\alpha}$

$\alpha = \frac{\omega\mu_0}{\rho}$

Γ is the wave propagation constant

V is the potential difference between the point (x, y) and remote earth

Now let us consider a point on the surface of the overhead wire, the electric field strength here is given by $R_0 I$ where R_0 is the internal resistance per unit length of the wire. This can be equated with equation C.1 and solved for Γ.

$$\Gamma^2 = (G + j\omega C)(R_0 + \frac{\omega\mu_0}{\pi}\int_0^\infty (\sqrt{\mu^2 + j} - \mu)e^{-(h' + y')\mu}\cos(x'\mu)d\mu - \frac{j\omega\mu_0}{2\pi}\ln\left(\frac{2h}{r_i}\right)$$
$$(C.2)$$

Where:

$(G + j\omega C)$ is the shunt admittance of the line per unit length

r_i is the radius of the overhead wire

And using the identity for the wave propagation constant $\Gamma^2 = (G + j\omega C)(R + jX)$ we find the self impedance of the circuit.

$$Z_s = (R_0 + \frac{\omega\mu_0}{\pi}\int_0^\infty (\sqrt{\mu^2 + j} - \mu)e^{-2h'\mu}d\mu - \frac{j\omega\mu_0}{2\pi}\ln\left(\frac{2h}{r}\right) \qquad (C.3)$$

Similarly if we have two overhead conductors at heights h_1 and h_2 under the same conditions as in Figure C.2 and undertaking the same analysis we can find the mutual impedance.
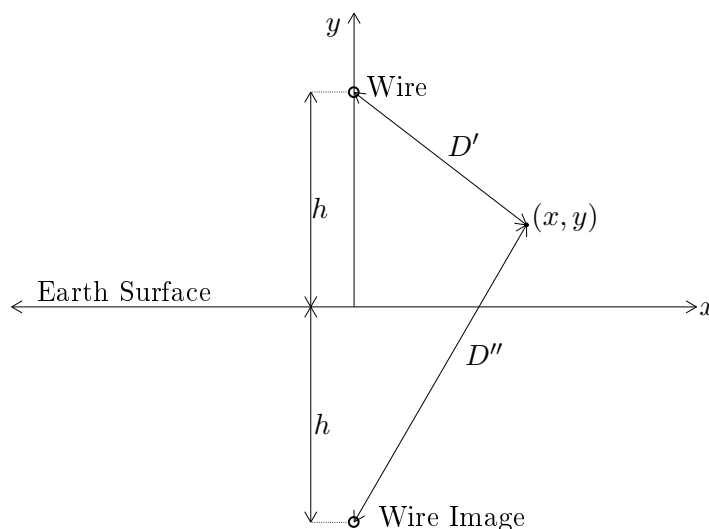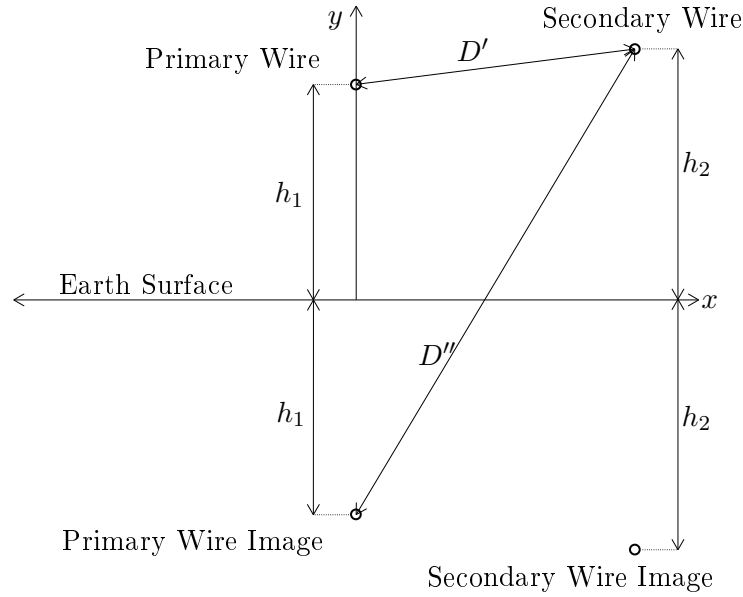

FIGURE C.2: Overhead wires with buried wire images showing the distances D' and D" from the primary wire and primary wire image, respectively, to the secondary wire.

$$Z_m = \frac{\omega\mu_0}{\pi}\int_0^\infty (\sqrt{\mu^2 + j} - \mu)e^{-(h_1' + h_2')\mu}\cos(x'\mu)d\mu - \frac{j\omega\mu_0}{2\pi}\ln\left(\frac{D''}{D'}\right) \qquad (C.4)$$

Now it can be seen that Equations C.3 and C.4 are both dependent on an integral of the form:

$$J(p,q) = \int_0^\infty (\sqrt{\mu^2 + j} - \mu)e^{-p\mu}\cos(q\mu)d\mu \tag{C.5}$$

To which Carson proposed the solution could be made to depend on the solution to the following integral:

$$\int_0^\infty (\sqrt{\mu^2 + \alpha^2})e^{-\beta\mu}d\mu \tag{C.6}$$

The solution to Equation C.6 is the sum of a first order Bessel function and an absolutely convergent series and they appear to be somewhat complicated but when applied to the two cases of concern of self and mutual impedance they rapidly simplify to the following.

$$J = (P + jQ) = \frac{\pi}{8} + j\left(\frac{1}{4} + \frac{1}{2}\ln\left(\frac{2}{e^\gamma r}\right)\right) \tag{C.7}$$

Where:
γ is Euler's constant (0.57722)
$r = 2h\sqrt{\alpha}$ for self impedance
$r = D''\sqrt{\alpha}$ for mutual impedance

Now we can substitute Equation C.7 in Equations C.3 and C.4 and evaluate the resulting expressions to arrive at the final self and mutual impedance equations.

$$Z_s = R_0 + \frac{\omega\mu_0}{8} + j\frac{\omega\mu_0}{2\pi}\ln\left(\frac{658}{r_i}\sqrt{\frac{\rho}{f}}\right) \tag{C.8}$$

$$Z_m = \frac{\omega\mu_0}{8} + j\frac{\omega\mu_0}{2\pi}\ln\left(\frac{658}{D'}\sqrt{\frac{\rho}{f}}\right) \tag{C.9}$$

Where:
f=frequency of AC current ($\frac{\omega}{2\pi}$)

D Field Measurement Protocols

The protocols for recording field data are shown here.

Soil Resistivity Measuring Protocol

Location:	Device:	Time, date:
Soil Type:	**Soil Moisture:**	**Weather, temp:**

Distance a (m)	Distance b (m)	Soil resistivity (Ωm)
3	Max 0.3	
4	Max 0.4	
5	Max 0.5	
6	Max 0.5	
7	Max 0.5	
8	Max 0.5	
9	Max 0.5	
10	Max 0.5	
11	Max 0.5	
12	Max 0.5	
13	Max 0.5	
14	Max 0.5	
15	Max 0.5	

Defects: ☐ no ☐ yes, what _____

Comments:

Inspector:

_____

(Name/company/signature)

Earth Resistance FOP Measuring Protocol

ENERPARC
Power of Excellence

Location:	Device:	Time, date:
Soil Type:	**Soil Moisture:**	**Weather, temp:**

Distance C (m)	Distance P (m)	Earth Resistance (Ω)
20	1	
20	2	
20	3	
20	4	
20	5	
20	6	
20	7	
20	8	
20	9	
20	10	
20	11	
20	12	
20	13	
20	14	
20	15	
20	16	
20	17	
20	18	
20	19	

Defects: ☐ no ☐ yes, what _____

Comments:

Inspector:
_____
(Name/company/signature)

E Drochtersen Stade Layout Drawing and Transformer Station Local Earthing System Drawing

The layout drawing for Drochtersen Stade PV plant and the local earthing system at each transofrmer station are presented here.

Legende

- Zaun
- Straße
- Modultisch
- Modulreihe
- A.065
- T140c / Trafo HVMV
- Trafostation
- Monitoring Container
- US — Übergabestation
- AC-Combiner
- ACB 01.01
- Rundleiter verzinkt RD10
- Erdung oberirdisch
- Modultisch-Verbinder (Kupfer 16 mm²)

Anschluss der Modultische an das Erdungsnetz

INV 014
INV 013
A.046
ACCB 01.07

Anschluss der Station an das Erdungsnetz

B.01
DRO-A-TST-05
(2000 kVA)
ACCB 01.07

Kabelgraben

Kabelgraben, Typ 1: Nur Erdung

Erde

N

Ansicht: Seite

Anschlussklemme für Tiefenerder
Art.-Nr.: 111357

Schlagspitze

min. 2 x Tiefenerder (L=1,5 m)

Leerrohr DN32 Würth

① ②

PAS

Trafostation

0,5

GOK

Stationserdung Ansicht Seite

Erster Erdungsring
Ansicht: Oben

Zweiter Erdungsring
Ansicht: Oben

Felderdung Runddraht RD10

Leerrohr DN32 Würth

Felderdung Runddraht RD10 Würth
Das Ende des Kabels muss mit grün-gelb Schrumpfschlauch markiert sein und in einem Leerrohr verlegt werden, um einen Kontakt zwischen den Erdungssystem zu verhindern

Multi-Klemme Ø 10 mm
Art.-Nr.: 1278

Anschlusspunkt am Stationsgehäuse

Anschlussklemme für Tiefenerder
Art.-Nr.: 111357

Erdungsseil E-Kupfer verzinnt 70 mm²

1 x KS Verbinder

PAS

Interne Erdung

Trafostation

1

min. 2 x Tiefenerder (L=1,5 m)
bis R < 2Ω erreicht sind.
Schlagspitze für Tiefenerder

Multi-Klemme Ø 10 mm
zum Schließen des Ringerders
Art. Nr. 1270

Anschlussklemme für Tiefenerder
Art.-Nr.: 111357

Erdungsseil E-Kupfer verzinnt 70 mm²

Multi-Klemme Ø 10 mm
zum Schließen des Ringerders
Art.-Nr.: 1278

min. 2 x Tiefenerder (L=1,5 m)
bis R < 2Ω erreicht sind.
Schlagspitze für Tiefenerder

Der Erdungsring muss mindestens 0,5 m
tief und 1 m entfernt von der Station sein.

Trafostation

0,5

0,5

Felderdung Runddraht RD10

Multi-Klemme Ø 10 mm
zum Schließen des Ringerders
Art. Nr. 1270
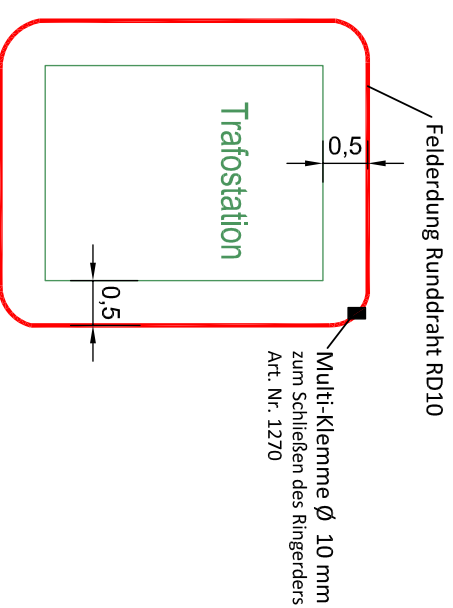
Der Erdungsring muss 0,5 m von
der Station entfernt sein.